universität wien

DIPLOMARBEIT / DIPLOMA THESIS

Titel der Diplomarbeit / Title of the Diploma Thesis

„Experimental Ionisation Yields of Fluoride Anions in a Middleton Type Sputter Ion Source“

verfasst von / submitted by

Xiaohe Zhang

angestrebter akademischer Grad / in partial fulfilment of the requirements for the degree of

Magistra der Naturwissenschaften (Mag. rer. nat)

Wien, 2018 / Vienna, 2018

Studienkennzahl lt. Studienblatt / degree programme code as it appears on the student record sheet:	A 190 344 412
Studienrichtung lt. Studienblatt / degree programme as it appears on the student record sheet:	Lehramtstudium UF Englisch UF Physik
Betreut von / Supervisor:	Univ.-Prof. Dipl.-Ing. Dr. Robin Golser
Mitbetreut von / Co-Supervisor:	Mag. Dr. Martin Martschini

Acknowledgements

The completion of the thesis could not have been possible without Robin Golser, who gave me the opportunity to work on this topic. My profound gratitude also goes to: my co-supervisor Martin Martschini for his support not only in experiments, but also in schedule organisation and, more importantly, motivation upkeep; Peter Steier for his expertise in AMS as well as programming, which made experimenting and data evaluation much easier for me; Johannes Lachner for his readiness to answer all my questions with patience; Karin Hain for involving me in useful discussions; Alfred Priller for explanation of the fundamentals; Mojmír Němec and Tomáš Prášek for providing me with sample materials as well as ideas; workshop staff Ewald Friedl, Gabi Obstmayer, Wolfgang Hiesz and Johann Lukas for the maintenance of the accelerator; Christoph Marek, Paul Wasserburger as well as the rest of the VERA team for keeping a positive atmosphere.

In the words of Shakespeare: *I can no other answer make but thanks, and thanks, and ever thanks*.

Abstract

The dominant application of anions in Accelerator Mass Spectrometry (AMS) necessitates the generation of a stable and intense anion beam on the basis of an efficient usage of the sample material. Generally, fluoride anions have shown to provide high ion currents and a considerable ability to suppress interfering isobars in a number of experiments (Zhao et al 2010). However, the overall fluoride ion formation efficiency needs to be determined to assess their applicability. Therefore, the objective of the study is an examination of factors that exert influence on the ionisation efficiency as well as the beam intensity of hafnium, caesium as well as uranium fluoride anions in a Middleton type Sputter Ion Source.

The first part of the thesis investigates the influence of target composition as well as manner of sputtering on HfF_5^- ion formation. It was revealed that sample materials consisting of HfF_4, PbF_2 and Ag, especially in the case of high PbF_2 proportion, not only generated a larger current, but also provided a higher ionisation efficiency of HfF_5^- than sample materials containing HfF_4 and Ag alone. Furthermore, targets that were sputtered in a continuous manner yielded ionisation efficiencies around 15% higher than targets that were sputtered for 10 min time spans in a consecutive manner. The highest HfF_5^- ionisation efficiency was 5.9%, achieved by continuous sputtering of a HfF_4, PbF_2 and Ag mixture with a mass ratio of 1:3:1.

The ion of interest in the second part of the thesis is CsF_2^-. Here, two fluorine donor materials (PbF_2 and LaF_3) in two different proportions were examined in their effectiveness. It was shown that PbF_2 yields stronger formation of CsF_2^- than LaF_3. Further, a Cs:F atom ratio of 1:3, when using PbF_2 as fluorine donor, suffices for a typical current of 40 - 100 nA and a maximum ionisation efficiency of around 0.08%.

The third part focuses on the formation of UO^- as well as UF_5^- ions in relation to different sample matrices, source parameter and target holder material. Adding Fe to a mixture of U_3O_8 and Fe_2O_3 improves the UO^- beam intensity as well as the ionisation efficiency. Under appropriate conditions of the ion source, U_3O_8 and Fe_2O_3 mixture added with Fe to a mass ratio of 1:2 yielded a typical UO^- current of 5-9 nA and a maximum ionisation efficiency of around 2.9%. Using gold and copper target holder inserts for UF_4 and PbF_2 mixtures with a mass ratio of 1:9 yielded a typical UF_5^- current around 10 nA and a maximal ionisation efficiency of 3.5%.

Zusammenfassung

Die vorwiegende Anwendung von Anionen in der Beschleuniger Massenspektrometrie (AMS) bedarf der Herstellung eines stabilen und intensiven Anionenstrahls bei gleichzeitiger effizienter Nutzung des Probenmaterials. Fluoridanionen machen im Allgemeinen intensive Ionenstrahlen und bieten potentielle Unterdrückung von Isobaren (Zhao et al 2010). Zur Feststellung ihrer Eignung muss jedoch die Effizienz der Fluoridionenformation untersucht werden. Daher ist das Ziel dieser Studie eine Untersuchung der Faktoren, die die Ionisationseffizienz und Strahlintensität von Hafnium-, Cäsium- und Uran-Fluorid-Anionen in einer Middleton Typ Sputter Ionenquelle beeinflussen.

Der erste Teil der Arbeit untersucht den Einfluss der Zusammensetzung der Probe und der Art des Sputterns auf die Bildung von HfF_5^- Ionen. Es wurde gezeigt, dass Probenmaterialien aus HfF_4, PbF_2 und Ag, insbesondere im Fall hoher PbF_2 Anteile, nicht nur höhere Spannung, sondern auch höhere Ionisationseffizienz an HfF_5^- erzielen als Probenmaterialien mit HfF_4 und Ag alleine. Außerdem wurde bei ununterbrochenem Sputtern eine um 15% höhere Ionisationsausbeute erreicht als wenn Targets nacheinander für jeweils nur 10 Minuten gesputtert wurden. Die höchste erzielte HfF_5^--Ionisationseffizienz betrug 5,9%, welche bei ununterbrochenem Sputtern einer Mischung von HfF_4, PbF_2 und Ag im Massenverhältnis 1:3:1 gemessen wurde.

Im zweiten Teil der Arbeit wurde CsF_2^- betrachtete. Zwei Fluordonatoren (PbF_2 und LaF_3) in zwei verschiedenen Verhältnissen wurden auf ihre Effektivität hin untersucht. Es wurde gezeigt, dass PbF_2 zu einer stärkeren Bildung von CsF_2^- führt als LaF_3. Darüber hinaus reicht ein Cs:F-Atomverhältnis von 1:3 bei der Nutzung von PbF_2 als Fluordonor aus, um einen Strom von 40-100 nA und eine maximale Ionisationseffizienz von etwa 0,08% zu erzielen.

Der dritte Teil konzentriert sich auf die Bildung von UO^-- und UF_5^--Ionen in Verbindung mit verschiedenen Proben-Matrix-Materialien, Quellen-Parametern und Probenhaltermaterialien. Zugabe von Fe zu einer Mischung von U_3O_8 und Fe_2O_3 verbessert die UO^--Strahlintensität sowie die Ionisationseffizienz. Bei entsprechender Einstellung der Ionenquelle ergab eine Mischung von U_3O_8 und Fe_2O_3 mit hinzugefügtem Fe in einem Masseverhältnis von 1:2 einen typischen UO^- Strom von 5-9 nA und eine maximale Ionisationsausbeute um 2.9%. Die verwendung von Gold- und Kupfer-Kathodeninserts für UF_4- und PbF_2-Mischungen in einem Masseverhältnis von 1:9 ergab einen typischen UF_5^--Strom von 10 nA und eine maximale Ionisationseffizienz von 3,5%.

Table of Contents

1. INTRODUCTION

Accelerator Mass Spectrometry (AMS), an ultrasensitive technique to measure trace isotopes, generally uses a focused positive ion beam (primary ion) bombarding sample material to obtain negative sample ions (secondary ion). One of the challenges it faces is the generation of stable negative ion beams with high intensity. Further, especially in the case of small sample sizes, it is important that elements of interest in samples are turned into anions efficiently (ionisation efficiency).

Fluoride anions are of growing interest for Accelerator Mass Spectrometry as they have shown high ion currents and a considerable ability to suppress interfering isobars in a number of experiments (Zhao et al 2010). In order to assess their applicability, however, it is necessary to determine their overall negative ion formation efficiency. The goal of this study is an examination of factors that influence the ionisation efficiency of fluoride anions (HfF_5^-, CsF_2^-, UF_5^-/UO^-) in a Middleton type sputter ion source.

This thesis is divided into two main parts: section 2 to section 5 gives a general theoretical overview as well as a description of the VERA facility, in which all the experiments were carried out. Section 6 to 8 provides an account as well as discussions of experiments conducted to examine factors influencing the ionisation efficiency of HfF_5^-, CsF_2^- and UF_5^-.

The investigation of HfF_5^- ion formation includes two experiments examining mainly the influence of matrix composition, composite proportion as well as mode of sputtering (consecutive and continuous sputtering); the examination of CsF_2^- ionisation includes one experiment investigating the impact of the sample matrix; further, four experiments were carried out focussing on the formation of UF_5^- as well as UO^- ions including different sample matrices, ion source parameters, sample masses and recess geometries.

2. ACCELERATOR MASS SPECTROMETRY AT VERA

Accelerator Mass Spectrometry (AMS) is a method for isotopic abundance measurements. By applying various mass and energy filters, isotope ratios down to the 10^{-16} level can be measured with great sensitivity and efficiency (Kutschera 2005).

The Vienna Environmental Research Accelerator (VERA) is based on a 3-MV Pelletron tandem accelerator by National Electrostatics Corporation (NEC). Operational since 1996, it underwent several modifications to incorporate measurement of a wide range of nuclides which form negative ions (Kutschera 2000; Steier et al 2004).

Figure 2.1 gives a schematic view of the current setup of VERA. As can be seen, VERA incorporates two ion sources (detailed in section 1.1). The negative ion beam is typically preaccelerated to 70 keV from the ion source (Steier et al 2004), making its subsequent filtering possible.

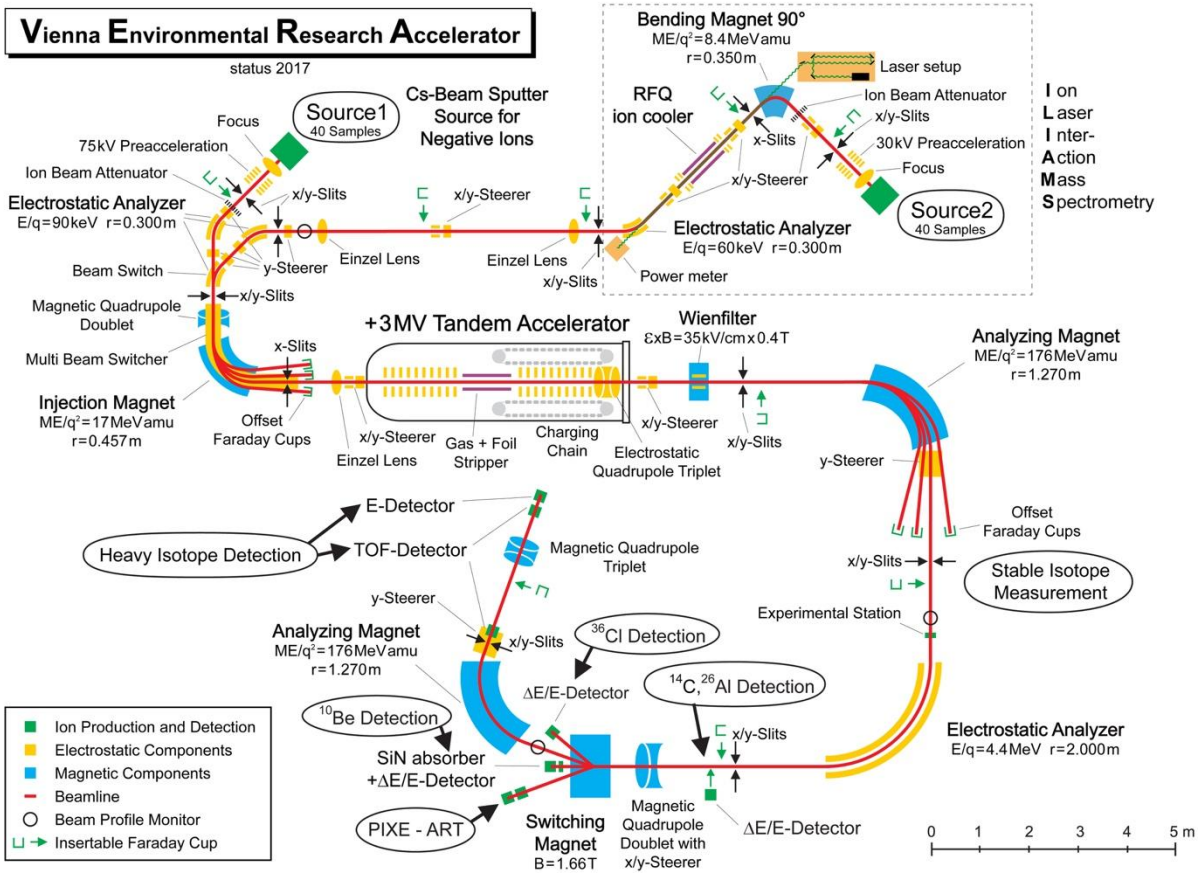

Figure 2.1 Schematic Diagram of VERA

2.1 THE ION SOURCES

VERA makes use of two so-called Multi-Cathode Source for Negative Ions by Caesium Sputtering, MC-SNICS in short. Its prototype is the high intensity source, which is shown in figure 2.2 (Middleton 1989).

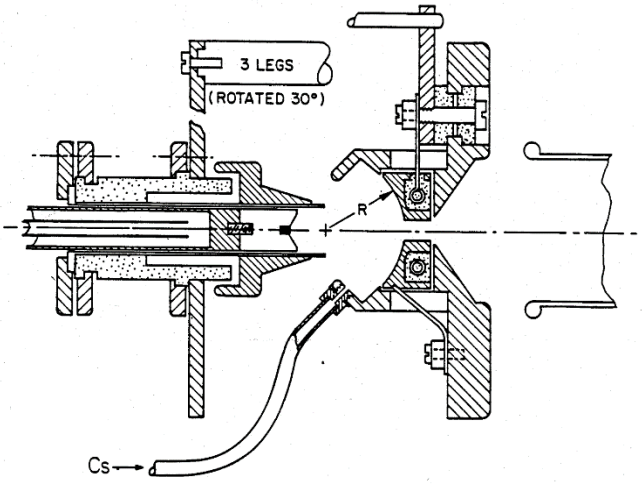

Figure 2.2 Middleton-Type High Intensity Source (Middleton 1989)

This high intensity ion source is also labelled as *Middleton-Type*, since it was first presented by Middleton. It is based on the SIMS technique (Secondary Ion Mass Spectrometry): by bombarding primary ions onto the sample material, the sample material ejects secondary ions, which will be extracted into an ion beam and analysed (Maden 2003).

Caesium is often (also in the case of VERA) used as the primary ion because of the advantages it offers: first, caesium has a relatively low electron affinity, which makes it an electron donator and thus contributes to the enhancement of extraction yield (Middleton 1989; Steier 2000); second, a layer of caesium on the target surface reduces the surface work function, which facilitates the desorption of the negative ions (Zhao et al 2016).

By heating the caesium reservoir, vaporised caesium atoms are produced, which then diffuse onto the hot spherical ioniser[1], which is usually made from tantalum, and are ionised (Middleton 1989). The ioniser has a focussing effect for the Cs^+ beam. Further improvement of the Cs^+ beam intensity at the target is achieved by an einzel lens between the ioniser and the target.

This Cs^+ beam undergoes an acceleration from the ioniser to the target, since the target has a lower electric potential than the ioniser: the target is usually kept at -70kV, and the ioniser at -65kV at VERA, which also explains the labelling of the target as cathode. In

[1] Source parameter for ioniser: IONPW, which has the greatest influence on the temperature in the source.

this way, this focussed Cs^+ beam gains kinetic energy and collides with the atoms / molecules of the sample material. With a thin neutral caesium layer on the target surface providing them with electrons and reducing the work function, sample material is ionised during this keV Cs^+ bombardment. These negatively charged sample ions will then be accelerated towards the spherical ioniser, which has a small opening in the middle, and go towards the rest of the AMS facility (Middleton 1989).

The difference between this prototype and the MC-SNICS is already indicated by their names. Instead of one single sample holder, VERA's MC-SNICS contain a target wheel which encompasses 40 sample holders (Vockenhuber 2005). Figure 2.3 shows a sketch applicable to both MC-SNICSs incorporated in the VERA facility.

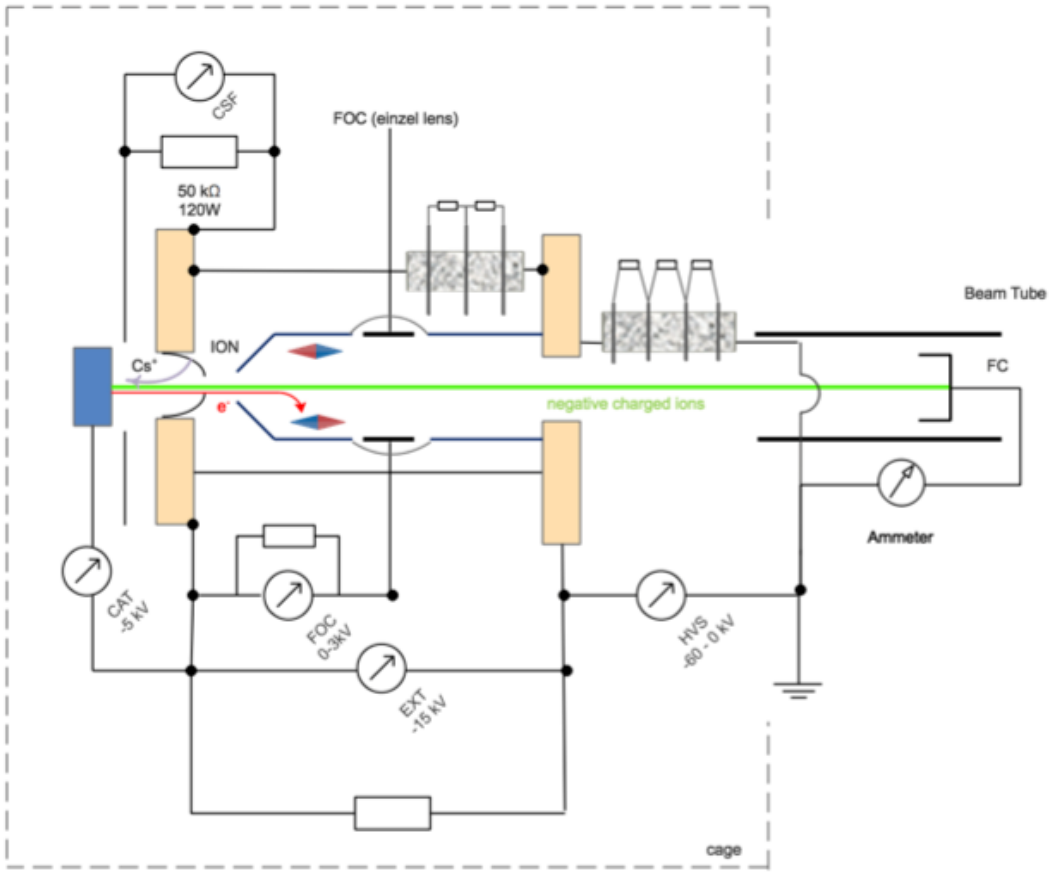

Figure 2.3 Sketch of the VERA MC-SNICS (Graph by author with the help of Dr. Alfred Priller) The primary Cs^+ ion beam is represented by the grey arrow. Due to the electric potential difference between the ioniser (ION) and the cathode (CAT), this Cs^+ beam is accelerated towards the cathode. The einzel lens CSF exists to improve the Cs^+ beam intensity. The bombardment of the keV Cs^+ on the sample surface leads to ionisation of sample material. These negative charged sample ions (green arrow) are accelerated by the extraction (EXT) as well as the pre-acceleration (HVS) voltage. An einzel lens (FOC) provides focussing of the secondary ion beam. The red arrow represents excessive electrons from the source (especially from ionisation of Cs atoms to Cs^+ ions), which are deflected by the magnets.

2.2 THE LOW ENERGY SECTION

The following section aims at a description of the filtering elements in the low energy section of VERA. All slits, lenses and steerers which contribute to either mass resolution or ion transmission are left out. For an overview of components, see figure 2.1.

The filtering element directly following source 1 (S1) is ESA 01-1, a 45° spherical electrostatic analyser with a radius of 300 mm and a gap of 50 mm. As a filter for E/q, it removes sputter tails, ions to which excess energy of the sputtering beam is imparted and which thus exit the ion source with a higher energy than the rest (Steier 2000). It provides "symmetrical 1:1 focussing from the slits after the source to the entrance lens of the beam sequencer" (Steier 2000).

In contrast to S1, source 2 (S2) is followed by a double focussing bending magnet BM I1-1 (Danfysik) with a nominal deflection angle of 90°, a radius of 350 mm and a pole gap of 50 mm. As a filter for magnetic rigidity mv/q, it offers preliminary ion filtering before their entrance into the Ion Laser InterAction Mass Spectrometry setup, ILIAMS in short.

The ILIAMS consists of a gas-filled radio frequency quadrupole (RFQ) and a laser. Ion beams up to several hundred nA first undergo deceleration and cooling by the RFQ and then a collinear overlapping with a continuous wave laser beam (Martschini et al 2017). By absorption of laser photons with an appropriate wavelength, the desired ions lose an electron and are neutralised, hence the name photodetachment. The deceleration inside the RFQ leads to an increased interaction time of the ion beam with the laser and, therefore, a greater detachment efficiency (Martschini et al 2017). Since photodetachment takes place with a photon energy equal to or greater than the electron affinity of an ion/atom and is thus a threshold process, it is only applicable when the ion of interest has a higher electron affinity than the interfering ions (Martschini et al 2017).

From ILIAMS, ions need to go through ESA I2-1 before entering ESA 01-1, the first filtering element following S1 and the element in which the beamlines from S1 and S2 are brought together. After passing through ESA 01-1, the ion beam is further filtered by ESA 01-2 and BM 01-1 (90° injector magnet) before its entrance into the tandem accelerator.

A fast sequential injection of various isotopes into BM 01-1 and the accelerator is made possible by swift switching (20 µs) of the voltage applied to the insulated vacuum chamber of the injector magnet. By changing the ion energy instead of the magnetic field,

which is subject to hysteresis effects, different isotopes are aligned in their magnetic rigidity and can pass through the magnet swiftly in sequence (Steier 2000).

2.3 The Tandem Accelerator and The High Energy Section

The main component of VERA's tandem electrostatic accelerator is its high voltage generator / Pelletron, which employs the same principle for high voltage generation as a Van de Graaf generator: transport and accumulation of charged particles. Instead of a moving belt, a Pelletron utilises a chain made of metal pellets linked with nylon connector to reduce terminal voltage instability and the sensitivity to spark damage, as well as to avoid the generation of belt dust from rubbing contacts (NEC 2001).

In the first stage, negatively charged ions are accelerated towards the positive high voltage terminal of the Pelletron and pass through the gas stripping tube for dissociation of molecular ions as well as removal of electrons (Steier et al 2004). The now positively charged ions are accelerated away from the terminal in the second stage.

After exiting the accelerator, the ion beam enters the high energy spectrometer consisting of a double focussing 90˚ analyser magnet with a bending radius of 1270 mm (BM 03-1) and a 90˚ electrostatic analyser with a radius of 2000 mm (ESA 04-1), providing bending power sufficient for the heaviest isotopes (Steier 2000). Stable reference isotopes are measured as currents by offset Faraday cups MFC 04-1, -2 and -3, whereas ions of interest are counted with an ionisation chamber after ESA 04-1. Components after ESA 04-1 provide possibility for further analysis if necessary (Steier et al 2004).

3. FLUORIDE AS SECONDARY ION

When the electron affinity of an element is low, it is difficult to gain a strong atomic anion beam. In this case, an application of molecular anion proves to be necessary (Middleton 1989). Since molecular anions have greater mass than the atomic ones, using molecular secondary anions means a reduction of the final kinetic energy of the elemental ion as well as a degradation of the final beam through the coulomb explosion in the stripper foil / gas (Middleton 1989). These two difficulties can be reduced by using light molecules.

The lightest possible is, logically, hydride. The multiplicity of hydrides, however, means a potential simultaneous injection of isotopes of the same element (Vockenhuber 2005). Therefore, devices are needed for separation after the accelerator. This also applies to the use of oxides because of the different isotopes of the oxygen atom (Vockenhuber 2005). In comparison, fluorides prove to be advantageous: first, there is a single stable isotope of fluorine; second, as a halogen, fluorine has a high electron affinity, which also leads to a high electron affinity of the respective molecule (Vockenhuber 2005).

An element M could take multiple fluorine atoms and form anions (MF_n^-). MF_{k+1}^- denotes fluoride anions, in which M is in its highest oxidation state. Hence, k represents the maximum formal valency of M. These anions are superhalogen anions with an electron binding energy greater than that of Cl^- and they prove to offer the most advantages for AMS: first, relatively large currents of superhalogen anions can be produced in a caesium sputter source because of their high electron binding energy; second, they offer significant isobar suppression potential since the number of fluorine atoms that the superhalogen anions of neighbouring elements contain is usually different by one (Zhao et al 2010). An extensive overview for the entire periodic table is shown in (Zhao et al 2010).

3.1 PbF_2 AS FLUORINE DONOR

PbF_2, compared with a number of other fluorides Zhao et al (2010) had used, is a particularly effective fluorinating agent for Cs^+ sputtering. This effectiveness was attributed to the crystal structure of PbF_2, which, after a phase transition at 250°C, "acts like a liquid electrolyte with fluorine atoms/ions released from their lattice bonds" (Zhao et al 2010).

Zhao et al (2010) also reported on the observation that PbF_2 became "an almost instant electric conductor upon Cs^+ sputtering". This means that metal binders for conductivity improvement can be spared for targets containing sufficient PbF_2, if time was allowed for targets to warm up.

4. IONISATION EFFICIENCY

4.1 THE IONISATION MECHANISM

The mechanism of negative ion production through sputtering, according to Middleton (1983), is similar to that of surface / thermal ionisation. The intensity of the negative ion is proportional, when neglecting statistical factors, to $\exp(E_A\text{-}W)/kT$, where W is the work function of the target surface, E_A the electron affinity, k the Boltzmann constant and T the absolute temperature of the sputter surface (Middleton 1983). The work function, per Middleton, can be reduced significantly by adding a thin layer of caesium on the sputter surface, leading to an immense improvement of negative ion intensity (1983). However, the theory of surface ionisation left questions unanswered which, per Vogel (2015), can be explained with the theory of Resonant Electron Transfer (RET).

According to Vogel (2015), surface ionisation converts merely a small fraction of sputtered atoms to anions. This is in accord with Middleton's (1999) conviction that the formation of most anions takes place in the plasma within a sputtered pit and prompted Vogel (2015) to an analysis of the interaction mechanism between "recessed Cs plasma and neutral sputter atoms". His analysis starts with a separation of sputtering from ionisation. Ionisation takes place when the sputtered neutral atom accepts an electron from a donor atom (caesium in the case of SNICS) and becomes an anion under the following conditions: first, the ionisation potential (IP) of an electron in the donor atom corresponds to the IP of an empty electron state in the acceptor; second, this IP almost equals the electron affinity (EA) of the anion, hence the term "Resonant Charge Transfer"/RET (2015).

4.2 DEFINITION OF IONISATION EFFICIENCY AND INFLUENCE FACTORS

Ionisation efficiency, according to Middleton (1989), is "the number of negative ions divided by the total number of sputtered particles expressed as a percentage". In our case, it is the number of the extracted ions of interest divided by the number of their corresponding atoms that a target contains (Vockenhuber 2005). The number of the aimed extracted anions can be obtained with an integration of the current over the whole lifetime of the target. Weighing the sample, of which the composition is known, provides the number of atoms contained in the targets.

The ionisation efficiency is an important factor in the overall detection efficiency of an AMS set-up, which also involves stripping efficiency, detector efficiency as well as transmission (Vockenhuber 2005; Child et al 2010). Therefore, an improvement of the ionisation efficiency means counting statistics improvement, which leads to potential sample size reduction (Shanks et al 2015) and thus a contribution to a sensitive detection. Especially in the case of a rare isotope or small sample, an increase of the ionisation yield is of significant importance.

Factors exerting influence on the ionisation efficiency are numerous. One of significant importance is the sample composition, which is linked with its electron affinity, chemical state of the target surface (which is prone to influence by the continued bombardment and thus implantation of caesium), crystal structures of the target which might be preferred for sputtering, chemical reactions of the sputtered surface with the unsputtered sample material, plasma ball formation as well as the distribution of the surface charge / conductivity (Child et al 2010). Other factors include temperature of the target, target mass, sample holder material, as well as sputter crater / pit, which is the exhumed profile of the target caused by caesium sputtering (Middleton 1989). The sputter crater depends on the intensity profile of the primary beam, which can be modified by a manipulation of the caesium focus. A modified recess geometry of the cathodes based on the crater provides improvement potential of the source efficiency. In the following section, two studies on the topic of recess geometry will be outlined.

4.2.1 Previous Research on Cathode Recesses

Since this thesis does not include experiments investigating recess geometries' influence on the anion formation, two studies are introduced in this section to spark ideas for further experiments. These two studies investigated the relationship between the source efficiency for C^- extraction and the cathode recess geometry as well as primary beam focus.

According to a study on ion source efficiency improvement by means of cathode modification conducted by Hlavenka et al (2016), there is a significant relationship between the target well diameter, target well depth, target holder material and the ionisation efficiency.

Their research included four experiments. First, a suite of aluminium target holders with 0.50, 0.75, 1.00, 1.25 and 1.50 mm well diameters (ø) and a standard well depth of 2.3 mm (3 cathodes for each variant) were filled with a mixture of graphite and iron powder at a 1:8 mass ratio. Targets masses varied so that a uniform depth of 1 mm from the top of the

sample well after pressing could be maintained. These targets were run for a measurement of $^{12}C^-$ beam intensity as a function of well diameter. The results showed higher ion beam currents for 0.75 and 1.00 mm diameters target wells. Second, by pressing the same amount of sample material into 1.0 mm diameter cathodes with well depths of 1.3, 2.3, 3.3, and 4.3 mm, the same test was carried out which showed a negative correlation between the well depth and the size of the initial ion beam current. Third, an ion source efficiency test for $^{12}C^-$ and $^{13}C^-$ was carried out using a set of aluminium target holders with 0.50, 0.75, 1.00 mm well ø and the standard 2.3 mm well depth, which were filled with approximately the same amount of sample material. An average efficiency of 14.9% was achieved by using target holders with a well ø of 0.75 mm. This was higher than the efficiency using target holders with a well ø of 1.00 mm (13.9%) and 0.50 mm (10.3%). Fourth, zinc inserts with 0.75 mm ø wells were brought into standard-sized aluminium cathodes (1.00 mm well ø, 2.3 mm well depth) for efficiency testing. These zinc inserts not only brought about a much higher beam intensity, but also an average ion source efficiency of 23.3%. The reason for this improvement, according to Vogel et al (2017), lies in the reduction of Cs^+ ions by aluminium ionisation, since the electron affinity of Al_2^- is greater than that of carbon (Hlavenka et al 2017).

The second study was carried out by Shanks et al (2015) at the Scottish Universities Environmental Research Centre (SUERC) which included additional source-related parameters: by casting the sputter crater profile with latex, they obtained data for a Gaussian / Super-Gaussian approximation and calculated a sample consumption of only 30% - 40% before a cathode burn-through. This provided a basis for an ion source modification including an adjustment of the cathode-ioniser distance and the caesium lens which leads to a modification of the electric field between the cathode and the ioniser and, as a consequence, an adjustment of the primary ion beam profile as well as sputter pit. However, it transpired that an increase of the sputter pit width leads not only to a sample consumption increase, but also to a reduction of the secondary ion beam current, which is due to a defocussed caesium sputtering of the cathode instead of the target. This conclusion led to their decision for a cathode modification. By pressing a powdered sacrifice material (Fe/Cu) into cathodes and drilling a hole with half the cathode's recess diameter in the sacrifice material, they prepared a target sleeve which was sputtered along with the commercial graphite target. The results show that the usage of an iron sacrifice, despite a reduction of target surface, has the potential of a source efficiency increase by a factor of up to four without a significant beam current reduction. The copper sleeve, though it also resulted in significant efficiency increase, had a poorer performance.

5. INVESTIGATION OF HAFNIUM IONISATION EFFICIENCY

According to Vockenhuber et al (2004), ^{182}Hf with a half-life of 8.9 Ma is significant in astrophysics as a chronometer for the early solar system or possible live supernova remnant on Earth. The significance of this isotope is further confirmed by Maji et al (2006), who asserted the long-lived radionuclides detection as potential evidence of million year BP incidents. The detection of minute traces in the earth's crust of the long-lived isotope ^{182}Hf, which is considered to be entirely formed by r-process during a supernova explosion, would show great significance (Maji et al 2006).

Due to the low activity of ^{182}Hf, its γ-Ray detection is unfeasible (Maji et al 2006). A direct detection using mass spectrometry would be an apt choice. An AMS measurement of ^{182}Hf, despite being the most sensitive technique so far, faces two challenges and therefore could not be conducted so far with environmental samples: first, a high mass resolution for isotope separation; second and more important, an effective ^{182}W suppression (Maji et al 2006). Further, the ionisation efficiency, a factor contributing to the overall AMS efficiency, carries significant importance.

5.1 CHOICE OF THE SECONDARY ION

Since the electron affinity of hafnium is low (normally referred to as 0 J/mol), it is difficult to gain a stable negative hafnium ion beam. For instance, Zhao et al (2010) measured a mere 0.001% of Hf^- ions among its fluorides when the pure metal as well as its oxide HfO_2 was embedded in a PbF_2 matrix and sputtered by Cs^+ ions. Thus, the application of molecular anions is inevitable.

Middleton's experiment (1989) with both hafnium hydride and oxide showed the presence of four hydrides and two oxides. The relative strengths of HfH^- : HfH_2^- : HfH_3^- : HfH_4^- were estimated to be 1 : 1 : 0.2 : 0.3. Among the oxide anions, the monoxide anion was prolific and the dioxide anion was very weak. Further, the $^{180}HfH^-$ current was much smaller (120 nA) in comparison with the $^{180}HfO^-$ current (2-4 µA). Thus, the conclusion was drawn that hafnium hydrides, due to their weakness and multiplicity, are not optimal for AMS in comparison with oxides.

Another option for secondary ions is the superhalogen anion, HfF_5^-. Using HfF_5^- for hafnium extraction offers a powerful suppression of its stable isobar ^{182}W. It was revealed that hafnium, if its pure metal as well as its oxide HfO_2 was embedded in a PbF_2 matrix and

sputtered by Cs^+ ions, took five fluorine atoms and formed 100% HfF_5^- (Zhao et al 2010). Under the same condition (though only pure metal of tungsten was used), the chances were much lower for tungsten to form the corresponding anion WF_5^-: tungsten formed around 30% of WF_5^- (Zhao et al 2010).

A study conducted at VERA showed that sputtering commercial hafnium hydride (HfH_2) and commercial hafnium fluoride (HfF_4) in a silver matrix yielded mostly HfH_3^- and HfF_5^- with a typical $^{180}Hf^{4+}$ current of 0.35 and 80 nA (Vockenhuber et al 2004) (table 5.1.1).

The relative strengths measured by Vockenhuber et al (2004) do not accord with the estimation by Middleton (1989). Based on the $^{180}Hf^{4+}$ current of 0.06 nA from HfH^- measured by Vockenhuber et al and the hydride transmission of 3%, a typical $^{180}HfH^-$ current of 2 nA can be calculated. This is only 1/60 of what Middleton measured with hafnium hydride (assumed to be HfH_2 by Middleton) without matrix material.

Further, Vockenhuber et al's experiment also revealed that HfF_5^- offers a powerful tungsten suppression and a low detection limit (table 5.1.1).

Different negative ions investigated for their ^{182}W suppression

Ion species	Sample material	Typical $^{180}Hf^{4+}$ current (nA)[a]	Typical ^{182}W count rate (s^{-1})	^{182}W suppression[b]	$^{182}Hf/^{180}Hf$ detection limit
Hf^-	HfH_2 + Ag, 1:1	0.004	141	~0.02	$\sim 10^{-4}$
HfH^-	HfH_2 + Ag, 1:1	0.06	454	0.1	3×10^{-5}
HfH_2^-	HfH_2 + Ag, 1:1	0.33	76	3	8×10^{-7}
HfH_3^-	HfH_2 + Ag, 1:1	0.35	55	4	5×10^{-7}
HfH_4^-	HfH_2 + Ag, 1:1	0.07	11	4	5×10^{-7}
HfH_5^-	HfH_2 + Ag, 1:1	0.31	2	100	2×10^{-8}
Hf^-	HfF_4 + Ag, 1:1	0.02	1800	0.0002	3×10^{-4}
HfF_2^-	HfF_4 + Ag, 1:1	0.3	1	5	1×10^{-8}
HfF_3^-	HfF_4 + Ag, 1:1	35	2	250	2×10^{-10}
HfF_5^-	HfF_4 + Ag, 1:1	80	0.2	6000	1×10^{-11}

[a] The transmission ($^{180}Hf^{4+}/^{180}HfH_x^-$) for the hydrides was around 3% because Ar was used as stripper gas, whereas for the fluorides a transmission of 6% was achieved with O_2 as stripper gas. The fluorides were measured with the ion source optimized for high output.
[b] The ^{182}W suppression is the relative formation probability of the various negative Hf ions (measured as $^{180}Hf^{4+}$ current) divided by the relative formation probability of the various negative W ions (measured as ^{182}W count rate in the detector).

Table 5.1.1 Negative molecular hafnium ions studied for their tungsten suppression (Vockenhuber et al 2004)

Vockenhuber (2005) further investigated HfF_5^- extraction efficiency using a HfF_4 target of 1.63 mg. According to him, it took three hours for the target, which generated an initial current of roughly 1750 nA, to be exhausted (after 3 hours of sputtering, only a few nA could be extracted from the target), resulting in an ionisation efficiency of 1% $^{180}HfF_5^-$.

A later study carried out by Fostner et al (2011) at VERA showed that, with a careful tuning of the S1, in which a maximum source output was not the aim, a much higher tungsten suppression was achieved with HfF_5^- extraction using the same sample matrix (table 5.1.2

left). Further, it was shown that embedding hafnium in a lead difluoride matrix with excessive fluorine provides perspective for HfF_5^- current improvement at the sacrifice of a high tungsten suppression (table 5.1.2 right).

Yield of the hafnium and tungsten atomic and fluoride anions collected as $^{180}Hf^{4+}$ current after the analyzing magnet and $^{183}W^{4+}$ count rate in the detector. In the case of HfF_6^- the current was too low and the count rate in the detector is given. The target material was HfF_4 mixed with silver powder with a ratio of 1:1.

Ion species	Typical $^{180}Hf^{4+}$ current [nA]	Ion species	Typical $^{183}W^{4+}$ count rate [1/s]	^{182}W suppression
Hf^-	0.001	W^-	2500	0.00024
HfF^-	0.092	WF^-	2000	0.027
HfF_2^-	1.26	WF_2^-	150	5
HfF_3^-	7.8	WF_3^-	6	770
HfF_4^-	0.037	WF_4^-	1	22
HfF_5^-	11	WF_5^-	0.18	36000
HfF_6^-	1000 cts/s	WF_6^-	0.01	0.12

Yield of the hafnium and tungsten atomic and fluoride anions collected as $^{180}Hf^{4+}$ or $^{183}W^{4+}$ ions after the analyzing magnet. In the case of Hf^- the current was too low and the count rate in the detector is given. The sample material was a mixture of Hf + W + PbF_2 powders with a ratio of 1:1:4.

Ion species	Typical $^{180}Hf^{4+}$ current [nA]	Ion species	Typical $^{183}W^{4+}$ current [nA]	^{182}W suppression
Hf^-	10^5 cts/s	W^-	0.025	0.008
HfF^-	0.02	WF^-	0.9	0.2
HfF_2^-	0.049	WF_2^-	0.22	0.2
HfF_3^-	0.64	WF_3^-	0.095	6.7
HfF_4^-	0.017	WF_4^-	1.1	0.015
HfF_5^-	190	WF_5^-	4.9	39
HfF_6^-	0.036	WF_6^-	0.055	0.7

Table 5.1.2 Negative molecular hafnium ions studied for their tungsten suppression (Forstner et al 2011)

In the sections to follow, two undertakings investigating the generation of a stable HfF_5^- beam and the ionisation efficiency are outlined.

5.2 EXPERIMENT 1

The first experiment aimed at an investigation of the relationship between the extraction efficiency of HfF_5^- and the sample matrix composition.

5.2.1 Methods

5.2.1.1 Sample Preparation

To achieve the above-mentioned aim, four sample materials with different proportions of hafnium tetrafluoride, lead difluoride and silver were prepared. Here, lead difluoride fulfils the function of fluorine donor and silver powder contributes to an increase of the sample's electric and thermal conductivity. The intended HfF_4:PbF_2:Ag mass ratios were 1:3:1, 1:1:1, 1:0:1 and 1:0:3, which corresponded to a Hf: F:Ag atom ratio of roughly 1:10:2, 1:6:2, 1:4:2 and 1:4:7.

The preparation procedures are as follows: first, an empty polypropylene tube (Eppendorf 3810X) was weighed; second, 99.9% pure HfF_4[2] powder with a formula mass of 254.48 (Alfa Aesar 45061) was brought into and weighed with the tube; third, 99+% pure lead fluoride powder (Aldrich 236152) with a formula mass of 245.20 as well as 99.9% pure

[2] Contained hafnium is in the natural abundance

silver powder (Alfa Aesar 00781) was added and weighed; at last, the mixture was ground and further mixed in a mortar to achieve greater homogeneity.

After the preparation, sample materials were pressed into copper target holders with 1 mm diameter recesses. The mass of the sample contained in each target holder was obtained by weighing the target holder before and after the pressing. For each sample material, three targets with the mass ratio 1:1:2 were intended. This mass ratio should correspond to a HfF_4 mass of 2 mg, 2 mg and 4 mg respectively, which functions as an indicator of the time needed for full sputtering (section 4.1) (Vockenhuber 2005).

Due to the fact that the material contained in a target holder could only be weighed after the sample material is pressed, and it was not possible to add material after pressing, the experiment design could not be realised exactly in practice. An overview of the sample materials' details is provided in table 5.2.1.

5.2.1.2 Measurement Principle

After the sample material and cathode preparation, these twelve cathodes were loaded, together with cathodes prepared for tuning, into the target wheel, which was then mounted in S1 of the VERA facility.

Before sputtering these cathodes with Cs^+ ions and starting the current test, parameters of VERA had to be adapted for hafnium measurement. This was achieved by loading a setup from previous measurements and subsequent parameter optimisation of the steering as well as the filtering elements with a cathode containing HfF_4, PbF_2 and Ag to a mass ratio of roughly 1:3:1.

All components from the ion source 1 to the Faraday cup directly following the accelerator (FC03-1) were included in the tuning process: the low energy section underwent automatic optimisation using the programme automax (Steier 2000) with the slits following BM01-1 set to 1 mm width; the terminal voltage (TPS TK-1 GvmVC) was also scanned to maximise the $^{180}Hf^{4+}$ current collected in the Faraday cup FC04-1 after the first magnet filter in the high energy section. Figure 5.2.1 shows a scan of the magnet chamber voltage (termed Multi Beam Switcher, MBS) for various HfF_5^- isotope currents collected in the Faraday cup after the injector magnet (FC02-1). It can be confirmed that the measured intensities are in agreement with the natural isotopic abundance.

During the measurement, only the section from the ion source to FC02-1, including the first filtering component ESA 01-1 and BM 01-1, was in operation. The width of the slit in front of FC02-1 was set to 1.5 mm to prevent beam loss. With all the relevant parameters

optimised and set for $^{180}HfF_5^-$ collection, a current test with FC02-1 was programmed for every two seconds, the results of which were documented, along with the MBS voltage and source parameters including cathode position, cathode current, HVS current (see figure 2.3) and ioniser power.

Any cathode change needed to be carried out manually, which means single cathodes were measured in a continuous manner. Further, a two-dimensional manual cathode position optimisation (cathode – ioniser distance not included) as well as a resulting parametric adaptation of the magnet chamber voltage proved to be necessary for sputtering of the sample residual in the target holders so that a thorough sputtering could be attained. Measurement termination of single cathodes was based on the current improvement potential that a position and a MBS scan offered: if the optimised current was less than 10% of the initial, the current measurement was stopped.

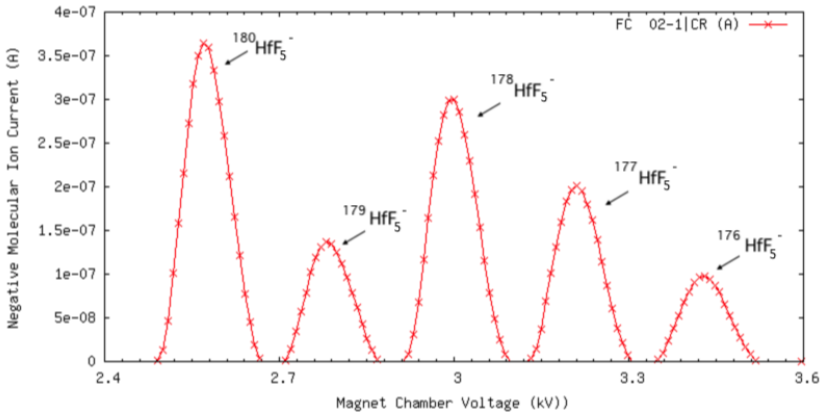

Figure 5.2.1 Scan of the Magnet Chamber Voltage against HfF_5^- negative ion current collected in FC 02-1 with 1mm slit opening. The isotopic intensities agree with the natural isotopic abundance.

5.2.2 Results and Discussion

As mentioned above, cathodes were sputtered in a continuous manner in this measurement. There were, however, two cathodes of which the measurement took a halt and continued at a later point without the cathodes being sputtered meanwhile (see table 5.2.1).

5.2.2.1 Current Development

The temporal development of the current extracted from all cathodes is shown in figure 5.2.2. The mass ratio of target components and the target mass can be read in the title and plot legend. A comparison of the left two with the right two figures shows that the matrix material,

lead difluoride, is crucial for the production of a relatively large and stable current in the first hour. In addition, a comparison of the top left and lower left figures led to the conclusion of a positive correlation between the proportion of lead difluoride and the intenisty of the initial current. With an absence of lead difluoride (upper left and upper right), the proportion of silver powder did not have a significant influence on the current intensity. Further, there is no obvious correlation between the average current intensity and the target mass.

The initial current extracted from targets with a HfF_4:PbF_2:Ag mass ratios of 1.0 : 3.3 : 1.1 was around 1 µA, comparable with the initial current of 1750 nA reported by Vockenuber (2005). However, partly thanks to the position as well as MBS optimisation during the measurement, this current lasted longer than the 3 hours in Vockenhuber's account, although the amount of HfF_4 was roughly in accord.

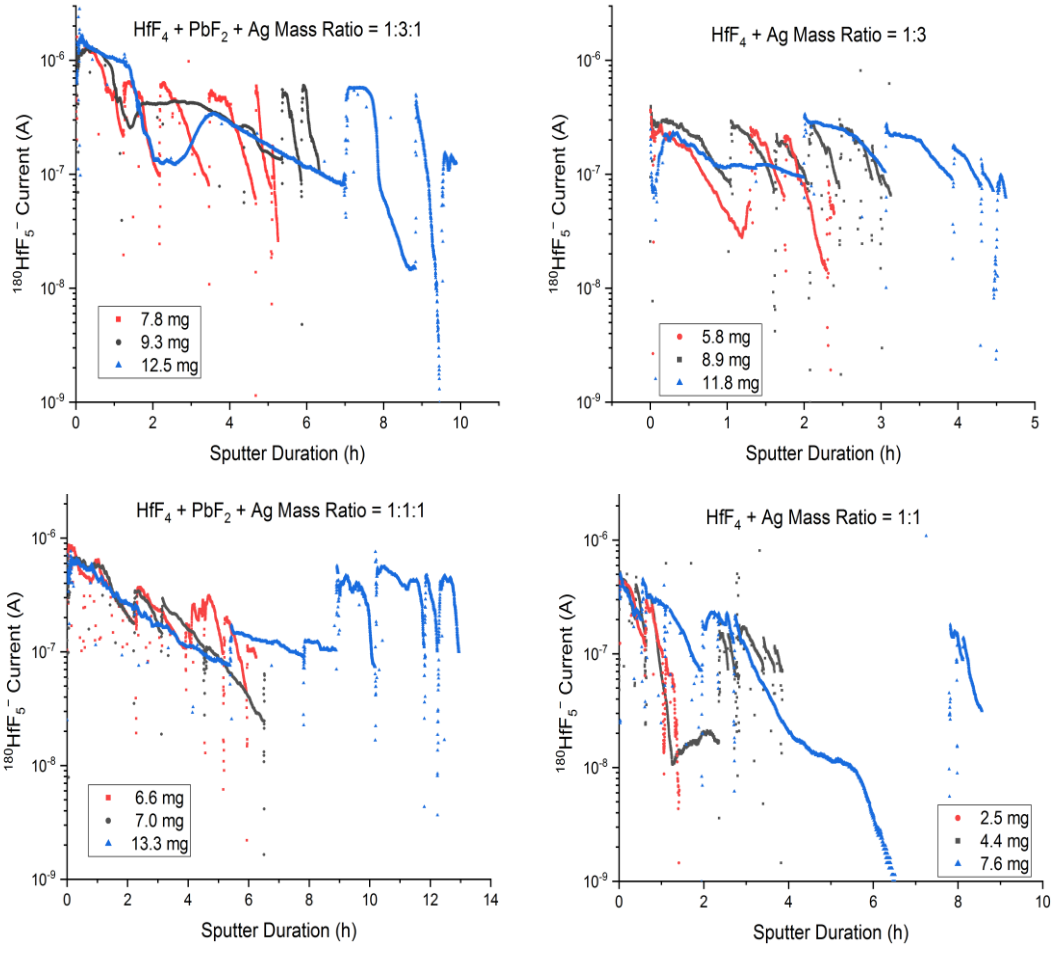

Figure 5.2.2 Temporal development of $^{180}HfF_5^-$ current collected in FC 02-1 (Legend label: target mass). Curve discontinuities were due to position as well as MBS optimisation. Observations: positive correlation between the PbF_2 proportion and the $^{180}HfF_5^-$ ion intensity and positive correlation between the target size and its life time.

5.2.2.2 Ionisation Efficiency

During the short time span (1-7 seconds) between two consecutive current measurements, the current was taken as stable. Hence, an integration of the current over time provides the number of the $^{180}HfF_5^-$ ions which were sputtered.
The results of the ionisation efficiency calculation are shown in table 5.2.1 and figure 5.2.3.

As was mentioned in section 5.2.1.2, the ioniser power during the measurement, which was subject to the source current regulation (HVS CR and CAT CR), was also documented. Since the regulation was on, the ioniser power was monitored and modified constantly. Since the ioniser power has a significant effect on the temperature in the source, which potentially affects the ionisation yield, it might offer some insight to average the ioniser power during the measurement of single cathode. The results as well as the standard deviation are shown in table 5.2.1.

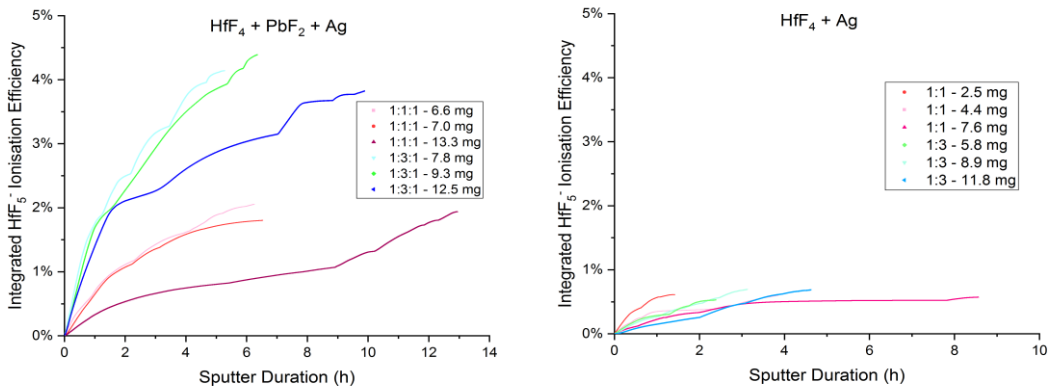

Figure 5.2.3 Temporal development of the integrated ionisation efficiency. Embedding HfF_4 in a PbF_2 matrix brought about an efficiency improvement up to a factor of 3.9. The greater the proportion of PbF_2, the better the ionisation efficiency. The proportion of Ag did not have a significant impact on the ionisation efficiency. Targets with the same material composition but different masses brought similar ionisation efficiencies.

As can be seen, cathodes containing different mass of the same sample matrix brought similar ionisation efficiencies (within 15.

As a fluorine donator, PbF_2 proved to be crucial for the ion formation. As far as can be observed, the more PbF_2 there was, the higher the ionisation yield. In contrast, an increase of the proportion of silver powder at the absence of PbF_2 did not result in an increase of the ionisation efficiency. Thus, it can be assumed that a Ag : HfF_4 mass proportion of roughly 1:1 would suffice for a satisfactory yield.

Since cathodes were sputtered in a continuous instead of a consecutive manner in this experiment, a second experiment was conducted investigating the influence of cathode change on the ionisation efficiency.

HfF_4 : PbF_2 : Ag Mass Ratio	Target Mass (mg)	HfF_4 Mass (mg)	Ioniser Power ± SD (W)	Sputter Duration (h)		Ionisation Yield (%)	
1.0 : 0.9 : 1.0	6.62	2.27	not logged	1.72	6.25	1.02	2.06
			224 ± 2	4.53		1.04	
	7.02	2.41	224 ± 3	6.53		1.80	
	13.34	4.58	218 ± 12	1.80	12.94	0.50	1.94
			218 ± 12	11.14		1.44	
1.0 : 3.3 : 1.1	7.83	1.47	212 ± 25	5.28		4.15	
	9.30	1.74	216 ± 21	6.35		4.40	
	12.49	2.34	216 ± 19	9.89		3.83	
1.0 : 0.0 : 1.1	2.54	1.24	197 ± 22	1.42		0.61	
	4.38	2.14	156 ± 3	3.86		0.60	
	7.59	3.71	153 ± 8	8.56		0.57	
1.0 : 0.0 : 3.1	5.84	1.42	166 ± 8	2.39		0.53	
	8.87	2.16	162 ± 2	3.13		0.70	
	11.79	2.87	177 ± 3	4.62		0.69	

Table 5.2.1 Targets specifications, measurement parameters and ionisation efficiencies in the first hafnium experiment

5.3 EXPERIMENT 2

The second experiment aimed at an examination of the relationship between the manner of sputtering and the ionisation yield. To achieve this, four cathodes containing roughly the same amount of sample were divided into two identical groups: group 1 underwent uninterrupted sputtering, whereas group 2 were sputtered consecutively, leaving one cathode time to cool down while sputtering the other.

5.3.1 Methods

The residual sample material with a PbF_2 : Ag : HfF_4 mass ratio of 3.3 : 1.1 : 1.0 from experiment 1 was utilised in this experiment, since it yielded the highest ionisation efficiency among the four sample matrices.

Since the ionisation efficiency may be, as was detailed in 4.1, source-dependent, the experiment had to be conducted with S1 to achieve results that are comparable with those from experiment 1.

Following the same procedure as described in 5.2.1.1, four targets containing roughly the same amount of sample material were produced, forming group 1 and 2 (detailed in table 5.3.1).

In contrast to the first experiment, this measurement was automated: current extracted from cathodes in group 1 was measured every 10 seconds, whereby a current optimisation was achieved by implementing a scan of the MBS voltage every 600 seconds (10 min) so that small changes in ion beam emission with deepening sputter craters during sputtering were accounted for; the same procedures applied to cathodes in group 2 except for a cathode switch every 10 min. Only the measurement termination based on judgement of the current development needed to be performed manually.

5.3.2 Data Feasibility

During this experiment, a spark in the accelerator led to an insertion of FC S1-1 before the injector magnet. From 18:45:41 to 18:50:59, the target was sputtered but no valid data for current measurement was recorded. A data modification was performed: the invalid data were replaced with an average of the 5 data points before and after the incident.

5.3.3 Results and Discussion

5.3.3.1 Current Development

The temporal development of the extracted current (after modification detailed in 5.3.2) is shown in figure 5.3.1. It is obvious that group 1 (continuous sputtering) showed a pattern different from group 2 (consecutive sputtering). In contrast to cathodes in group 1, which produced a current which decreased steadily, cathodes in group 2, although following the pattern of group 1 overall, produced a much higher current immediately after the cathode change, which dropped to roughly 50% in around 2 minutes. The typical current immediately after cathode switch in group 2 was higher than the typical current extracted from cathodes in group 1.

5.3.3.2 Ionisation Efficiency

The evaluation of the ionisation efficiency followed the same procedures detailed in 5.2.2.2. Results are shown in figure 5.3.2 and in table 5.3.1.

All in all, cathodes which underwent continuous sputtering delivered an ionisation yield around 15% higher than those which underwent consecutive sputtering, which indicates that a high temperature in the source and maintaining the sputtering equilibrium should facilitate the fluoride anion formation. However, since a conventional hafnium measurement calls for consecutive cathode change, measures other than the manner of sputtering should be taken into consideration for yield improvement.

The results of this experiment deviated from that of the first experiment by roughly 20%, hence the results of the first experiment can be taken as reproducible. However, since the source parameters in the first experiment were different from those of the second and the caesium vapour control as well as the ioniser power were subject to regulation mechanisms, further experiments would be needed for a better understanding.

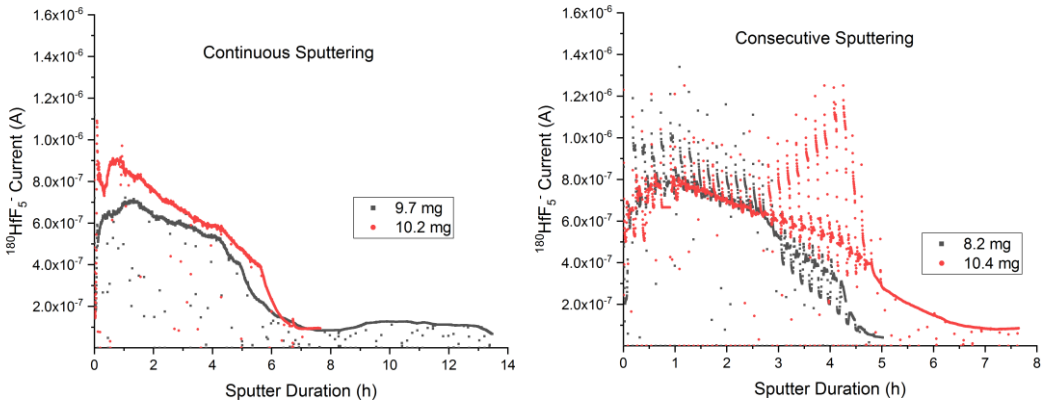

Figure 5.3.1 Temporal development of $^{180}HfF_5^-$ current (left: group 1, right: group 2) (legend entry denotes target masses). Currents produced by targets in group 1 decreased steadily. Cathodes in group 2 produced high currents immediately after cathode changes, which deceased to about 50% in 2 minutes.

HfF_4 : PbF_2 : Ag Mass Ratio	Manner of Sputtering	Sample Mass (mg)	HfF_4 Mass (mg)	Ioniser Power ± SD (W)	Sputter Duration (h)	Ionisation Efficiency
1.0 : 3.3 : 1.1	Consecutive	8.24	1.54	174 ± 15	5.02	4.66%
		10.35	1.94	182 ± 17	7.65	4.97%
	Continuous	9.68	1.81	194 ± 9	13.47	5.86%
		10.23	1.92	180 ± 16	7.65	5.69%

Table 5.3.1 Targets specification and results of ionisation efficiency measurement

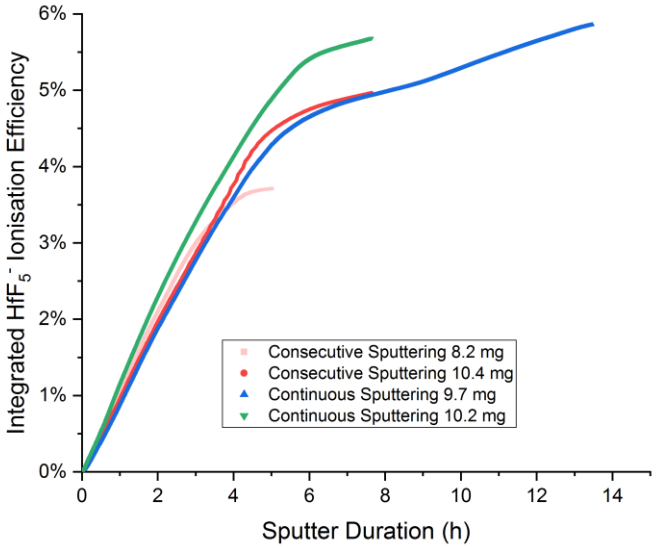

Figure 5.3.2 Temporal development of the integrated HfF_5^- ionisation efficiency. Overall, targets that underwent continuous sputtering yielded ionisation efficiencies about 15% higher than those underwent consecutive sputtering.

5.4 Conclusion and Outlook for Future Hafnium Experiments

The two experiments for HfF_5^- extraction showed the importance of lead difluoride not only for a high current output, but also in ionisation yield improvement. Further, it was shown that the temperature /sputter equilibrium also has an impact: frequent cathode switch during an experiment provides a larger initial current at the sacrifice of the overall yield.

Figure 5.4.1 Sputtered copper cathodes

In addition, a preliminary investigation of the sputter pit was started: two copper cathodes (target holder and metal pin) with an even surface were put in a target wheel for sputtering to gain a profile of the sputter pit. The results are shown in figure 5.4.1. Similar measures as those taken by Shanks et al (2015) (section 4.2.1) could be used to investigate the hafnium ionisation yield. It might be interesting to not only compare different sacrifice material, but also to press the sacrifice material based on the sputter pit for a comparison with the sacrifice sleeve used by Shanks et al.

Further, it might be interesting to see if pre-pitting targets would have influence on the size of the HfF_5^- current as well as its ionisation yield (see section 7.4).

6. INVESTIGATION OF CAESIUM IONISATION EFFICIENCY

Radioactive isotopes of the element caesium, ^{134}Cs, ^{135}Cs and especially ^{137}Cs, are direct as well as indirect nuclear fission products of elements such as plutonium, thorium and uranium (IAEA, "Fission Product Yields"). With uranium being a basic fuel in most current reactors and ^{137}Cs being one of its favoured fission products (average fission yield of ^{137}Cs for uranium: 6.4% (IAEA, "Fission Product Yields")), ^{137}Cs shows a high abundance in spent nuclear fuel. Therefore, ^{137}Cs, with its medium half-life of 30.2 years, and given its high water solubility as well as high-energy beta-decay (0.5 MeV), poses a serious danger to the environment as well as human health in case of nuclear contamination (Wessells 2012). On the other hand, its ratio to its long-lived isotope ^{135}Cs ($T_{1/2}$ > 1.3 Myr[3]) holds significance in its function as a tracer for radiocaesium releasing sources and seawater circulation (Zheng et al 2014), as well as in sediment dating (Taylor et al. 2015; Yang et al 2016).

Isotope detection of caesium as well as the investigation of the ^{135}Cs/^{137}Cs ratio have been carried out using Thermal Ionisation Mass Spectrometry (TIMS), e.g. Lee et al. 1993, Inductively Coupled Plasma-Mass Spectrometry (ICP-MS), e.g. Yang et al. 2016, and Accelerator Mass Spectrometry (AMS), e.g. Eliades et al. 2013. According to Zhao et al. (2016), one of the main limiting factors of an AMS-based ^{135}Cs measurement is the production of a "steady, large (> 100 nA) and lasting (>0.5 h)" negative ion current containing caesium from "samples containing mg quantities of Cs".

6.1 CHOICE OF THE SECONDARY ION

Caesium, similar to hafnium, does not readily form stable negative atomic ions due to its relatively low electron affinity, which amounts to 0.47 eV (Anderson et al. 1999). An application of the negative molecular ions, thus, might appear necessary. The common AMS ion sources use Cs^+ as the primary sputtering ion. If one wants to investigate the Cs content of a sample, the sputtering agent has to be changed. Rubidium is an alternative that was also used in this work. In the following, an overview of the reported performance of Cs anions and molecular ions is given:

Middleton (1989) observed a Cs^- current of nearly 2 µA after 1 hour of sputtering targets with Cs for the extraction of polyatomic negative ions of aluminium. In this case, the growth of this $^{133}Cs^-$ as well as $^{27}Al^-$ ion beam was characterised by a pale blue plasma ball

[3] The value is debated. MacDonald et al (2016) determined the half-life to be (1.6 ± 0.6) Myr with AMS and (1.3 ± 0.2) Myr with ICPMS, which deviate from the quoted value of 2.3 Myr by ~40%.

in the sputter pit. This puzzle found an explanation in Vogel's application of the Resonant Electron Transfer (RET) theory (see section 3.1): the IP of Cs^0 (0.66) is close to the EA of Al (0.441 eV) and Cs (0.472 eV), which not only enables a direct RET between Al^- and Cs, but also initiates a competition of the two elements on the Cs (7d) and, more importantly, on each other (Vogel 2015). He later referred to this process as Competitive Ionisation (Vogel 2017).

Further, Middleton (1989) observed strong peaks of carbon polymers of caesium when sputtering graphite targets with Cs. Among them, CsC_6^- produced the highest peak of 1.18 µA. This observation could be taken to suggest an adoption of CsC_6^- as the secondary ion (see section 6.4), despite problems resulting from the existence of two stable carbon isotopes.

Currently, either the atomic negative ion Cs^- or the superhalogen difluoride CsF_2^-[4] are applied (Lachner et al. 2015; Yin et al. 2015; Zhao et al. 2017).

At VERA, several tests on negative ion formation of caesium were conducted (Kasberger 2015; Lachner et al 2015): by sputtering a Cs_2SO_4 and Cu 1:1 volume mixture with rubidium, a typical $^{133}Cs^-$ current of 10 nA was obtained with a sputter duration of roughly 15 min; the same test with pure Cs_2SO_4 delivered a Cs^- current up to 60 nA and that with a Cs_2SO_4, $BaSO_4$ and PbF_2 mixture (Cs : Ba : F atom ratio = 1:1:8) a CsF_2^- current around 14 nA. Further, CsF_2^- showed greater potential for isobar suppression of Ba than the atomic ion Cs^- (see section 3).

At the China Institute of Atomic Energy (CIAE), samples including CsF and Ag, $CsNO_3$ and Ag as well as AgI and Ag[5] mixture in various mass ratios were sputtered with caesium for anion extraction (Yin et al 2015). The results showed that CsF_2^- (typically around 2.8 nA) and Cs^- (highest peak: roughly 6 nA from $CsNO_3$ in Ag matrix) are the two main components of the negative ion beam. Although the extracted currents were much smaller than that achieved at VERA, this experimental finding points out that the application of the Cs^- ion can produce a higher current than that of CsF_2^-.

At the AEL-AMS laboratory, a novel approach of recycled sputtering without primary ion supply was adopted by Zhao et al (2016) for CsF_2^- extraction. It yielded a large but unstable and short-lived CsF_2^- current averaging 400 nA. This was achieved by an insertion of PbF_2 targets before inserting measurement targets consisting of CsF and PbF_2.

[4] It was reported by Zhao et al (2010) that CsF_2^- was the fluoride anion produced in the largest amount (100%), when sputtering a mixture of the pure Cs metal and PbF_2 with Cs+ ions.
[5] Since caesium was used here as the primary ion, primary ion extraction needed to be determined.

Due to the very low transmission of Cs^- through the RFQ as well as the isobar suppression potential that the superhalogen offers, CsF_2^- is currently applied for caesium measurement at VERA. Since CsF_2^- was reported to either offer a lower beam intensity (Kasberger 2015; Lachner et al 2015; Yin et al 2015), or a higher intensity but lower stability than Cs^- (Zhao et al 2016), an achievement of a CsF_2^-beam with high intensity and stability, as well as a high ionisation efficiency, would be of benefit. Since sample composition could easily be adapted, it was taken as the first experiment variable for the achievement of the above-mentioned aim. Therefore, cathodes with different mixtures of CsX, fluorine donors and conducting materials were studied.

6.2 EXPERIMENT

In this experiment, PbF_2 (see section 3.1) was compared with LaF_3 in the effectiveness as a fluorine donor. Further, two proportions of the fluorine donor were compared in their influence on the anion beam intensity as well as ionisation efficiency.

6.2.1 Methods

Samples with different proportions of caesium sulphate, a fluorine donor and copper[6], were prepared to fulfil a Cs:F:Cu atom ratio of 1:7:3 and 1:3:3, respectively. Caesium sulphate instead of caesium fluoride was utilised since the highly hygroscopic nature of caesium fluoride renders its application inconvenient.

6.2.1.1 Sample Preparation

The same preparation procedures detailed in section 5.2.1.1 applied. Materials used were: $^{133}Cs_2SO_4$ powder with a purity of 99.997% (Alfa Aesar 11112), 99% pure lanthanum fluoride powder (Alfa Aesar A16673) with a formula mass of 195.90, 99+% pure lead fluoride powder (Aldrich 236152) with a formula mass of 245.20, 99.9% pure copper powder (Alfa Aesar 42623).

Standard copper target holders with 1 mm diameter sample wells were used in this experiment. For each sample material, three targets with the mass ratio 1:1:2 were intended, corresponding to a Cs_2SO_4 mass of 2 mg, 2 mg and 4 mg. However, as in the case of hafnium

[6] Copper was used to increase the electric and thermal conductivity of the sample material.

(section 5.2.2.1), the intended proportion could only be roughly achieved. An overview of the sample materials and the targets is provided in table 6.3.1.

6.2.1.2 Measurement Principle

To avoid potential interference from the primary ion, the targets were sputtered by rubidium instead of caesium. Since ion source 2 of the VERA facility was mounted with a rubidium reservoir at the time of the experiment and the ILIAMS following S2 offers potential elimination of interfering isobars, the experiment was carried out at S2 and the caesium difluoride anions were collected with the faraday cup FC02-1 after the injector magnet to the accelerator.

With I^- (127 amu) extracted from a AgI target, the current generating the magnetic field of BMI1-1 was scaled for CsF_2^-, which, however, needed subsequent optimisation due to magnetic hysteresis.

Although only the section of the accelerator from S2 to FC02-1 was deployed within the framework of this study, it proved to be necessary to utilise mass filters in the high-energy section to make sure that it was the target isotope that was measured. It transpired that LaO_2^-, with the same mass number as CsF_2^-, was the major interference anion from the ion source. This means that the ILIAMS needed to be in operation for the elimination of LaO_2^-. The CsF_2^- current extracted from targets without LaF_3, however, was also reduced in intensity by the transmission through the RFQ (see section 6.3.2).

With a few unexhausted cathodes from previous measurements which contained either the same material as the measurement cathodes or CsF with a fluorine donor, all the parameters from S2 to FC02-1 were optimised either using automax or by scanning and setting the optimum value.

After the assignment of the optimised parameter to the respective element, an automated measurement was started. Taking the potential influence of the cathode's temperature into account, which is partly determined by the sputtering duration, the measurement was arranged in cycles. Each target was sputtered for 2000 seconds (33 minutes and 20 seconds) in a cycle, from which 100 data points should be recorded[7]. This means that 1 data point corresponded to a measurement duration of 20 seconds. Within these 20 seconds, the current was taken as stable. However, the amount of measurement cycles was not determined and a manual termination of the measurement was required.

[7] It turned out to be 101 data points in practice.

Since S2 only offers manual cathode position adjustment, a position scan and optimisation to improve the sample consumption efficiency could not be attained.

The measurement was stopped when the extracted current was less than 10% of the typical value during the first 3 hours.

6.2.3 Results

6.2.3.1 Data Feasibility

A verification of the feasibility of the collected data for further evaluation was carried out prior to the analysis. First, not all 101 data points were evaluated, since the final current measurement was carried out directly before the cathodes were switched and thus does not correspond to another period of 20s of sputtering. Therefore, final data points of all the cycles were excluded from the analysis.

Further, potential influences of an unforeseen outage of the laser (RFQ was still running) should be accounted for: during this period, the CsF_2^- beam intensity was reduced by the RFQ and the interfering anion LaO_2^- was not eliminated (see section 2.2, 6.2.1.2). This took place during the 5^{th} cycle (sputter duration: 2.2 – 2.8 h).

Figure 6.2.3.2 shows the development of the current extracted from all targets in FC02-1 over time. Due to the contribution of LaO_2^-, samples with LaF_3 produced an irregularly high current during the laser outage. Therefore, data collected for samples with LaF_3 during this time were not included for analysis.

6.2.3.2 Ion Transmission

The CsF_2^- ion transmission through the RFQ was calculated based on measurements of currents extracted from 9 cathodes containing PbF_2 in the faraday cup FCI1-1 after BMI1-1 (I_1) and FC02-1 after BM01-1 (I_2).

Since ion transmission changes with time, its measurement was carried out three times. However, not all 9 cathodes were included in each measurement. The first transmission measurement provided only one data point combinable with data from later measurements.

The ion transmission I_2/ I_1 are shown in Figure 6.2.3.1, in which 0:00 of the first measurement day was taken as the zero point on the time axis.

Figure 6.2.3.1 contains either simple connection of two measurement points of a cathode or plotted linear regression of several measurement points of the same cathode, if it was measured twice on the same day (therefore the unconnected points).

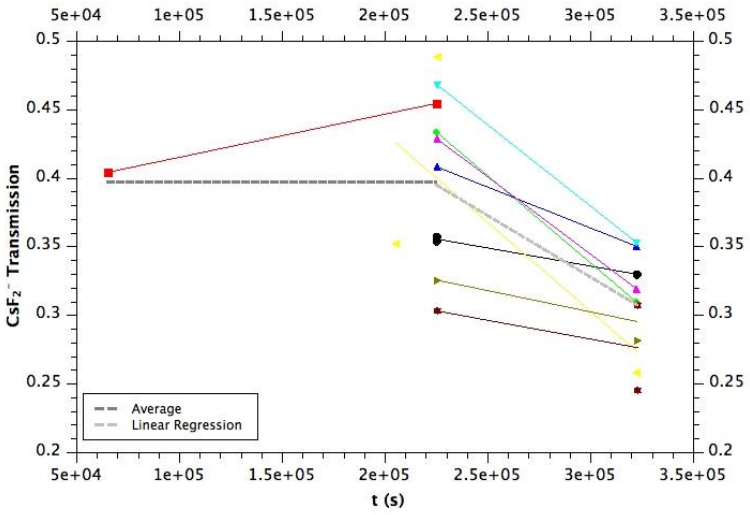

Figure 6.2.3.1 Measurement of CsF_2^- ion transmission through RFQ. Currents extracted from 9 cathodes containing Cs_2SO_4, PbF_2 and Cu were measured in FCI1-1 (I_1) and FC02-1 (I_2). Y axis: ion transmission I_2/ I_1. X axis: time (0:00 of the first day of measurement was defined as the 0 point on this axis)

The CsF_2^- currents in FC02-1 recorded in the first 4 cycles[8] were modified using the average transmission (0.398 ± 0.062) in the time span, which is represented by the dashed dark grey line in Figure 6.2.3.1. CsF_2^- currents in FC02-1 recorded after the first 4 cycles were modified using the linear regression of the measured transmission from the second and the third measurement, which is represented by the dashed light grey line in Figure 6.2.3.1. The function used for interpolation was CsF_2^- transmission = A t + B with A = $-8.97*10^{-7} \pm 2.3*10^{-7}$ and B = 0.597 ± 0.063

6.2.3.3 Current Development

As can be read in figure 6.2.3.2, CsF_2^- currents generally larger than 20 nA could be collected in FC 02-1 from the PbF_2 matrices for the first 2.2 hours (first 4 cycles). In most cases, these current dropped to half of their peak values after 2 - 3 hours of sputtering. Hence, the first 2.2 hours of the sputter duration warrant a closer look.

[8] From the begin of the experiment to the time of the second transmission measurement

a. PbF_2 Matrices

As can be read in figure 6.2.3.3, it generally took 10 min for the CsF_2^- current in FC02-1 extracted from PbF_2 matrices to develop to a typical value of 40-100 nA (transmission corrected; ± 16%), which was not the case with hafnium fluoride in PbF_2 matrix (see section 5.2.2.1). A possible explanation would be that it took time to free caesium atoms from the Cs_2SO_4 crystals for a recombination with fluorine to form CsF_2^-.

The current cliffs at cathode changes suggest that a discontinuation of the sputtering equilibrium generally had a negative influence on the current especially for smaller targets (less than 15 mg).

In general, there was a positive correlation between the target mass and current intensity. However, there was no obvious correlation between the PbF_2 proportion and current intensity. It seemed that a mass ration of $CsSO_4$ and PbF_2 of 1:2 (Cs:F atom ratio around 1:3) would suffice for a relatively stable CsF_2^- current of 40 - 100 nA. Further fluorine atom excess did not provide any current intensity improvement.

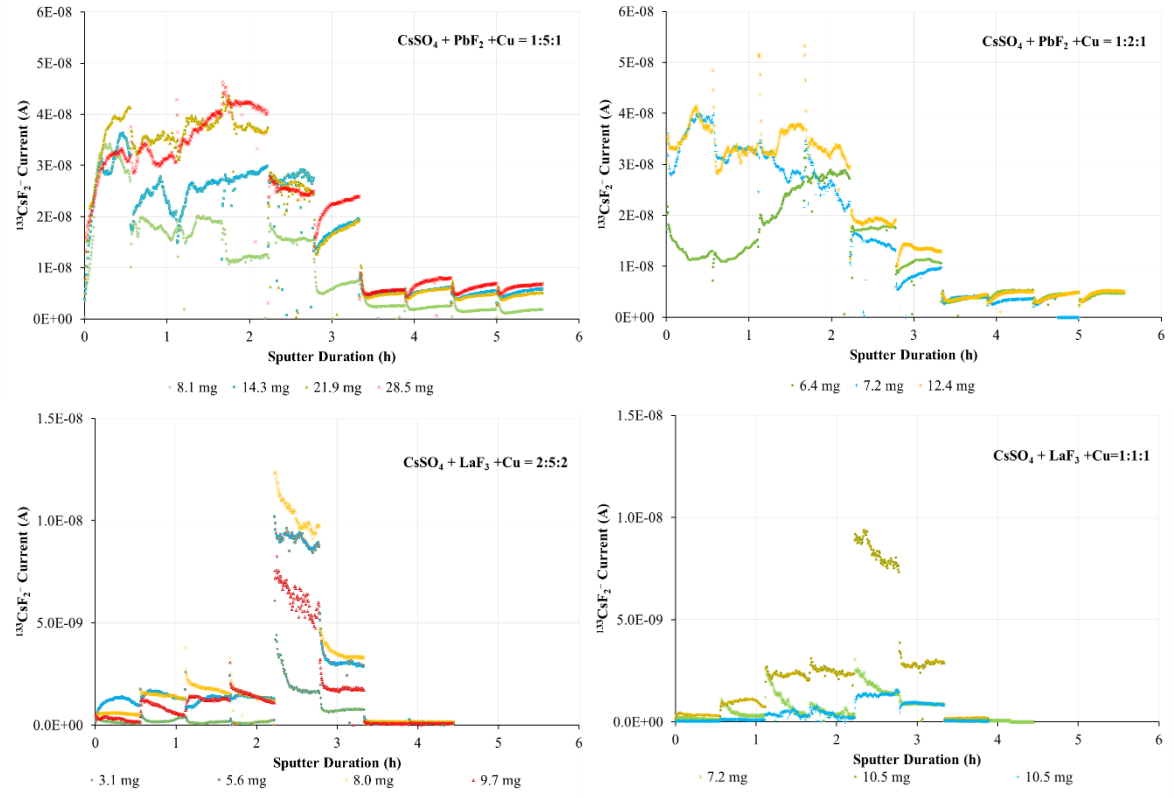

Figure 6.2.3.2 Temporal development of the $^{133}CsF_2^-$ current in FC02-1 (upper right corner: mass ratio of sample composite; legend entry: target mass). Note: different scales of the vertical axes. Laser outage took place from 2.2 to 2.8 h of the sputter duration. During this time, LaO_2^- with the same mass number as CsF_2^- was not neutralised, resulting in irregularly high currents for the targets mixed with LaF_3.

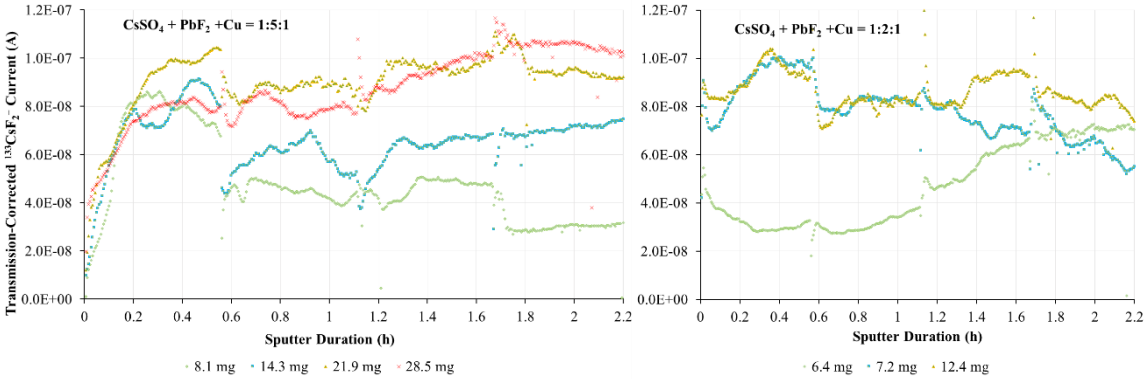

Figure 6.2.3.3 Temporal development of the transmission-corrected $^{133}CsF_2^-$ current in FC02-1(± 16% error due to the standard deviation of the transmission) extracted from targets using PbF_2 as matrix (first 2.2 hours). Currents from larger targets were generally larger than those from smaller targets. However, there was no obvious correlation between the PbF_2 proportion and the current intensity.

b. LaF_3 Matrices

In comparison with PbF_2 matrices, LaF_3 matrices generated much weaker CsF_2^- currents. Most of them were less than 10 nA (transmission corrected, see figure 6.2.3.4). A comparison of the current before and during the laser outage in figure 6.2.3.1 suggested that the LaO_2^- current was, if there was no sudden increase of CsF_2^- current during the time, much larger than that of CsF_2^-.

Targets with more than 5 mg total sample material produced a reasonable current intensity of around 2-3 nA. An increase of the fluorine donor proportion seemed to have an impact on the current intensity only at the beginning. Furthermore, the CsF_2^- current generally grew in the first 2.5 hours, which could be taken to suggest that LaF_3 is less volatile than PbF_2: it not only took time to free Cs from $CsSO_4$, but also F from LaF_3, whereas PbF_2 offers fluorine atom at the onset of the Cs^+ sputtering (Zhao et al 2010). In contrast to targets using PbF_2 as matrix, cathode changes brought about current intensity improvement overall.

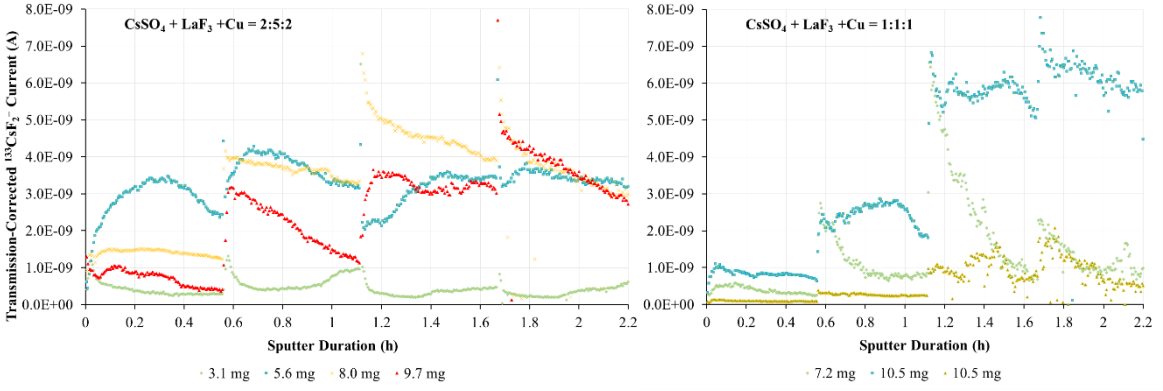

Figure 6.2.3.4 Temporal development of the transmission-corrected $^{133}CsF_2^-$ current in FC02-1(± 16% error due to the standard deviation of the transmission) extracted from targets using LaF_3 as matrix. The current intensity grew over time. LaF_3 proportion did not have a consistent influence on the current intensity.

Figure 6.2.3.5 shows the development of the transmission-corrected current extracted from a cathode used in an earlier measurement. Contained in the target was Cs_2SO_4 and LaF_3 with a Cs:F atom ratio of 1:3. As can be seen, CsF_2^- current extracted from this cathode, at least in the first 0.55 hour, was much larger than from the cathodes prepared specifically for the ionization yield tests. This could be taken to suggest that either copper powder in the targets was disadvantageous for the formation of the CsF_2^- ion, or the existence of a sputter pit before the measurement facilitated the anion formation.

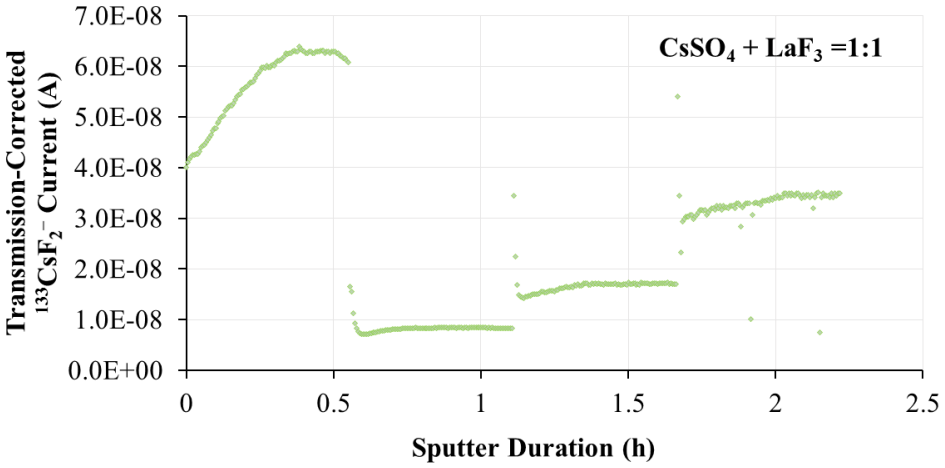

Figure 6.2.3.5 Temporal development of the transmission-corrected $^{133}CsF_2^-$ current in FC02-1 (± 16% error) extracted from a target used in an earlier measurement (unweighed) which was measured along with the targets prepared for the actual measurement. Compared with measurements targets using LaF_3 matrix, this target generated a much higher initial current of around 50 nA.

6.2.3.4 Ionisation Efficiency

Calculation of the ionisation efficiency roughly followed the procedures detailed in section 5.2.2.2 except for a transmission-based correction (see section 6.2.3.2). There is an evident measurement time difference for each cathode, resultant from either parameter optimisation or deletion of unfeasible data.

With weighing imprecision usually lower than 1‰, the uncertainty of the transmission contributed the most to the uncertainty of the ionisation efficiency. An error calculation was carried out based on either relative error (averaged transmission rate) or the variance formula (transmission rate calculated with linear regression). The results are shown in table 6.2.3.1 as well as figure 6.2.3.6.

Overall, it can be concluded that PbF_2 matrices delivered a notably higher ionisation yield than LaF_3 matrices. Further, the conclusion in section 6.3.3.1 applies also to the ionisation efficiency: a Cs:F atom ratio 1:3 would suffices for a reasonable CsF_2^- ion formation efficiency, further fluorine excess generally brought about no improvement.
The performance of the LaF_3 matrices was generally poor, partly due to the deletion of the invalid data. In addition, there was a positive correlation between the proportion of fluorine and the ionisation efficiency.

Further, sample consumption efficiency played a role in this experiment, since the sample material in cathodes was not completely sputtered. A logical consequence is a negative correlation between the sample mass and the ionisation yield (figure 6.2.3.7). It revealed that an optimal sample size was about 5-8 mg, corresponding to a Cs_2SO_4 mass of about 1-2 mg. This sample size brought about an ionisation efficiency up to 200% of those by cathodes with much more, and in one case, much less material. In the case of targets with PbF_2 matrix (especially when the proportion of the matrix material is high), however, using samples less than 10 mg meant an increase of the ionisation efficiency at the sacrifice of the beam intensity (see section 6.3.3.3.a).

F-Donor	$CsSO_4$:F-Donor:Cu Mass Ratio	Sample Mass (mg)	Cs_2SO_4 Mass (mg)	Sputter Duration (h)	Ionisation Yield ± Uncertainty (‰)
PbF_2	1.0 : 4.7 : 1.0	8.06	1.21	5.56	0.858 ± 0.091
		14.31	2.15	5.56	0.781 ± 0.071
		21.88	3.29	5.56	0.618 ± 0.064
		28.49	4.28	5.56	0.495 ± 0.048
	1.0 : 2.0 : 0.9	6.43	1.67	5.56	0.730 ± 0.066
		7.17	1.86	4.74	0.817 ± 0.098
		12.42	3.22	5.56	0.578 ± 0.063
LaF_3	2.0 : 4.9 : 2.4	3.05	0.66	3.89	0.027 ± 0.002
		5.58	1.21	3.89	0.072 ± 0.007
		7.96	1.72	3.89	0.054 ± 0.005
		9.74	2.11	3.89	0.028 ± 0.003
	1.0 : 1.0 : 1.0	7.23	2.38	3.60	0.013 ± 0.001
		10.50	3.46	3.33	0.0006%[9]
		10.51	3.46	3.33	0.026 ± 0.003

Table 6.2.3.1 Targets Specification and Ionisation Efficiency Measurement Results

[9] The calculated error is too small to be significant.

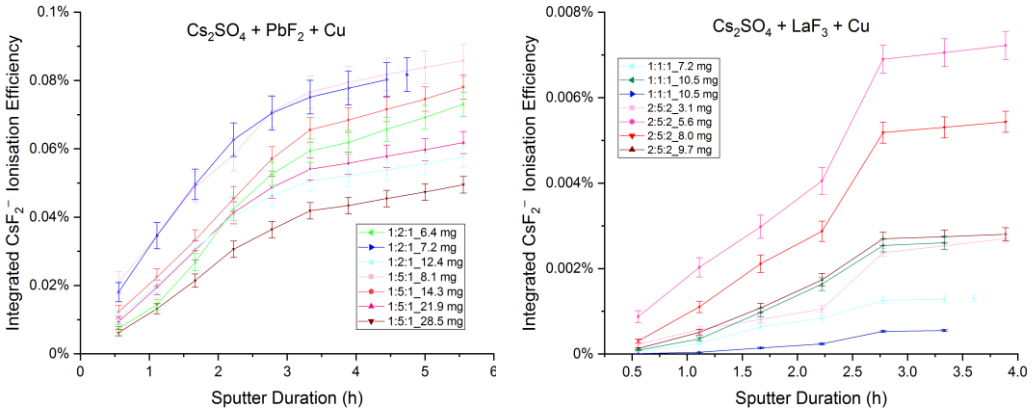

Figure 6.2.3.6 Temporal development of the integrated CsF_2^- ionisation efficiency of PbF_2 (left) and LaF_3 (right) matrices (legend entry denotes mass ratio_target mass). Note: different scales of the vertical as well as the horizontal axes. It shows that PbF_2 is a much more effective fluorine donor than LaF_3.

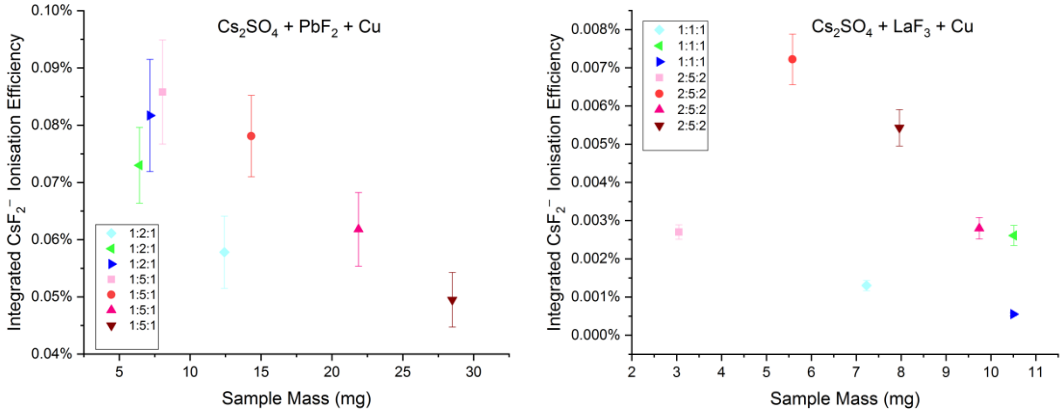

Figure 6.2.3.6 Correlation between the sample mass and the ionisation yield of targets with PbF_2 (left) and LaF_3 (right) matrices. Note: different scales of the vertical as well as horizontal axes.

6.2.4 Conclusion and Outlook for Future Caesium Experiments

This experiment showed that PbF_2 was a more effective fluorine donor than LaF_3 and a Cs:F atom ratio of 1:3 is sufficient for a typical current of 40 - 100 nA, comparable with what was achieved at VERA (Kasberger 2015; Lachner et al 2015), and an ionisation efficiency of around 0.08%.

Potential measures for ionisation efficiency improvement might include a cathode modification to increase the sample consumption as well as a composition change from $CsSO_4$ to CsF to reduce potential competitive ionisation.

6.3 Feasibility of CsC_6^- as the Secondary Ion

As was mentioned in section 6.1, Middleton's (1989) measurement of a CsC_6^- ion beam current of 1.6 µA tempts the application of caesium carbide as secondary ion. To judge its applicability, two carbon cathodes containing graphite and iron from a previous measurement (hence pre-pitted) was sputtered by Cs^+ in S2 to see if the data collected by Middleton could be reproduced.

Figure 6.3.1 shows the mass scan generated with procedures detailed in section 7.2.1.2. Before the mass scan was made, currents from targets with graphite and iron were measured with the first cup after S2 (FCS2-1). They were around 50 µA, a value that can be expected from a carbon cathode.

It can be read that most caesium carbide anions did not amount to 10 nA. The CsC_6^- ion beam current did not outperform that of other caesium carbon polymer anions. However, the CsC_{10}^- current was much smaller here than measured with a KkU D30 and graphite target (see figure 7.5.2).

Since the caesium carbide ion intensities observed in this experiment were not comparable with that of the CsF_2^- (see section 7.2.2.1) and the application of caesium carbide implies difficulties with sample matrix, the conclusion was drawn that CsC_6^- was, within the framework of this measurement, not feasible as a secondary ion for caesium measurement.

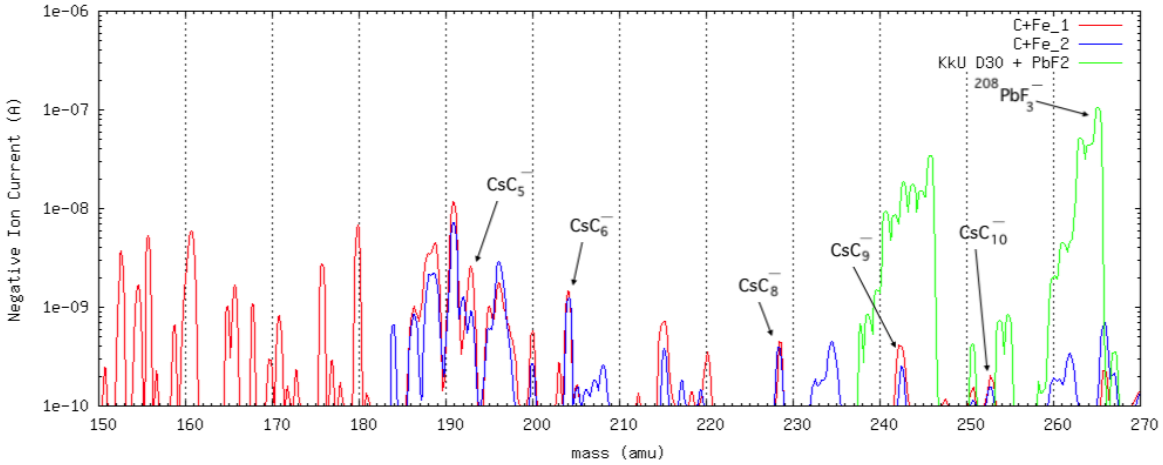

Figure 6.3.1 Mass scans of targets containing graphite and iron. Scale calibrated with a target containing KkU D30 and PbF_2 (see Appendix A). Intensities of all caesium carbide anions are under 10 nA.

7. INVESTIGATION OF URANIUM IONISATION EFFICIENCY

Since ^{235}U and ^{239}Pu are widely used in nuclear weaponry and power plants, nuclear weapon testing and the application of nuclear energy leads to the formation and release of anthropogenic ^{236}U (neutron capture by ^{235}U), ^{239}Pu (neutron capture by ^{238}U) as well as other actinides (Wilcken et al 2007).

Due to their long half-lives, ^{236}U ($t_{1/2}$=23.4 Ma) (Zhao et al 1997) and ^{239}Pu ($t_{1/2}$=24.4 ka) (Farewell et al 1954) are used as tracer for nuclear releases (Quinto et al 2009) as well as for environmental changes such as desertification and sediment transport (Hirose et al 2017).

In particular, ^{236}U has become widely accepted as oceanographic tracer (Winkler et al 2012) and is routinely analysed at VERA (Winkler et al 2015). The measurement of the $^{236}U/^{238}U$ ratio in environmental samples, which typically is in the order of 10^{-9} in the oceans (Casacuberta et al 2014, Eigl et al 2016, Nomura et al 2017), is usually conducted with AMS, since conventional mass spectrometry like TIMS, ICP-MS and RIMS does not offer a sufficiently low detection limit (Steier et al 2010). However, the low overall detection efficiency of uranium and other actinides leads to a rather laborious sample preparation and prevents the use of even smaller sample masses, shorter measurement durations and the general application of a multi-actinide analysis approach (Quinto et al 2016). Therefore, an improvement of the ionisation efficiency is of significant importance.

7.1 CHOICE OF THE SECONDARY ION

Due to its relatively low electron affinity (theoretical prediction: 0.3 eV) (Middleton, 1989), uranium does not readily form stable atomic anions. Hence, AMS ^{236}U measurements are conventionally conducted with UO^- as the secondary ion, which offers an intensity about two orders of magnitude higher than the atomic anion (Fifield et al 2008).

According to Fifield et al (1996), who extracted singly charged uranium anions as well as uranium mono-, di-, tri- and tetroxide anions with the SNICS ion source of the 14 UD at the Heavy Ion Accelerator Facility of the Australian National University, UO^- ion offered the largest current (table 7.1.1) and also the highest sputtering efficiency, when a mixture of UO_3, FeO and Ag powder with a uranium and iron atom ratio of 1:1 is utilised for sputtering. In his experiment, the UO^- current averaged 380 nA for 4 hours before exhaustion, resulting in an extraction efficiency of 0.3%.

Negative ion currents from a UO_3 sample

U^- (nA)	UO^- (nA)	UO_2^- (nA)	UO_3^- (nA)	UO_4^- (nA)
0.9	390	55	6	1.2

Table 7.1.1 Negative molecular ion current extracted from UO_3, FeO and Ag mixture with a uranium and iron atom ratio of 1:1 using a NEC SNICS source (Fifield et al 1996)

The usage of carbide anions was first put forward by Middleton (1989), who extracted a UC_2^- and UC^- current of 0.25 µA and 75 nA respectively from a cathode containing uranium metal powder mixed with powdered graphite. This was further investigated by Buompane et al (2015), who extracted an average UC_2^- and UC^- current of 171 and 102 nA respectively from cathodes containing uranyl nitrate $UO_2(NO_3)_2$ baked at 800°C and mixed with graphite and aluminium powder. It took 5.55 hours for this relatively stable current to be exhausted, providing a UC_2^- and UC^- ionisation efficiency of 0.36% and 0.21% respectively.

UF_5^-, which has the highest intensity amongst all uranium fluoride anions (Zhao et al 2010) offers itself as secondary ion due to merits of superhalogen anions mentioned in section 3.

In the sections to follow, four experiments examining the applicability of UF_5^- for uranium measurement and options for optimisation of ionisation yield as well as current output for UO^- and UF_5^- will be outlined.

7.2 EXPERIMENT 1

The main aim of the 1st measurement was to compare the current intensity as well as the yield of UF_5^- extracted from UF_4 samples and U_3O_8 mixed with PbF_2. Furthermore, different matrices for UO^- extraction were studied in their effectiveness. Extracting UF_5^- and UO^- in the same experiment should also provide a foundation for a comparison of these two secondary ions in their intensity and yield.

To enable an assessment of various fluoride as well as oxide anions produced by every material over the entire sputter time, continuous mass - beam intensity scans were made.

7.2.1 Method

7.2.1.1 Sample Preparation

Four samples prepared at the VERA laboratory and eight prepared at the Faculty of Nuclear Sciences and Physical Engineering of the Czech Technical University in Prague were included in this experiment. One sputter target was prepared from each sample material.

a. Samples Prepared at VERA

The uranium-containing material used at VERA in this experiment is the in-house standard, Vienna KkU: uranyl nitrate $UO_2(NO_3)_2 \cdot 6H_2O$ prepared before 1918 in the "K.k. Uranfabrik Joachimsthal". Its uranium concentration is about 500,000 µg/g and the $^{236}U/^{238}U$ ratio is $(6.98 \pm 0.32) \times 10^{-11}$ (Steier et al 2008). By baking it at 800°C, a mixture of UO_2, UO_3 and U_3O_8 is obtained for AMS use.

A dilution of the KkU can be achieved with the following procedures: first, dissolve $UO_2(NO_3)_2 \cdot 6H_2O$ and a certain amount $Fe(NO_3)_3$ in water according to the dilution factor; by adding NH_3, precipitated $UO_2(OH)_2$ and $Fe(OH)_3$ is obtained; this precipitate is then baked at 800°C for dehydration. A diluted KkU thus contains Fe_2O_3 and U_3O_8, which is similar to the final matrix of environmental uranium samples prepared for AMS measurements.

To increase their thermal and electric conductivity, uranium samples are embedded in a metal matrix. In this experiment, two materials were tested on their effectiveness for the enhancement of the UO^- formation: niobium and iron [10][11].

The following sample materials were prepared at VERA: KkU D30[12]; KkU D30 mixed with niobium with a mass ratio of 1:1; KkU D30 mixed with iron with a mass ratio of 1:1 as well as KkU D30 mixed with PbF_2 with a mass ratio of 1:8. The preparation basically followed the routine introduced in 5.2.1.1 except that aluminium instead of copper sample holders were used. Aluminium target holders are used conventionally in uranium measurements, since copper easily forms clusters. The cluster $^{65}Cu^{63}Cu_3$ has the same mass

[10] The thermal conductivity of niobium: 54 W/(m K); of iron: 80 W/(m K); of uranium (pure metal): 27 W/(m K). The electric resistivity at room temperature (293/298 K) of niobium: 15×10^{-8} Ω m; of iron: 10×10^{-8} Ω m; of uranium (pure metal): 28×10^{-8} Ω m (James 1992).

[11] The advantage of using iron is that environmental uranium samples prepared for AMS measurement contain primordial iron. Therefore, adding more iron will not add any other background ions.

[12] D30 means the diluted material contains 1/30 (mass) of KkU.

number as ^{238}UO and creates, thus, obstacles for mass separation in uranium measurement using UO^-.

Specifications of the used material as well as samples are listed in Table 7.2.1.

Category	Added Matrix Material Code	Mass Ratio KkU D30 : Added Matrix	Sample Mass (mg)	Uranium Mass (µg)	Uranium Concentration (µg/g)
KkU D30 + PbF2	Aldrich 236152	1.0:8.5	14.75	26	1760
KkU D30 + Nb	Alfa Aesar 040510	1.0:1.0	11.48	97	8400
KkU D30 + Fe	Alfa Aesar 000737	1.0:1.0	5.88	50	8430
KkU D30	None	1.0:0.0	3.94	66	1670

Table 7.2.1 Specification of samples prepared at VERA

b. Samples Prepared in FNSPE CTU Prague

Samples prepared in FNSPE CTU Prague are UF_4 samples. They underwent the following fluorinating procedures to increase the uranium oxide / uranium fluoride ratio, which was a limiting factor for experiments with uranium fluoride in the past: "Weighted amount of $UO_2NO_3.6H_2O$ is dissolved within 1,0 ml of demi-water (or 1 ml of 12% HCl when Nd_2O_3 is used as a carrier). The solution is heated up to 80 °C and the chosen carrier[13] ($CaCl_2$ or Nd_2O_3) is added. Reducing agent ($N_2H_4.2HCl$ or $SnCl_2$) together with the copper catalyst ($CuCl_2$) are then dissolved in the solution. By adding concentrated hydrofluoric acid, a precipitate is obtained. The reaction mixture is then maintained at 80 °C for 2 hours with occasional stirring. Resulting white precipitate of CaF_2 containing uranium is centrifuged. After decanting the solution above, the precipitate is washed with MetOH[14] and dried under vacuum at 30°C for several hours. Obtained product can be modified by heating to 310 °C under reducing Ar-H2 atmosphere" (written by Tomáš Prášek, FNSPE CTU Prague).

Specifications of the samples are listed in Table 7.2.2 (page 41).

7.2.1.2 Measurement Principle

This measurement was performed with source S2. The targets were sputtered by the conventional caesium ions. The negative ions were collected by FCI1-1 directly after the first magnetic mass filter BMI1-1.

Except for the 12 cathodes mentioned in 7.2.1.1, two carbon targets, one gold target and two cathodes containing KkU were put into the target wheel. They fulfilled the following

[13] Carriers were used to prevent uranium from oxidation.
[14] Methanol

purposes: parametric optimisation for current maximisation (KkU); mass scale calibration (gold); parking cathode (carbon) as well as monitoring the state of the ion source (KkU) to ensure regular operation conditions of the ion source.

The detailed procedures of the measurement can be found in Appendix A *Checklist for Ionisation Yield Measurements with S2*, which was compiled after the second experiment.

In regular isotope measurements, the energy of the extracted ion from the source is kept constant, which is predominantly determined by the extraction (EXT) and preacceleration (HVS) voltage. A variation of the magnetic field results in different masses of ions collected in a Faraday cup. In this way, mass scans are created.

During this measurement, the magnetic field generated by BMI1-1 was kept constant, whereas the HVS (high voltage source, see section 2.1) voltage, thus the ion energy, underwent gradual variation. The reason was the magnetic field of BMI1-1 cannot be set directly, since there was no in-built Hall sensor so that only the current in the coils can be read.

The intensity of the beam current collected in FCI1-1 was plotted against the HVS voltage value. Since there is a linear relationship between the mass and the energy of the ion passing through the magnet ($ME = (Brq)^2/2$), a constant was introduced to turn the HVS voltage – ion current (energy - ion current) plot into a mass – ion current plot. This constant, in fact $(Brq)^2/2$, could be found by sputtering a gold target, from which the highest peak of the ion current is known to be $^{197}Au^-$.

To ensure the inclusion of the uranium atomic anion as well as its oxide and fluoride ions, the mass range from roughly 235 amu to 345 amu was chosen, which corresponded to a HVS voltage range from 3.33 to 13.33 kV.

For measurement automation, a batch program was used which called in three consecutive HVS voltage scans of each cathode before changing to the next cathode (see Appendix B). The two cathodes containing KkU were scanned once per turn of the sample wheel to monitor the ion source.

It took the program in average (300±50) seconds to produce one HVS voltage scan with a 10kV range containing 400 measurement points.

The measurement was stopped when the UF_5^- and UO^- beam intensity reached the sensitivity limit of the Faraday cup of 10^{-10} A.

Sample Code	A5	A5-TA	E2	E2-TA	V4	V4-TA	W4	W4-TA
Date of Prep.	03/01	04/01	03/01	04/01	03/01	04/01	03/01	04/01
Uranium Compound	$UO_2(NO_3)_2 \cdot 6H_2O$ (12.0 mg)		$UO_2(NO_3)_2 \cdot 6H_2O$ (11.9mg)		$UO_2(NO_3)_2 \cdot 6H_2O$ (12.3 mg)		$UO_2(NO_3)_2 \cdot 6H_2O$ (12.1 mg)	
Solvent	H_2O (1.0 ml)				12% HCl (1.0 ml)			
Carrier	Ca (as $CaCl_2$) (99.6 mg)		Ca (as $CaCl_2$) (99.5 mg)		Nd (as Nd_2O_3) (133 mg)			
Reducing Agent	$N_2H_4.2HCl$ (12.0 mg)		$SnCl_2$ (11.9 mg)		$SnCl_2$ (12.3 mg)		$N_2H_4.2HCl$ (12.1 mg)	
Catalyst	Cu (as $CuCl_2$) (13.8 mg)		Cu (as $CuCl_2$) (13.6 mg)		Cu (as $CuCl_2$) (13.5 mg)			
Precip. Agent	40% HF (1ml)							
Drying	30 °C, vacuum							
Heating	-	310 °C, $Ar+H_2$	-	310 °C, $Ar+H_2$	-	310 °C, $Ar+H_2$	-	310 °C, $Ar+H_2$
Samples Mass (mg)	2.17	4.22	5.65	8.46	13.93	11.92	11.19	9.96
Uranium Mass (µg)	150	310	320	500	470	420	410	390
Uranium Conc. (µg/g)	69100	73500	56600	59100	33700	35200	36600	39200

Table 7.2.2 Specification of samples prepared in FNSPE (compiled by Tomáš Prášek and edited by the author)

7.2.1.3 Source Regulation

The source regulation coordinates the caesium inflow and the ioniser power to reach the set value of either the HVS or the CAT current[15] (see section 2.1). During the first eight turns (around 2 hours of sputtering duration for each cathode), this regulation was used for output maximisation. After the first eight turns, the source regulation modus "Slow" was used so that the source parameters were only subject to minor changes[16].

Excessive caesium made the EXT insulator conductive and led to an insertion of the Faraday cup FC S2-1 directly after S2 during the 15th as well as the 16th turn. Therefore, scans made showed no currents despite the targets being sputtered. During this period, each target was sputtered for roughly 30 minutes (life time of targets in this experiment averaged 12 hours). It was necessary, thus, to carry out an interpolation. By averaging five data points

[15] Depending on the control parameter of the source regulation. If the control parameter is HVS_CR, then a value set for CAT_CC is only a maximum limit.

[16] In fact, the "slow" modus should be used during the whole measurement. At the point of the measurement, there was no established procedures to follow and the source regulation in the first eight turns was left in the modus of lnhfastC by an oversight.

before and after the interruption of normal source operation and using them as substitutes, the influence of this disorder was accounted for.

7.2.1.4 Data Evaluation

The large size of the generated data renders the usage of a semi-automated evaluation convenient. Hence, a batch program was utilised to select a current peak in a HVS voltage range defined for ions of interest (see Appendix C). Taking the source output as stable during each scan, the ionisation efficiency was calculated.

7.2.2 Results and Discussion

7.2.2.1 Samples Prepared at VERA

a. Mass Scans

Figure 7.2.2 shows the first scans of the first turn (sputter duration: around 5 min) of all cathodes prepared at VERA. One can see that cathodes for uranium oxide anion extraction produced roughly equal amount of uranium mono- (254 amu), di- (270[17] amu), tri-(286 amu) oxide anion (around 2 nA). The KkU D30 and PbF_2 mixture produced UF_5^- (333 amu) with an intensity of roughly 3 nA, a UF_4^- (314 amu) current less than 0.2 nA and a UO^- current around 0.3 nA.

Further, the highest peak in the scan of the KkU D30 and PbF_2 mixture is $^{208}PbF_3^-$ (265 amu). Thanks to the isotopic ratio of ^{208}Pb, ^{207}Pb and ^{206}Pb, this peak showed a distinct pattern which provided a reference point for mass scale calibration in later experiments.

Figure 7.2.3 shows the third scan of the third turn (sputter duration: around 45 min) of all cathodes prepared at VERA. A comparison of this figure with figure 7.2.2 revealed a decrease of UO_3^- and UO_4^- and an increase of UO^- (to 4-5 nA) in the first 45 min, which probably resulted from an oxygen excess at the beginning of the measurement[18]. Further, the UF_5^- current from the KkU D30 and PbF_2 mixture decreased from around 10 nA to 1 nA.

[17] The aluminium cluster Al_{10}^- has the same mass number. However, since these scans were made at the beginning of the measurement and the Al_9^- and Al_{11}^- peak are much smaller, we considered it legitimate to claim the peak to be predominantly UO_2^-.

[18] The source was cleaned one week prior to the measurement.

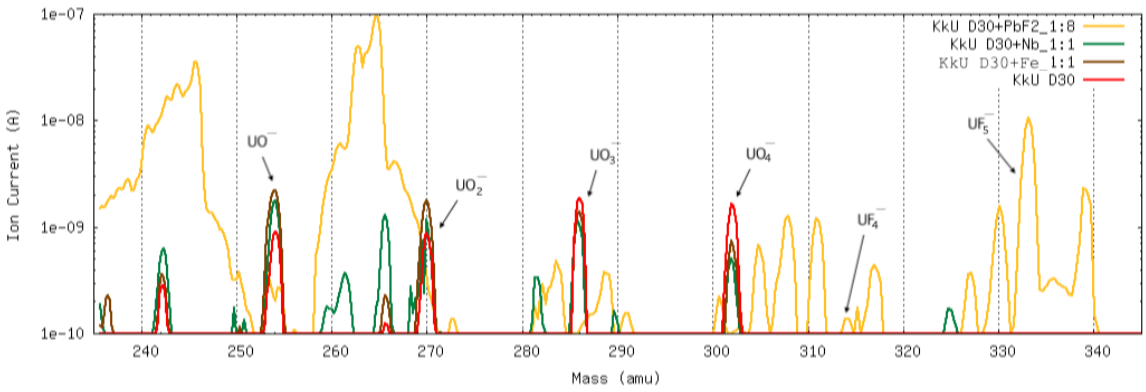

Figure 7.2.2 1st turn, 1st mass scan (sputter duration: around 5 min) of cathodes prepared at VERA. Four UO_x^- peaks with comparable intensities and two UF_x^- peaks with UF_5^- being the dominant fluoride were identified.

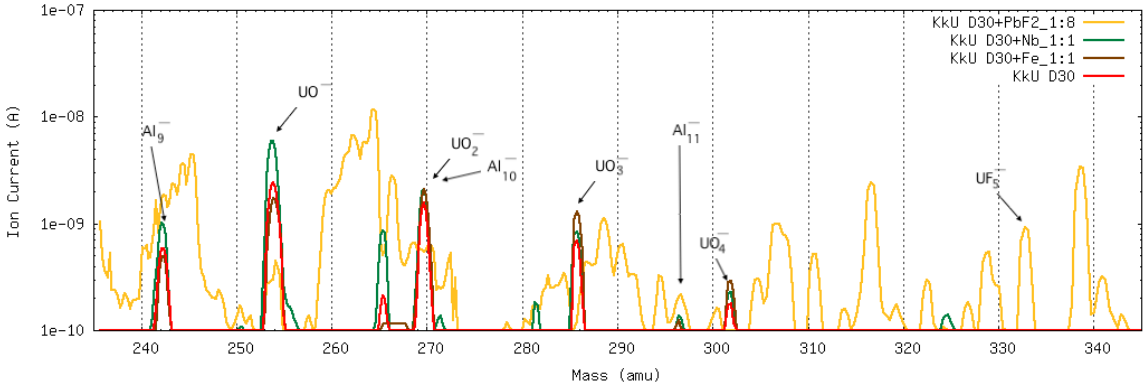

Figure 7.2.3 3rd turn, 3rd mass scan (sputter duration: around 45 min) of cathodes prepared at VERA. In comparison with figure 7.2.3, intensities of UO_3^- and UO_4^- decreased whereas that of UO^- increased. Also, intensities of aluminium cluster ions Al_x^- increased.

b. Current Development

Figure 7.2.4 a) shows the temporal development of UF_5^- and UO^- beam intensity extracted from relevant cathodes.

As can be seen, it generally took 20 minutes for the UO^- current to develop to a reasonable value (3 – 4 nA). A possible explanation was the relatively high yield of uranium oxide anions of higher order at the beginning of the measurement, as was mentioned in section 7.2.2.1.a. This beam intensity is around 1% of what Fifield (1996) measured using a mixture of UO_3, FeO and Ag powder.

The UF_5^- current produced by the KkU D30 and PbF_2 mixture had the highest intensity at the beginning (10 nA), however, it dropped to less than 1 nA after 30 minutes of sputtering. It might, however, be a result of the source regulation for output maximisation at the beginning (see section 7.2.1.3), which needs further investigation.

A comparison among the UO^- currents by KkU D30 mixed with Nb, KkU D30 mixed with Fe and KkU D30 showed that embedding KkU D30 in either niobium or iron matrix

improved the intensity of the UO^- current. In the first four hours, the niobium matrix outperformed the KkU D30 and the iron matrix. However, the conclusion should not be drawn immediately that niobium was a better matrix material than iron for UO^- intensity improvement, since these three samples were of different sizes; they contained different amount of uranium and the uranium concentrations were different.

The temporal development of UF_5^- and UO^- current normalised to the mass and concentration of uranium are shown in figure 7.2.4 b) and c) respectively. A combined view of 7.2.4.a) b) c) reveals that niobium matrix not only provided a higher UO^- ion intensity overall, but also a higher UO^- current normalised to the uranium concentration. However, the iron matrix outperformed the niobium matrix in the case of UO^- current normalised to uranium mass. In addition, it is interesting that the UO^- current from KkU D30 and PbF_2 mixture normalised to uranium concentration was higher than that from KkU D30.

Further, all materials prepared for UO^- extraction (KkU D30+Nb, KkU D30 +Fe, KkU D30) experienced a decreasing and increasing instability of the UO^- current from the fourth to the tenth hour. Since the UO^- current from the KkU D30 and PbF_2 mixture was generally low, it was not affected to a great extent.

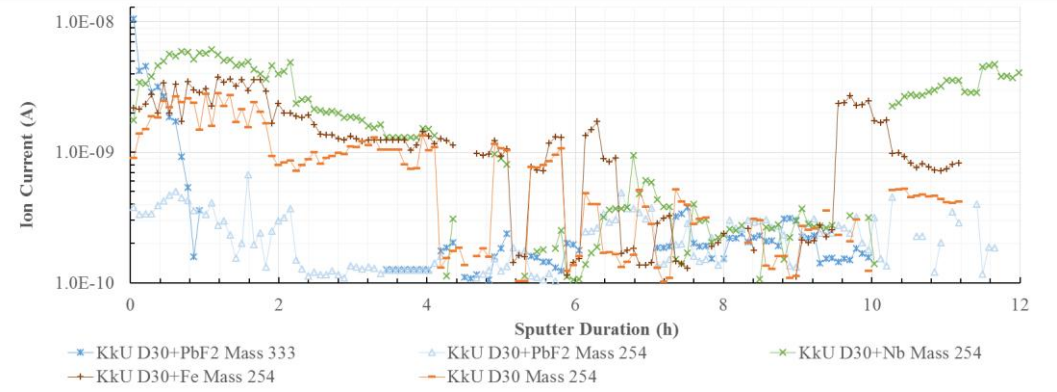

Figure 7.2.4 a) Temporal development of UF_5^- (333 amu) and UO^- (254 amu) beam intensity (first 12 hours). The rapid increase and decrease of the UO^- currents lasted from the 4th hour to roughly the 10th hour of sputtering. The end of this phase corresponds with the end of UF_5^- extraction from the KkU D30 + PbF_2 target.

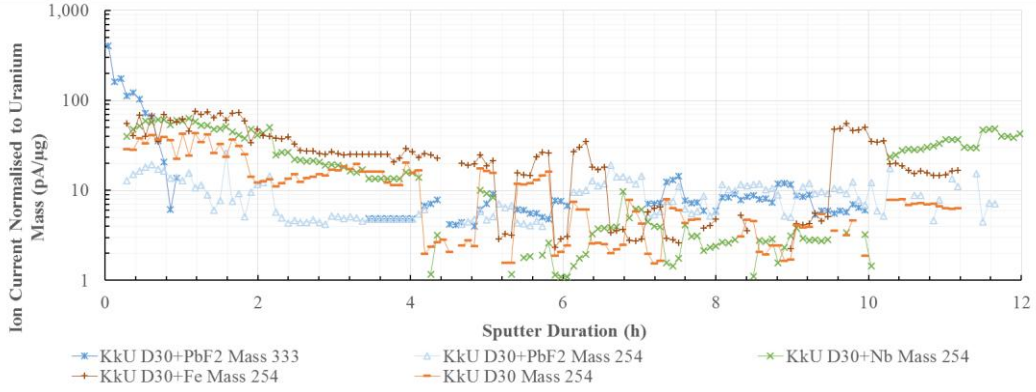

Figure 7.2.4 b) Temporal development of UF_5^- (333 amu) and UO^- (254 amu) beam intensity normalised to uranium mass (first 12 hours)

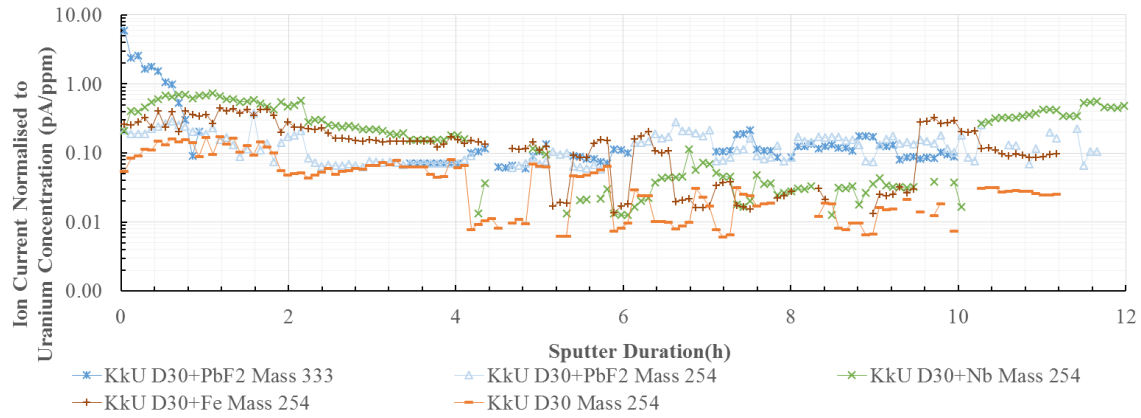

Figure 7.2.4 c) Temporal development of UF_5^- (333 amu) and UO^- (254 amu) beam intensity normalised to and to concentration (first 12 hours)

A possible explanation for this UO^- ion formation disturbance was that the target containing PbF_2 were sputtered alternatingly with targets containing no PbF_2: the target containing PbF_2 was sputtered right before the following three targets: KkU D30+Nb, KkU D30 +Fe, KkU D30. Since PbF_2 is highly volatile (Zhao et al 2016), its vapour stayed in the source after its sputtering and probably disturbed the formation of UO^-. As can be seen in figure 7.2.4 a), the UO^- currents increased again when no UF_5^- current, but only UO^-current, could be extracted from the KkU D30 and PbF_2 mixture. This also indicates that PbF_2 was exhausted before KkU D30 in the same target (after around 10 h of sputter duration). Further, as can be seen in figure 7.2.4 c) (right), a UF_5^- current of around 0.2 nA could be extracted from samples without PbF_2 after 4 hours of sputtering, which lasted for 6 hours until PbF_2 was exhausted.

Target containing mixture of KkU D30 and Nb had the greatest mass and, thus, the longest life time. A comparison of the development of UO^- currents from iron and niobium matrices in a full-time scale is shown in figure 7.2.4 c) (left)

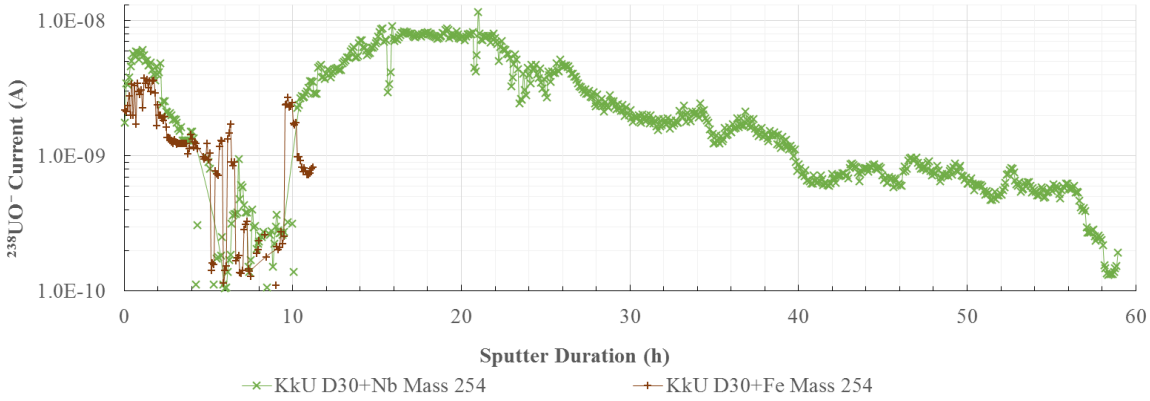

Figure 7.2.4 d) Temporal development of $^{238}UO^-$ beam intensity of KkU D30 + Nb and KkU D30 + Fe in full time scale. The KkU D30 + Nb target had the greatest mass and thus the longest life time.

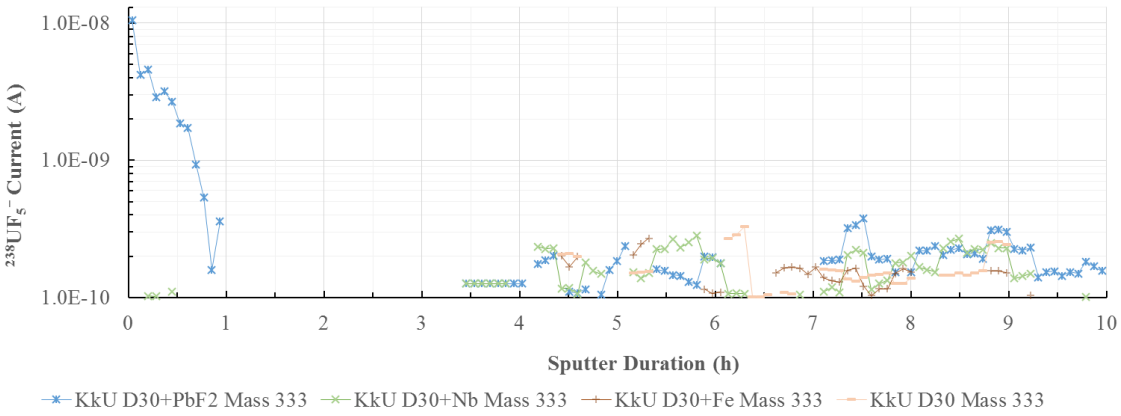

Figure 7.2.4 e) Temporal development of the $^{238}UF_5^-$ beam intensity (first 11 hours). The PbF_2 vapour stayed in the source after the sputtering of the target containing PbF_2, resulting the formation of UF_5^- from targets containing no fluorine donor.

c. Ionisation Efficiency

Figure 7.2.5 shows the temporal development of the integrated ionisation efficiency for the first 12 hours. As was discussed in section 7.2.2.1 b, only KkU D30+Nb produced UO^- after 12 hours of sputtering, which exceeded the normal measurement duration by far. Sputtering time 12 -60 hours is, thus, of no significant importance. The final results are shown in table 7.2.3.

The uncertainty of the scan duration (see section 7.2.1.2) led to a very small standard deviation of the mean, which had less influence on the uncertainty of the ionisation efficiency than, for instance, changes of the source parameters. Thus, a calculation of the uncertainty was left out.

As was indicated earlier, the KkU D30 and PbF_2 mixture reached 70% of its final UF_5^- yield after half an hour of sputtering. Adding additional iron to KkU D30, which contains almost 96.7% of Fe_2O_3, doubled the ionisation yield of UO^- in 3 hours.

The UO^- ionisation efficiency of the KkU D30+Nb and KkU D30+Fe increased considerably after 10 hours of sputtering, corresponding to the end of the UO^- ion formation disturbance discussed in section 7.2.2.1 b. Due to the different target sizes (see table 7.2.2), the KkU D30+Nb target could still produce UO^- for a longer time, whereas the KkU D30+Fe target was exhausted after around 11.2 hours.

With a final ionisation efficiency comparable to what Fifield achieved with a mixture of UO_3, FeO and Ag, iron appeared to be the most suitable matrix material for a normal measurement with 2-3 hours of duration, although the final yield of UO^- by the niobium matrix proved to be higher in the long run (see table 7.2.3).

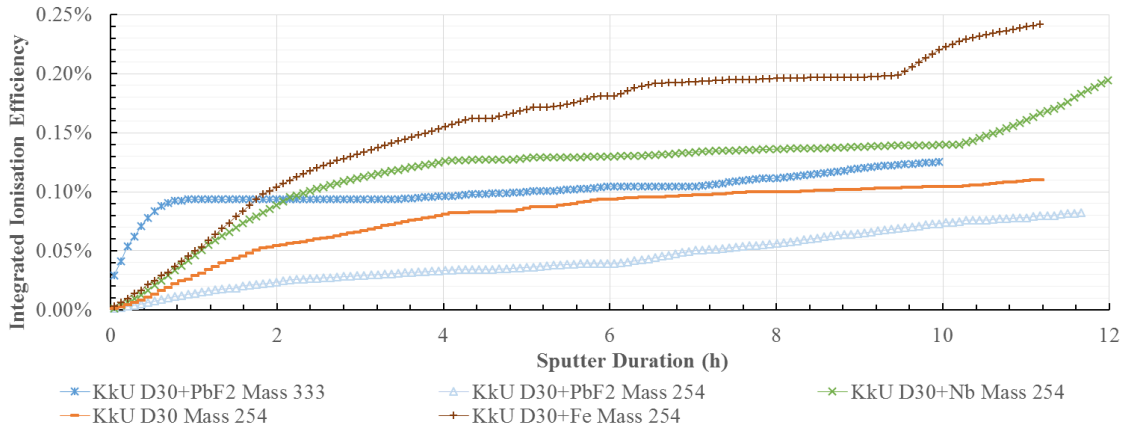

Figure 7.2.5 Temporal development of the integrated UF_5^- (333 amu) and UO^- (254 amu) ionisation efficiency. The rapid increase after around 10 hours of sputtering corresponds with the end of the UF_5^- extraction from the KkU D30 + PbF_2 target. In the first 12 hours, iron was a better matrix for UO^- extraction. The UF_5^- ionisation efficiency with KkU D30 and PbF_2 was comparable with that of UO^- from KkU D30.

Uranium-Form	Added Matrix	Sample Mass (mg)	Uranium Mass (µg)	UF_5^- Yield (‰)	UO^- Yield (‰)
KkU-D30	PbF_2	14.75	26	1.25	0.82
KkU-D30	Nb	11.48	97	0.08	13.70
KkU-D30	Fe	5.88	50	0.07	2.42
KkU-D30	None	3.94	66	0.06	1.10

Table 7.2.3 Ionisation efficiencies of samples prepared at VERA. In the long run, KkU D30 + Nb yielded the highest UO^- ionisation efficiency.

7.2.2.2 Samples Prepared in FNSPE CTU Prague

a. Mass Scans

Figure 7.2.6 a) shows the third scan of the first turn (sputter duration: around 15 min) of A5, A5TA, E2 and E2TA with H_2O as solvent and $CaCl_2$ as carrier. A5 & A5TA (TA: sample underwent the last procedure of heating) were reduced by $N_2H_4.2HCl$ and E2 & E2TA by $SnCl_2$ (see table 7.2.2).

Figure 7.2.6 b) shows the third scans of the first turn of V4, V4TA, W4 and W4TA with 12% HCl as solvent and Nd_2O_3 as carrier. W4 & W4TA was reduced by $N_2H_4.2HCl$ and V4 & V4TA by $SnCl_2$ (see table 7.2.2).

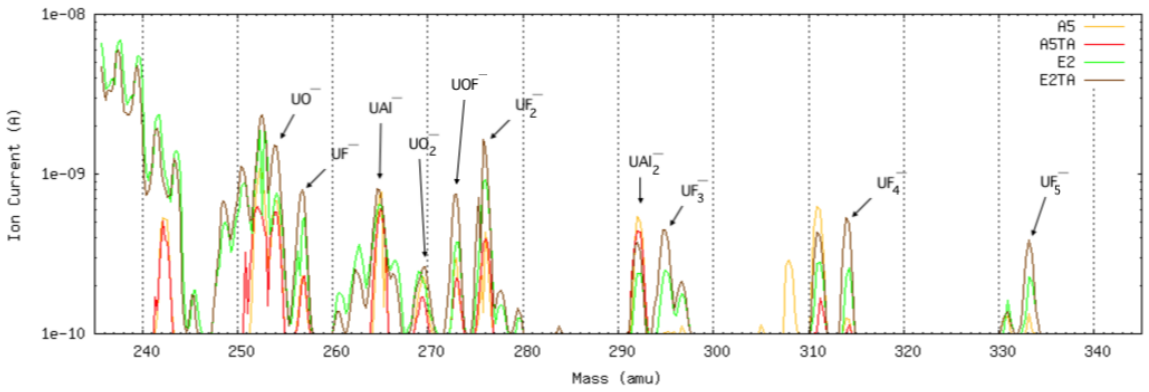

Figure 7.2.6 a) 1st turn, 3rd mass scan of A5, A5TA, E2 and E2TA: H_2O as solvent and $CaCl_2$ as carrier

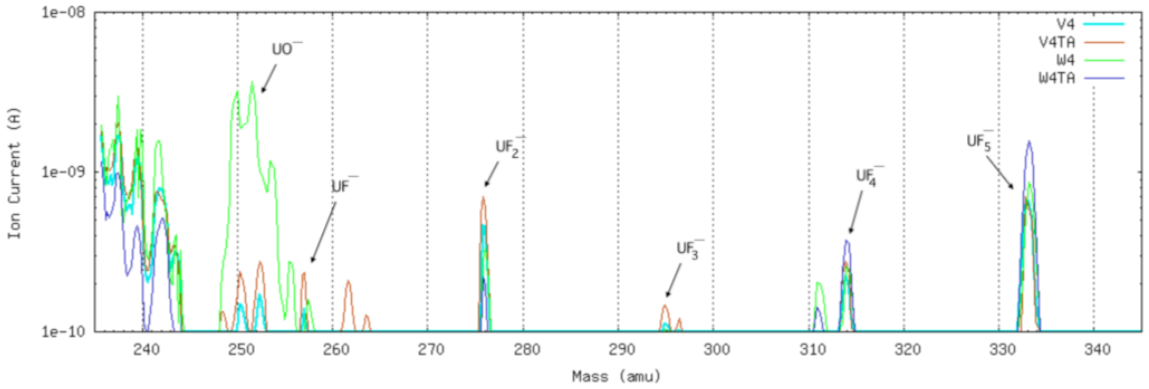

Figure 7.2.6 b) 1st turn, 3rd mass scan of V4, V4TA, W4 and W4TA: 12% HCl as solvent and Nd_2O_3 as carrier: in comparison with A5, A5TA, E2 and E2TA, these targets produced more UF_5^-, less UO_x^- and UOF^-

Code	UO^- (254 amu) (nA)	UO_2^- (270 amu) (nA)	UF^- (257 amu) (nA)	UF_2^- (276 amu) (nA)	UF_3^- (295 amu) (nA)	UF_4^- (314 amu) (nA)	UF_5^- (333 amu) (nA)	UOF^- (273 amu) (nA)	UAl^- (265 amu) (nA)	UAl_2^- (292 amu) (nA)
A5	0.7	0.2	0.2	0.4	0.1	0.1	0.1	0.3	0.8	0.5
A5TA	0.6	0.2	0.2	0.4	x	0.1	x	0.2	0.6	0.4
E2	0.8	0.3	0.5	0.9	0.3	0.3	0.2	0.4	0.6	0.3
E2TA	1.5	0.3	0.8	1.8	0.5	0.5	0.4	0.6	0.8	0.4
V4	0.2	x	0.1	0.5	0.1	0.2	0.7	x	x	x
V4TA	0.3	x	0.2	0.7	0.1	0.3	0.7	x	x	x
W4	1.1	x	0.1	0.3	0.1	0.3	0.9	x	x	x
W4TA	x	x	x	0.2	x	0.4	1.1	x	x	x

Table 7.2.4 Maximum beam currents of different uranium compounds read from figure 7.2.6 a) and b) (rough values, x indicates that the current is under the sensitivity level of the Faraday cup)

Maximum beam currents of different uranium compounds read from the mass spectra in figure 7.2.6 a and b are shown in table 7.2.4. Based on these values, it could be judged that using H_2O as solvent and $CaCl_2$ as carrier generally facilitated the formation of UO_x^-, UOF^- as well as UAl_x^-, whereas using 12% HCl as solvent and Nd_2O_3 as carrier facilitated the formation of UF_x^-.

Interestingly, UF_5^-, in contrast to Zhao et al's (2010) findings with uranium metal in a PbF_2 matrix, is not always the highest peak in the fluoride spectrum. Especially in the case of A5&A5TA and E2&E2TA, uranium fluoride anions with less than 5 fluorine atoms, especially UF_2^-, had an intensity higher than that of UF_5^-. It seemed that a fluorine donor is needed in this case to facilitate the formation of the superhalogen anion.

b. Current Development

Figure 7.2.7 shows the temporal development of UF_5^- and UO^- beam intensity. Apparently, the UF_5^- and UO^- currents developed in a complimentary manner: a high UF_5^- intensity meant low UO^- intensity and vice versa.

The conclusion that using 12% HCl as solvent and Nd_2O_3 as carrier facilitated the formation of UF_5^- can be confirmed. Further, the procedure of heating in $Ar+H_2$ at 310 °C, especially in the case of V4&V4TA, W4 & W4TA, reduced the UO^- intensity.

Only two data points recorded for UF_5^- produced by A5 were above the sensitivity limit, which correspond to the observation in section 7.2.2.2.a that A5&A5TA, E2 & E2TA produced more UO_x^-, UOF^- as well as UF_x^- with U in lower oxidation states, especially UF_2^- than UF_5^-.

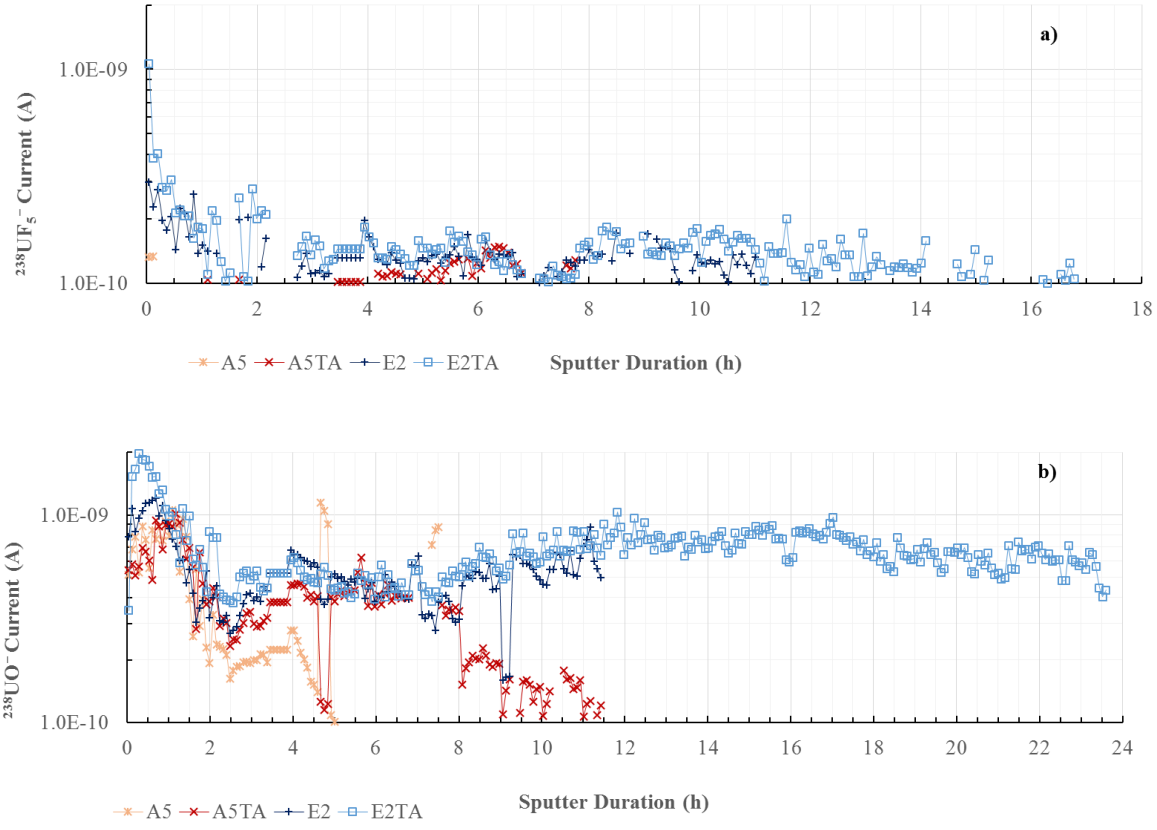

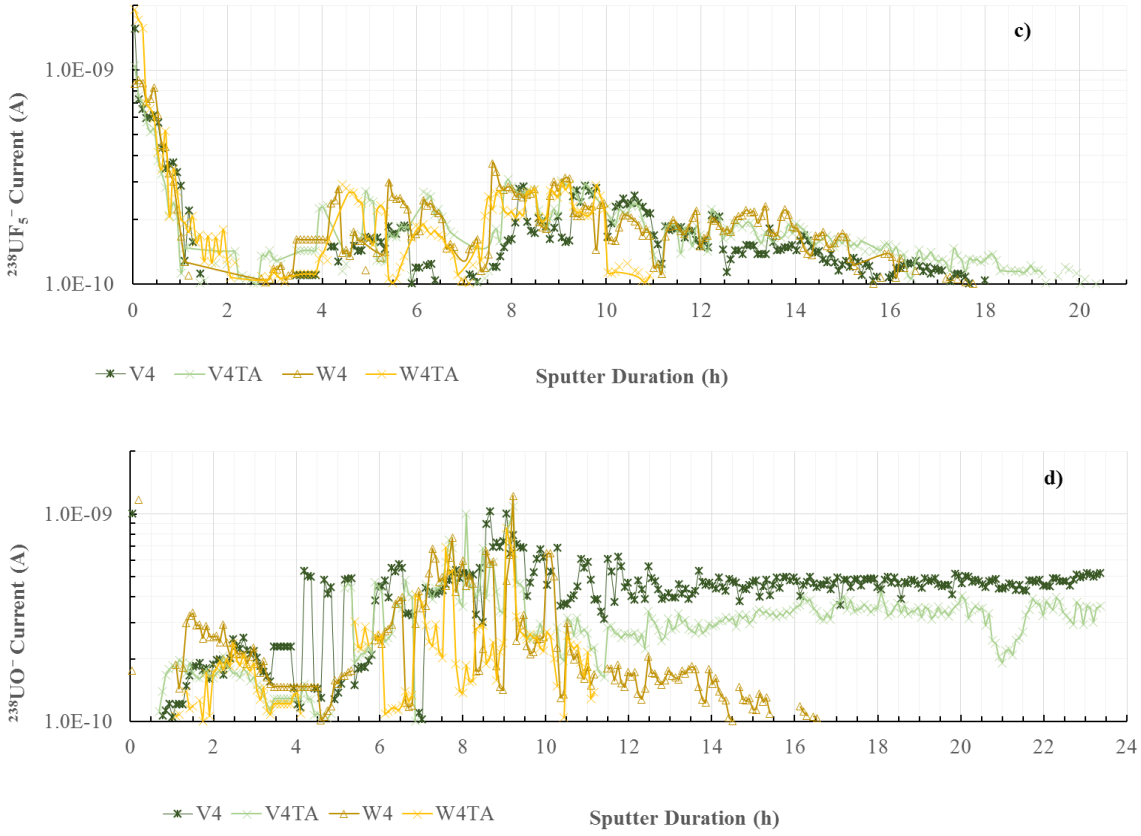

Figure 7.2.7 Temporal development of $^{238}UF_5^-$ (a, c) and $^{238}UO^-$ (b, d) currents[19] extracted from A5&A5TA, E2 & E2TA (a, b) and V4&V4TA, W4 & W4TA (c, d). Note: different scale of the horizontal axes. A5&A5TA, E2 & E2TA produced more UO^- than V4&V4TA, W4 & W4TA. All targets produced more UO^- than UF_5^-.

Moreover, as was observed also in the case of cathodes prepared at VERA, it took 10 to 15 minutes for the UO^- current to develop to a peak value, the UF_5^- current, in contrast, was at its maximum at the very beginning and experienced a rapid decrease in the first half hour. This might, however, be influenced by the source regulation in the first eight turns, corresponding to 2 hours of sputtering (see section 7.2.1.3).

c. Ionisation Efficiency

Figure 7.2.8 shows the temporal development of the integrated UF_5^- and UO^- ionisation efficiency. The results are also shown in table 7.2.5.

Overall, all UF_4 samples provided much poorer UF_5^- (max. 0.0071%) and UO^- (min. 0.0280%) ionisation efficiencies than those by VERA samples: UF_5^- (0.125%) and UO^- (max. 0.0110%). The UO^- ionisation efficiencies were better than UF_5^-, especially in the case of A5&A5TA and E2 & E2TA. Moreover, it can be reaffirmed that the heating procedure supressed the production of UO^-.

[19] Part of the data underwent modification detailed in section 7.2.1.3, resulting in the section with constant current value at a sputter duration around 4 h.

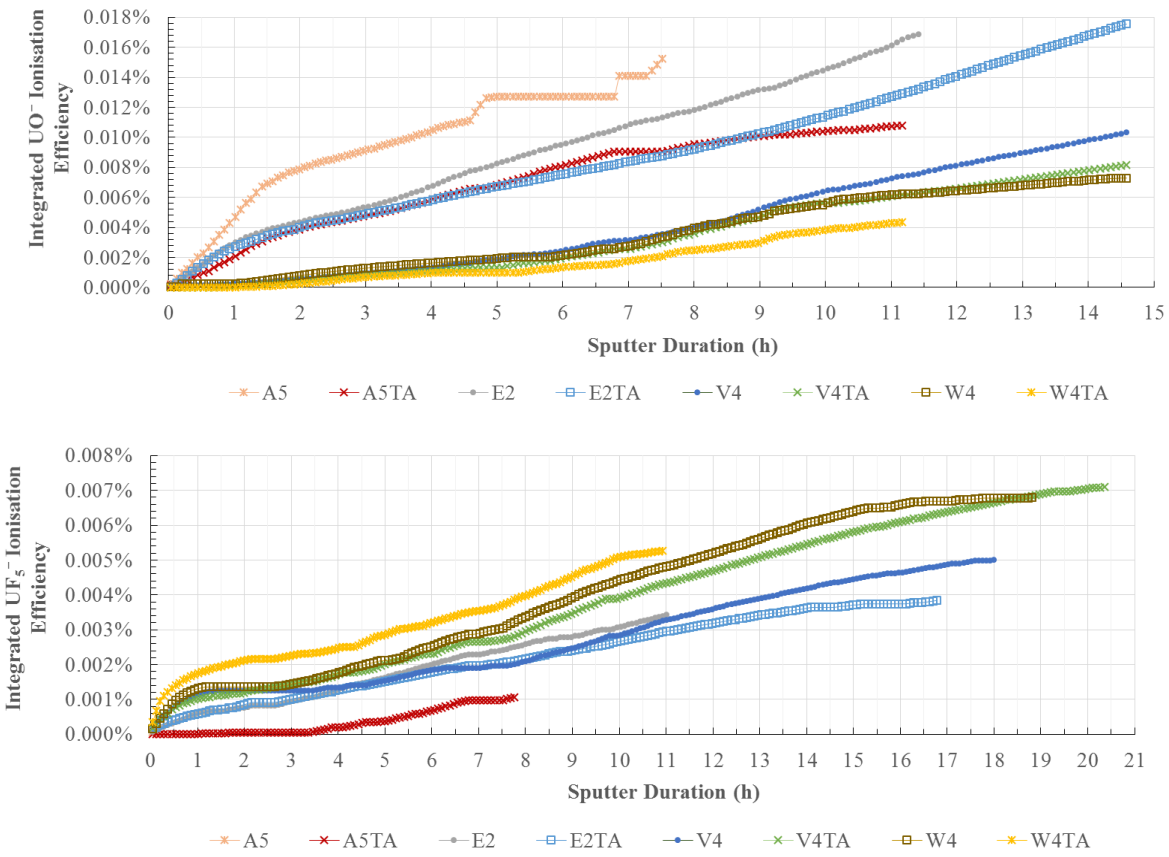

Figure 7.2.8 Temporal development of the integrated UF_5^- (up) and UO^- (down) ionisation efficiencies. Note: different scales of the horizontal as well as vertical axes

Uranium-Form	Code	UF_5^- Yield ($\times 10^{-5}$)	UO^- Yield ($\times 10^{-5}$)
UF_4	A5	0.1	15.3
	A5TA	1.1	10.8
	E2	3.4	16.9
	E2TA	3.8	28.0
	V4	5.0	17.9
	V4TA	7.1	14.3
	W4	6.8	7.5
	W4TA	5.3	4.3

Table 7.2.5 Ionisation efficiency of samples prepared in FNSPE CTU Prague

7.2.3 Conclusion from Experiment 1

Figure 7.2.9 shows a picture of the sample wheel after sputtering. Since not only the sample itself, but also the sample holder as well as the wheel was sputtered, the sample consumption efficiency can be assumed to be almost 100%.

As was discussed in section 7.2.2.2, the KkU D30 and Fe mixture provided a satisfatory UO^- ionisation efficiency despite a UO^- formation disorder for 6 hours. This

disorder appeared to be caused by PbF_2, which should nevertheless restore an ioniser surface "poisoned" by the coverage of UO_x which has a high melting point (Zhao et al 2016). Therefore, cathodes for UF_5^- and UO^- extraction should be separated in the experiments to follow.

This experiment, with a big range of variables, laid the foundations for a second one: as was discussed in section 7.2.2.2.a, some of the UF_4 samples produced more UF_x^- with U in lower oxidation states as well as UO_x^- and did not deliver a satisfactory yield of UF_5^-. Adding further fluoride donor into the matrix might provide chances of yield improvement. In order to gain more information about the influence of the sample size in the target holder on the yield, a set of targets containing different amounts of the same material should be studied. Further, various proportions of lead difluoride and KkU D30 would provide more data on the influence of the fluorine donor proportion on the formation of UF_5^-.

Figure 7.2.9 Sample wheel after sputtering

7.3 EXPERIMENT 2

As indicated in section 7.2.3, the second experiment had three goals:

- an investigation of possible performance improvement with an embedment of UF_4 in a lead difluoride matrix.
- an examination of the existence of a correlation between sample mass and ionisation efficiency.
- a study of the influence of the mass ratio of KkU D30 to PbF_2 on the UF_5^- ionisation efficiency.

7.3.1 Method

7.3.1.1 Sample Preparation

To achieve the aims mentioned above, five UF_4 samples prepared in FNSPE CTU: E2, V4&V4TA as well as W4&W4TA (see table 7.2.2 for specification) were mixed with PbF_2

to a rough mass ratio of 1:8; KkU D30 was mixed with lead difluoride to mass ratios of 1:8, 1:3 and 1:1 respectively; KkU D30 was mixed with Fe powder to a mass ratio of 1:2 for three samples with different masses. All mixtures were homogenised using a mortar. Further, the mixture of KkU D30 and PbF_2 with a mass ratio of 1:8 prepared roughly one months ago for the first experiment was included to inspect possible deterioration of the substance over time due to, e.g., possible water absorption. Thus, there were 13 targets included in this measurement. Specifications of these 13 targets are shown in table 7.3.1 (for specifications of the sample material see also table 7.2.1 and table 7.2.2).

Category	Mass Ratio UF_4:Matrix	Sample Mass (mg)	Uranium Mass (µg)	Uranium Concentration (µg/g)
E2 + PbF_2	1.0 : 7.7	2.60	17	6549
V4 + PbF_2	1.0 : 7.8	4.97	19	3880
V4TA + PbF_2	1.0 : 9.0	4.89	17	3479
W4 + PbF_2	1.0 : 8.2	4.23	17	4011
W4TA + PbF_2	1.0 : 8.6	2.41	10	4075
Category	**Mass Ratio KkU D30: Added Matrix**	**Sample Mass (mg)**	**Uranium Mass (µg)**	**Uranium Concentration (µg/g)**
KkU D30 + PbF_2	1.0 : 3.0	2.18	9	4178
KkU D30 + PbF_2	1.0 : 1.0	4.45	37	8415
KkU D30 + PbF_2 (old[20])	1.0 : 8.5	2.83	5	1759
KkU D30 + PbF_2	1.0 : 8.4	6.35	11	1769
KkU D30 + Fe (L)	1.0 : 2.1	4.50	24	5343
KkU D30 + Fe (S)	1.0 : 2.1	1.92	10	5343
KkU D30 + Fe (M)	1.0 : 2.1	2.85	15	5343

Table 7.3.1 Targets specifications

7.3.1.2 Measurement Principle

This measurement used roughly the same procedures as the first experiment (see Appendix A for details), except that the 2 mm instead of the 1 mm slit in front of FCI1-1was utilised for the automax current optimisation due to an oversight. For parking, parametric optimisation, mass calibration as well as source monitoring, two carbon cathodes from previous measurements as well as a non-weighed KkU were added to the target wheel.

[20] Prepared roughly 1 months before the experiment

The targets were put into two groups: targets containing lead difluoride took position 2-11; targets containing no lead difluoride took position 12-14. Cathodes 2-11 were not measured before the exhaustion of cathodes 12-14 so that there would be no interference from PbF_2 residue in the source during the extraction of UO^-. In addition, the scanned range was different according to the extracted ion: during the extraction of UF_5^-, the scanned HVS voltage range also covered mass 352, corresponding to UF_6^-[21].

The mass calibration was done with a target containing KkU and PbF2, since it was known from the first experiment that the highest peak at the beginning is $^{208}PbF_2^-$ neighboured by the $^{206}PbF_2^-$ and $^{207}PbF_2^-$ peak.

During the mass calibration, it was noticed that the mass resolution of this measurement was not optimal. A possible explanation was the application of the 2 mm instead of the 1 mm slit in front of FCI1-1 for current optimisation.

During the measurement, the same ion source issues detailed in section 7.2.1.3 occurred, hampering the six turns (roughly 1.5 h out of roughly 20 h measurement time) in the UO^- measurement. Consequently, data interpolation was necessary for this time span.

7.3.2 Results

7.3.2.1 UO^- Ionisation Efficiency & Sample Mass

a. Mass Scans

Figure 7.3.1 shows the mass scans 1, 3, 5, 7 of KkU D30 and Fe (S), which corresponds to 5 min, 15 min, 25 min and 35 min of sputter duration. As can be read from the figure, there were equidistant peaks at the position of 254 amu, 270 amu[22], 286 amu as well as 302 amu, which corresponds to UO^-, UO_2^-, UO_3^- and UO_4^-.

The UO_2^-, UO_3^- and UO_4^- peaks experienced steady reduction from the 1st to the 7th scan, whereas the UO^- peak experienced growth. This was also observed in the first experiment (see section 7.2.2.1.a).

[21] The scanned mass range from the first time did not cover UF_6^- since it was reported that UF_5^- shows a higher intensity than UF_5^- when sputtering a mixture of uranium metal and PbF_2 with Cs^+ (Zhao et al 2010). UF_6^- was covered in the second experiment to see if this also applies to the sample matrices applied here.
[22] See page 38

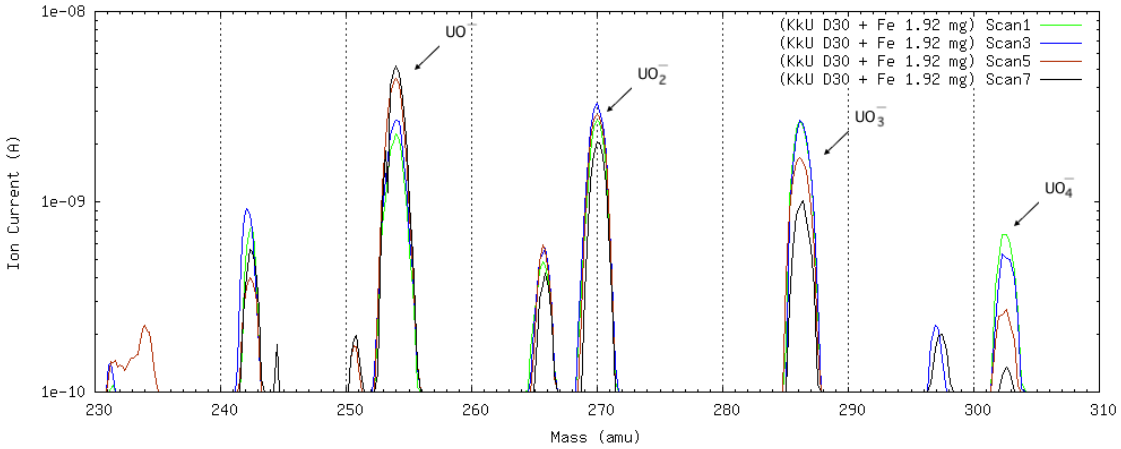

Figure 7.3.1 Mass scans 1, 3, 5, 7 (sputter duration: 5, 15, 25, 35 min) of KkU D30 and Fe mixture (S). An increase of UO^- and decrease of UO_2^-, UO_3^- and UO_4^- beam intensity was observed.

b. Current Development

Figure 7.3.2 shows the temporal development of the UO_x^- currents.

Overall, the UO^- intensity was comparable with that of the first experiment: target L produced a steady current of UO^- over 2 nA for the first 5.5 hours; the UO^- intensity from target M reached almost 9 nA at one point, but dropped to 2 nA after 4 hours; target S produced a UO^- current over 2 nA for only an hour. There was a positive correlation between the sample mass and the UO^- current most of the time.

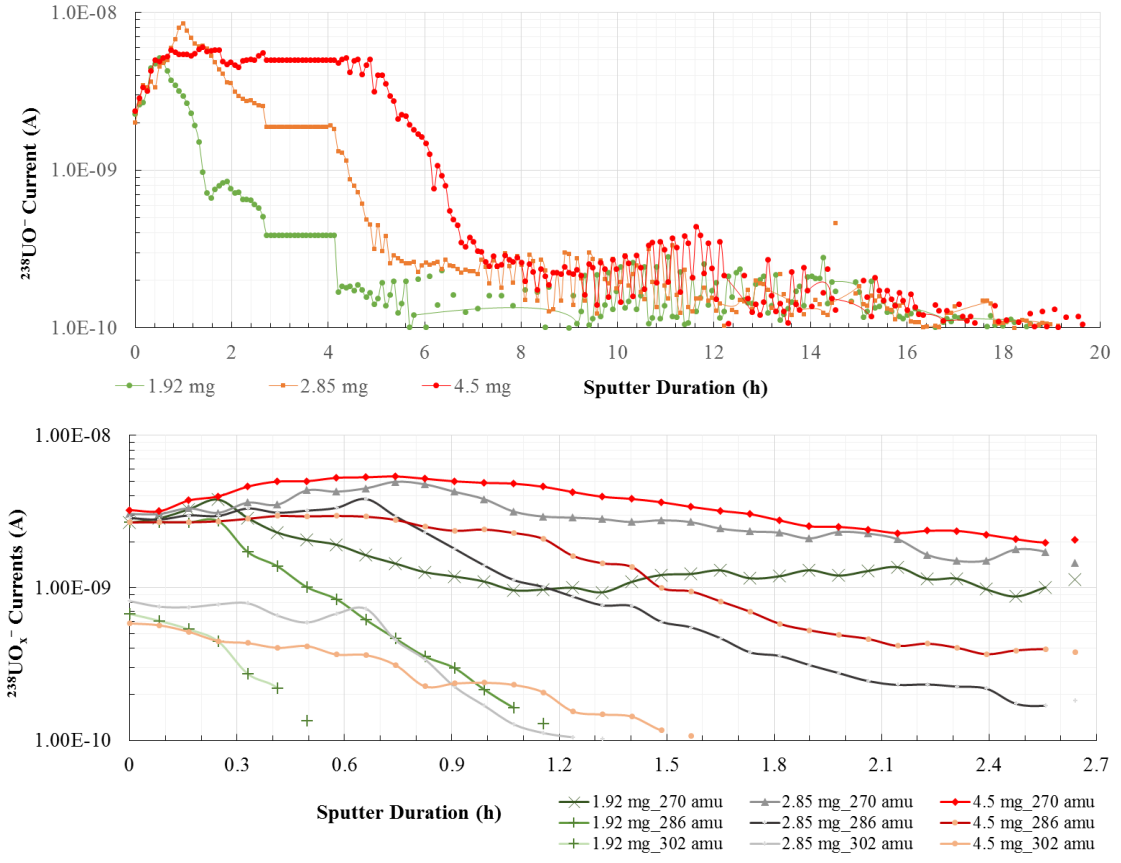

Figure 7.3.2 Temporal development of $^{238}UO^-$ (up) and $^{238}UO_x^-$ (down) currents. Note: different scales of the x-axes. UO_x^- currents with x>1 were at their peak values at the beginning and lasted only for around 2 hours. UO^- currents needed 15 min to develop to a reasonable value. These UO^- currents lasted for around 5 hours.

An UO^- ion current disturbance like that described in section 7.2.2.1.b did not occur, which could be taken as evidence that PbF_2 lingering in the source caused the observed UO^- formation disturbance in the first experiment.
Like in the first experiment, it took around 15 min for the UO^- current to develop to a reasonable value. Meanwhile, most of the UO_2^-, UO_3^- and UO_4^- currents were reduced.

With respect to the uranium contained, target S (figure 7.3.2 left) produced a considerable amount of UO_x^- of higher orders at the beginning. During the increase and stabilisation of the UO^- ion formation, target S was sputtered, partly to produce UO_x^- of higher orders, which led to its exhaustion after the stabilisation of the UO^- output.

c. Ionisation Efficiency

Figure 7.3.3 shows the temporal development of the UO_x^- ionisation efficiencies. The results are also shown in table 7.3.2.

Overall, UO^- ionisation was almost four times more efficient than in the first experiment, which could be a result of the increased Fe proportion in the material (see table 7.2.1) and the absence of potential ion formation obstruction caused by lead difluoride.

Ionisation efficiencies of UO_2^- [23] and UO_3^- were significant. Target S, with the shortest lifetime, rendered a considerable amount of uranium into UO_2^- and UO_3^-, which could be taken as a reason for its relatively low UO^- yield.

Material Composition	**Sample Size**	**Sample Mass (mg)**	**IE UO^-**	**IE UO_2^-**	**IE UO_3^-**	**IE UO_4^-**
KkU D30 + Fe (Mass Ratio 1.00 : 2.12)	S	1.92	0.68%	0.36%	0.13%	0.02%
	M	2.85	1.06%	0.46%	0.22%	0.04%
	L	4.50	1.11%	0.37%	0.16%	0.02%

Table 7.3.2 UO_x^- ionisation efficiencies (IE)

[23] see page 38

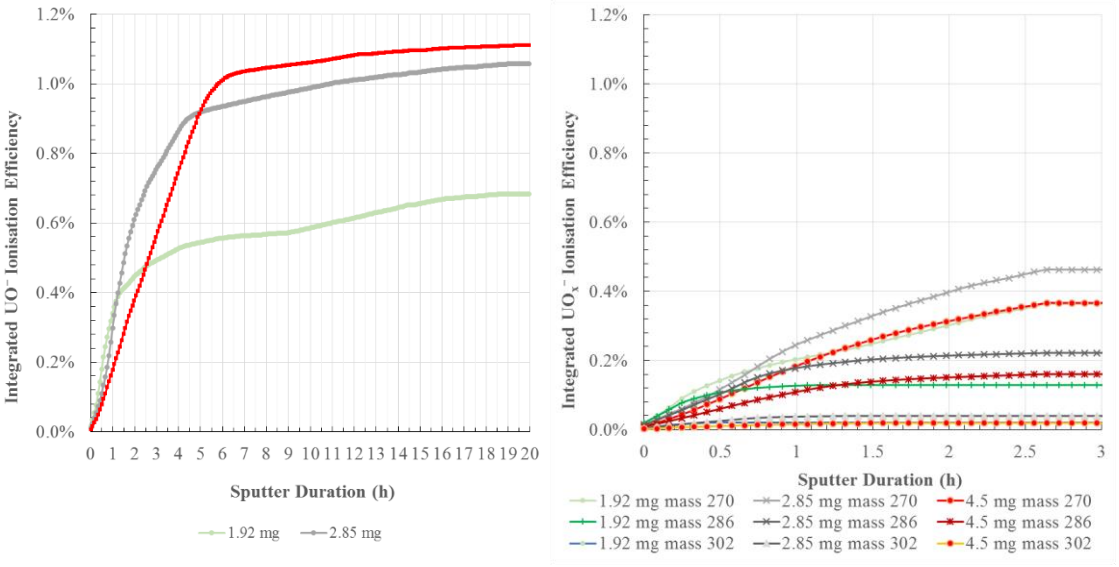

Figure 7.3.3 Temporal development of the integrated UO_x^- ionisation efficiencies. Vertical axes of both figures have the same scale for a better comparison

7.3.2.2 UF_5^- Ionisation Efficiency & PbF_2 Proportion

a. Mass Scans

Figure 7.3.4 shows the third mass scans (sputter duration: 15 min) of KkU D30 and PbF_2 mixtures. As can be seen, the non-optimal mass resolution led to merging of peaks and hampers the evaluation of the UF_5^- measurement.

Evidently, the KkU D30 and PbF_2 mixture with a mass ratio of 1:1 produced significant UO^-, UO_2^- and UO_3^- currents at the beginning.

Following UF_x^- peaks can be identified: UF_3^- (295 amu), UF_4^- (314 amu), UF_5^- (333 amu) and UF_6^- (352 amu)[24], amongst which UF_5^- is the highest. This observation is in general accord with Zhao et al's report (2010).

Further, target prepared roughly one months earlier than others produced more UF_3^- , UF_4^- as well as UF_6^-, for which there is currently no explanation at hand.

[24] Due to the poor mass resolution, the UF_6^- peak was merged with the Al_{13}^- peak after the full consumption of the sample.

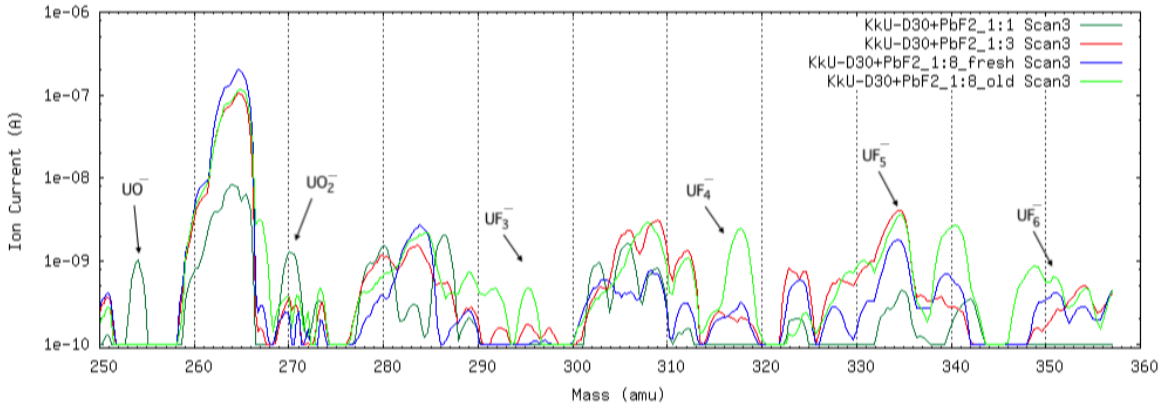

Figure 7.3.4 Mass scans 3 (sputter duration: 15 min) of KkU D30 and PbF_2 mixtures. Target with a KkU D30 and PbF_2 mass ratio of 1:1 produced much more uranium oxide ion than others. Further, target prepared roughly one month earlier than others (old) produced more UF_3^- , UF_4^- as well as UF_6^-.

b. Current Development

Figure 7.3.5 shows the temporal development of the UF_5^- and UO^- currents.

There seemed to be no obvious correlation between the PbF_2 proportion and the UF_5^- beam intensity. Generally, the UF_5^- output ranged from 1 to 3 nA before it dropped to 1/10 of its original value after roughly 1 hour of sputtering. In comparison with the output of the same material in the first experiment, the output at the beginning was more moderate and this 1 to 3 nA output lasted longer (1 hour instead of 0.5 hour in the first experiment). Factors that contributed to this could be: first, a source regulation aiming at output-maximisation was used at the beginning of the first experiment, which is not the case in this experiment (see Appendix A); second, although the size of the KkU D30 and PbF_2 target (14.75 mg) in the first experiment was considerably larger than those in the second experiment, a great portion of it was consumed right at the beginning.

As was described in section 7.3.2.2.a, KkU D30 and PbF_2 mixture with a mass ratio of 1:1 produced a considerable amount of UO^-: it is shown in figure 7.3.5 that its UO^- beam had a higher intensity than that of the UF_5^- most of the time. Generally, the higher the PbF_2 proportion, the lower the UO^- current.

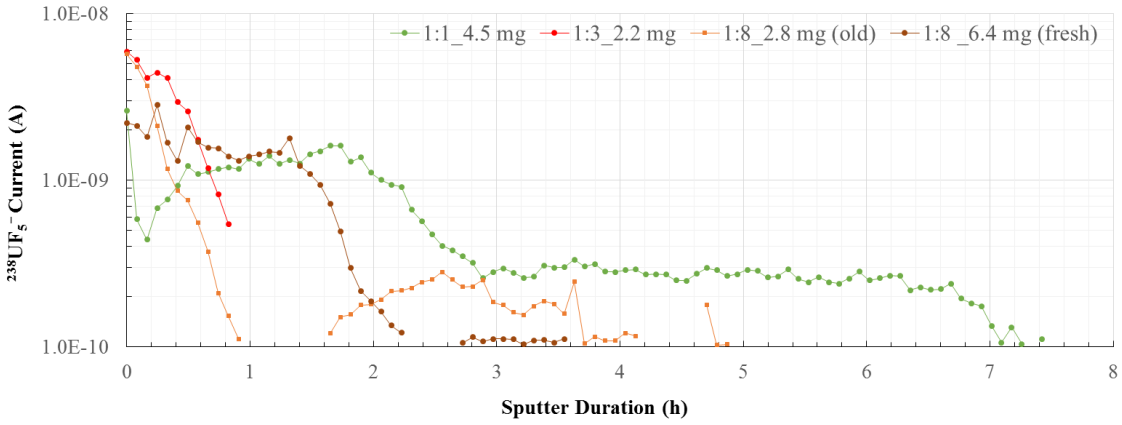

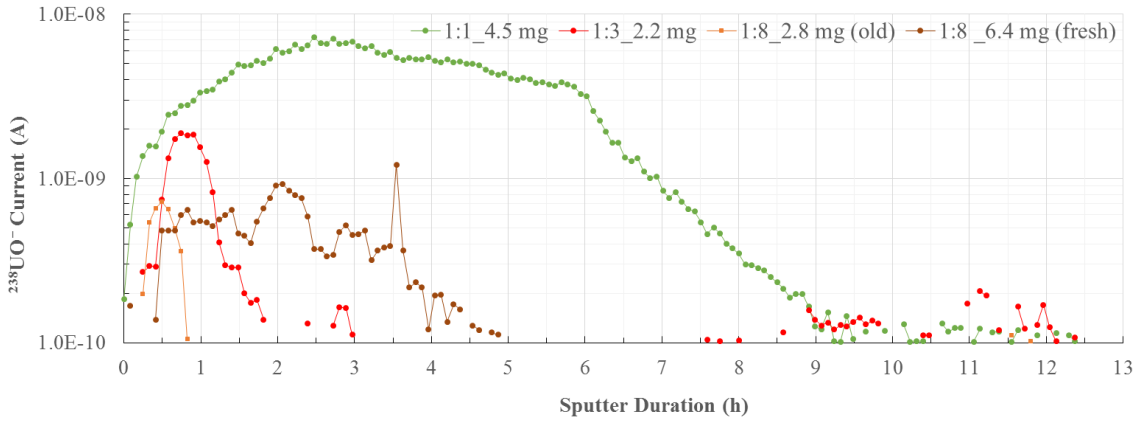

Figure 7.3.5 Temporal development of $^{238}UF_5^-$ and $^{238}UO^-$ currents extracted from targets containing KkU D30 and PbF_2 (legend: mass ratio_target mass): the target with the smallest PbF_2 proportion produced the lowest UF_5^- and highest UO^- intensity.

c. Ionisation Efficiency

Figure 7.3.6 shows the temporal development of the UF_5^- and UO^- ionisation efficiencies. The results are also shown in table 7.3.3.

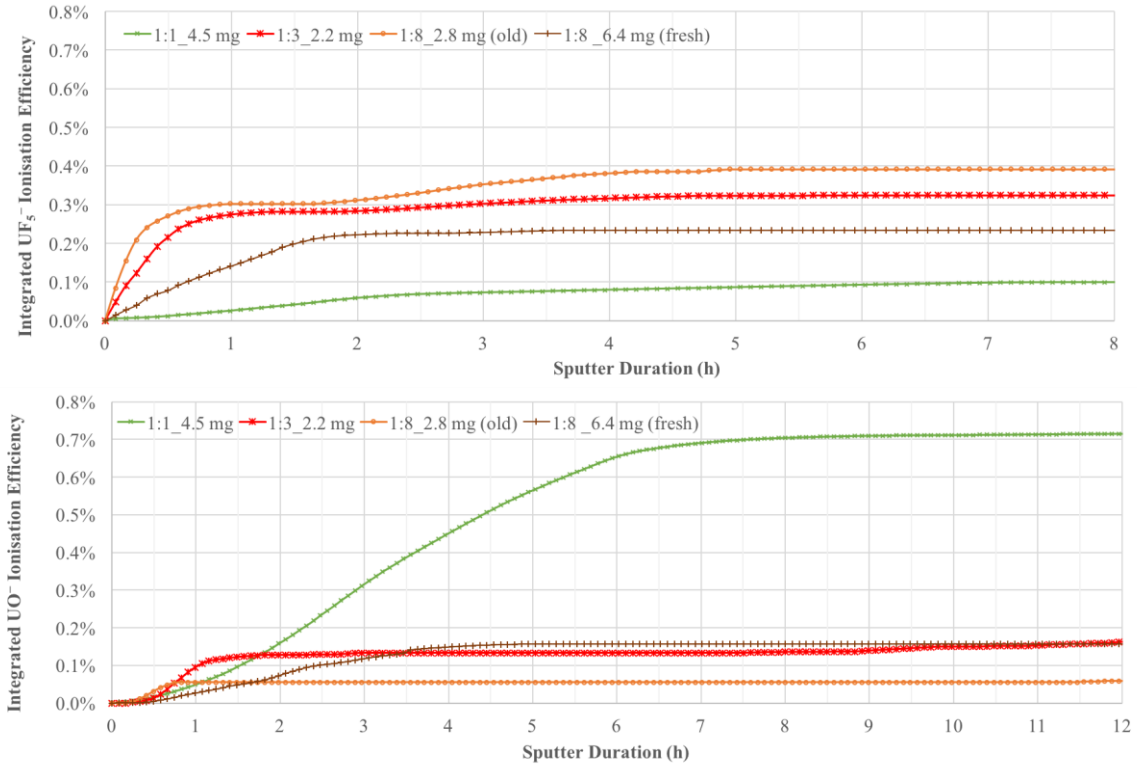

Figure 7.3.6 Temporal development of the integrated UF_5^- and UO^- ionisation efficiencies from targets containing KkU D30 and PbF_2 (legend: mass ratio_target mass): PbF_2 proportion more than ½ provided better UF_5^- ionisation efficiencies; PbF_2 proportion of ½ provided better UO^- ionisation efficiency. The vertical axes were set to the same scale to facilitate comparison.

The UF_5^- ionisation efficiencies of samples with PbF_2 mass proportions greater than 1/2 were much higher than that in the first experiment. A KkU D30 and PbF_2 mass ratio of 1:3 is sufficient for a reasonable ionisation efficiency. Further, deterioration of KkU D30 and

PbF_2 mixture over time can be ruled out: although the sample prepared on February the 6th of Feb had roughly half the mass of that prepared on the 13th of March, it outperformed the latter.

Date of Preparation	Material	Mass Ratio	Sample Mass (mg)	IE UF_5^-	IE UO^-
13th Mar.	KkU D30 + PbF_2	1.0 : 1.0	4.45	0.10%	0.72%
	KkU D30 + PbF_2	1.0 : 3.0	2.18	0.32%	0.16%
	KkU D30 + PbF_2	1.0 : 8.4	6.35	0.23%	0.16%
06th Feb.	KkU D30 + PbF_2	1.0 : 8.5	2.83	0.39%	0.06%

Table 7.3.3 UF_5^- and UO^- ionisation efficiencies

7.3.2.3 UF_4 Samples in PbF_2 Matrix

a. Mass Scans

Figure 7.3.7 shows the third mass scans of UF_4 and PbF_2 mixtures. A comparison of it with figure 7.2.6 a) and b) in the first experiment shows that embedding UF_4 in a PbF_2 effectively supressed UF_x^- of orders lower than 5 and facilitated the formation of UF_5^-. However, there was still a considerable amount of UAl_2^- (292 amu) generated.

Further, only the E2 and PbF_2 mixture showed a UO^- peak, which is in accordance with the observation in the first experiment.

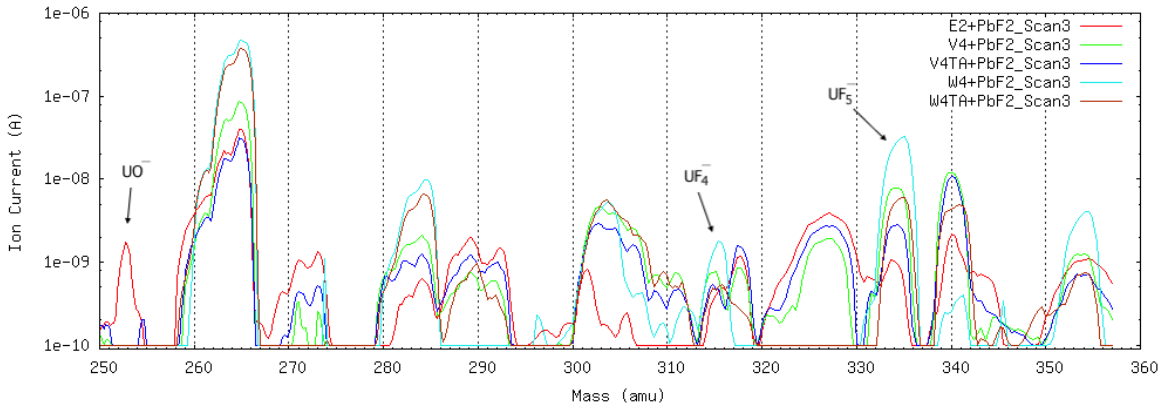

Figure 7.3.7 Mass scans 3 (Sputter duration: 15 min) of UF_4 and PbF_2 mixtures. Embedding UF_4 in PbF_2 matrix effectively supressed the formation of UF_x^- with x<5 (compare: figure 7.2.6 a and b).

b. Current Development

Figure 7.3.8 shows the temporal development of the UF_5^- and UO^- currents. The UF_5^- currents were much larger (around 10 nA) than those in the first experiment (around 1 nA) at the beginning, but decreased rapidly after the first 30 minutes. The targets' life time was around 14 hours, though the currents were generally reduced to below 1 nA after the first 3 hours. These small currents then continued for another 10 hours before it was exhausted.

E2 in PbF_2 matrix produced a UO^- current around 0.4 nA in the first five hours. This further supports the assumption in the first experiment that using H_2O as solvent and $CaCl_2$ as carrier facilitated the formation of UO^- ion. As contrasted with V4 and V4TA, which produced a UO^- current around 0.4 nA in the first three hours, W4 and W4TA produced only a negligible amount of UO^-.

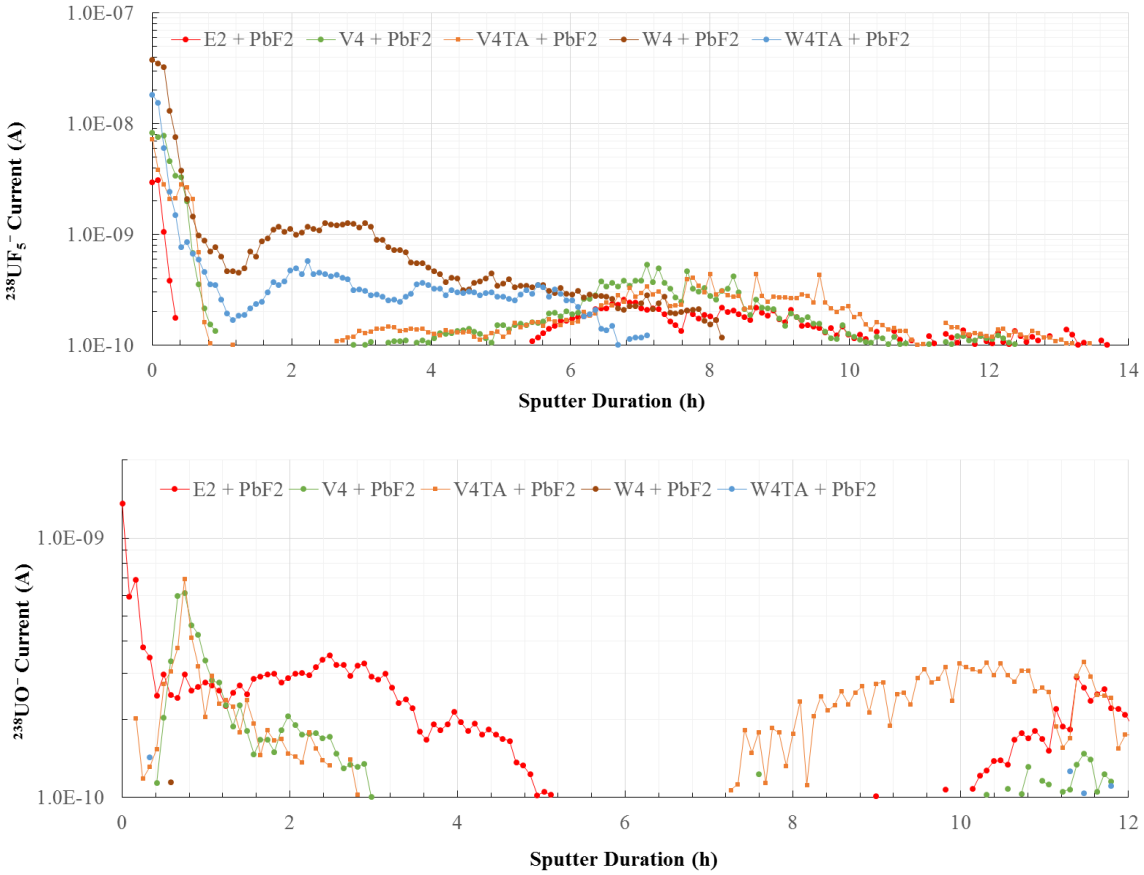

Figure 7.3.8 Temporal development of $^{238}UF_5^-$ and $^{238}UO^-$ currents from UF_4 and PbF_2 mixtures. Embedding UF_4 in PbF_2 matrix effectively supressed the formation of UO^-.

c. Ionisation Efficiency

Figure 7.3.9 shows the temporal development of the UF_5^- and UO^- ionisation efficiencies. The results are also shown in table 7.3.4.

Judging by the results, embedding UF_4 in PbF_2 matrix improved the UF_5^- ion formation considerably. Not only the beam intensity, but also the ionisation efficiency of UF_5^- was much higher. Unlike in the first experiment, ionisation efficiencies of UF_5^- is generally much higher than that of UO^-. Mixtures with W4 / W4TA produced, as was observed in 7.3.2.3.a and b, almost at all. E2, V4 as well as V4TA, however, provided a UO^- ionisation efficiency greater than that of the first experiment.

In comparison with KkU in PbF_2 matrix, UF_4 in PbF_2 matrix offered not only potemtial improvement of the UF_5^- beam intensity at the beginning, but also its ionisation efficiency (W4 and W4TA).

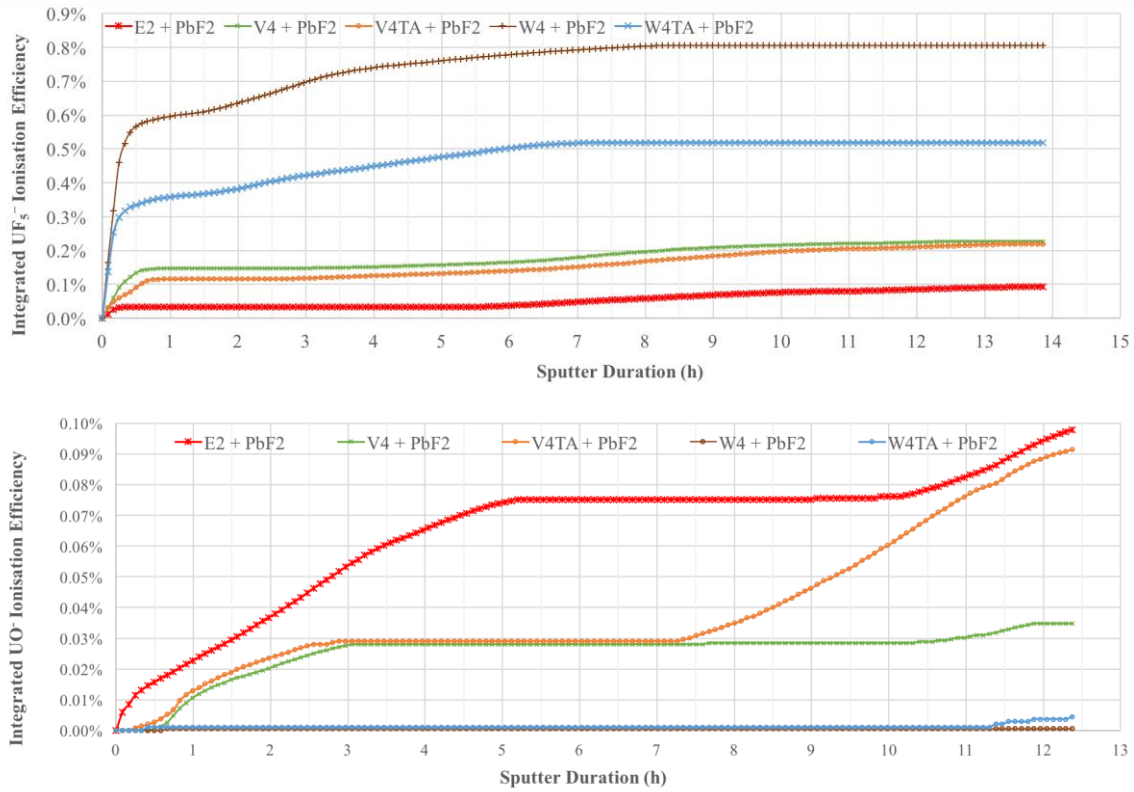

Figure 7.3.9 Temporal development of the integrated UF_5^- and UO^- ionisation efficiencies. Note: different scale of the axes

Code (Uranium Form)	Matrix	Mass Ratio	IE UF_5^-	IE UO^-
E2 (UF_4)	PbF_2	1.0 : 7.7	0.09%	0.10%
V4 (UF_4)	PbF_2	1.0 : 7.8	0.23%	0.03%
V4TA (UF_4)	PbF_2	1.0 : 9.0	0.22%	0.09%
W4 (UF_4)	PbF_2	1.0 : 8.2	0.81%	0.00%
W4TA (UF_4)	PbF_2	1.0 : 8.6	0.52%	0.00%

Table 7.3.4 UF_5^- and UO^- ionisation efficiencies

7.3.3 Conclusion from Experiment 2

This experiment showed that adding further iron powder to a mixture of KkU D30 and iron powder with a mass ratio of 1:1 and having a PbF_2-free ion source for UO^- extraction increased the UO^- ionisation efficiency.

For UF_5^- extraction using KkU D30 and PbF_2 mixtures, a mass ratio of 1:3 was sufficient for a UF_5^- ionisation efficiency of 0.32%. Further, UF_4 in a PbF_2 matrix has a better

applicability than UF_4 alone for the formation of UF_5^-. However, UF_4 samples produced small currents (usually under 1 nA) of UF_5^- after an initial 0.5 hours, in which strong 1-30 nA UF_5^- current were produced. These small currents lasted for around 13 hours until the target holder as well as the wheel itself was sputtered (see figure 7.2.9[25]). Therefore, it was postulated that F^-, a chemically reactive material and available in a great quantity during the sputtering process, attacked the aluminium target holder and the uranium compounds penetrated/diffused in the aluminium target holders, which made the extraction at the end only possible when the target holder itself was sputtered.

Furthermore, it was observed during the measurement that the ion source was in an unstable condition during UF_5^- extraction. Since the targets made only for UO^- extraction and those for UF_5^- extraction were measured under the same set of source parameters, it was proposed that an adoption of another set of parameters for UF_5^- extraction might provide potential performance improvement.

Therefore, further experiments should be conducted for:

I. an examination of source parameters for UF_5^- formation;
II. a confirmation of the positive correlation between sample mass and the ionisation efficiency for UF_5^-;
III. an application of sample holders that do not react with fluorine;
IV. an examination of the relation between proportion of the matrix material and the UO^- ionisation efficiency by mixtures of KkU D30 and iron.

7.4 EXPERIMENT 3

The third experiment had aim I and II in section 7.3.3.

According to Zhao et al (2016), lead difluoride undergoes diffuse phase transition, when the target temperature is above 250 °C, which leads to high F^- ion mobility in PbF_2 and renders the material, an insulator in other conditions, electrically conducting. High temperatures, furthermore, causes effective mixing of elements and chemical reactions generating fluoride anions. This finding led to the decision to take the ioniser power (IONPW, see section 2.1) as a first source parameter to examine, since this parameter contributes the most to the temperature in the source.

[25] The wheel not only looked like this after sputtering in the first experiment, but also in all experiments with uranium.

7.4.1 Method

This experiment included only KkU D30 mixed with PbF_2 to a mass ratio of roughly 1:8, prepared with the same procedures detailed in section 5.2.1.2. Sample specifications are shown in table 7.4.1.

7.4.1.1 Measurement Principle

To examine the impact of the IONPW on the target anion output and its ionisation efficiency, all other source parameters should be kept constant. Therefore, samples were divided into three groups to be sputtered with three different IONPW, each group containing three to four targets of roughly 5 mg, 3 mg and 1 mg. This means the measurement can be divided in two three sub-measurements with three different IONPW.
However, the insertion of all cathodes into one wheel at the beginning of the measurement would result in the exposure of all cathodes to caesium vapour during the first sub-measurement, which might influence the ionisation efficiency, having only one group of cathodes in the wheel during one sub-measurement would be advantageous. Thus, the target wheel was taken out of the source after each sub-measurement to have the same initial conditions.

Three cathodes containing same material as measurements cathodes were used for parametric optimisation and scale setting. All sub-measurements followed the routine procedures detailed in Appendix A.

During measurements with IONPW set as 187 and 160 W, the source regulation HVSCR was set as Slow. However, setting the IONPW to 205W and having the regulation HVSCR on at the same time made the maintenance of the IONPW impossible, since the source regulation turned the IONPW to a lower value almost immediately. Thus, during the measurement with IONPW set as 205 W, source regulation was turned off.

7.4.2 Results

The temporal developments of the UF_5^- currents and the integrated UF_5^- ionisation efficiencies are shown in figure 7.4.1 and 7.4.2, respectively. Since the formation of UO^- was not the primary goal of this experiment, its ionisation efficiencies are only shown in table 7.4.1 as reference.

All targets were exhausted within 3 hours. A high ioniser power meant a shorter life time of a target. However, there seemed to be no obvious correlation between the ioniser power and the beam intensity. There seems, however, to be a weak positive correlation between the ioniser power and the ionisation efficiency (except for the 2.58 mg target measured with IONPW 160). An ionisation efficiency improvement of around 3-10% could be achieved with an ioniser power of 205 W instead of 187 W. It could be taken to suggest that high temperature in the source may have facilitated the plasma ball formation and the ionisation process, leading to a higher beam intensity normalised to uranium mass (see table 7.4.1), an earlier exhaustion of the target and a higher ionisation yield overall.

Further, a large sample (5-6 mg) generally provided a current of a few nA for a longer time than small ones and the ionisation efficiency tended also to be better than smaller samples (max.: 30% ionisation efficiency increase by using a sample of 5-6 mg).

In comparison with the results of UO^- ionisation efficiency using KkU D30 and iron mixtures (see section 7.3.2.1), the UF_5^- ionisation efficiencies were still relatively low and the currents were rather unstable. A solution of this problem needs to be seeked.

Sample Material	IONPW (W)	Sample Mass (mg)	Avg UF_5^- Current Normalised to Uranium Mass (pA/µg)	IE UF_5^-	IE UO^-
KkU D30+PbF_2 Mass Ratio 1.0 : 8.4	160	2.02	221	0.17%	0.03%
		2.58	319	0.30%	0.02%
		5.85	106	0.27%	0.08%
	187	1.17	359	0.17%	0.13%
		2.20	269	0.21%	0.14%
		3.09	173	0.19%	0.12%
		6.16	160	0.30%	0.12%
	205	1.12	404	0.19%	0.04%
		2.56	257	0.24%	0.03%
		3.01	217	0.29%	0.06%
		4.01	196	0.31%	0.07%

Table 7.4.1 Samples specifications, average UF_5^- currents normalised to uranium mass, UF_5^- and UO^- ionisation efficiencies

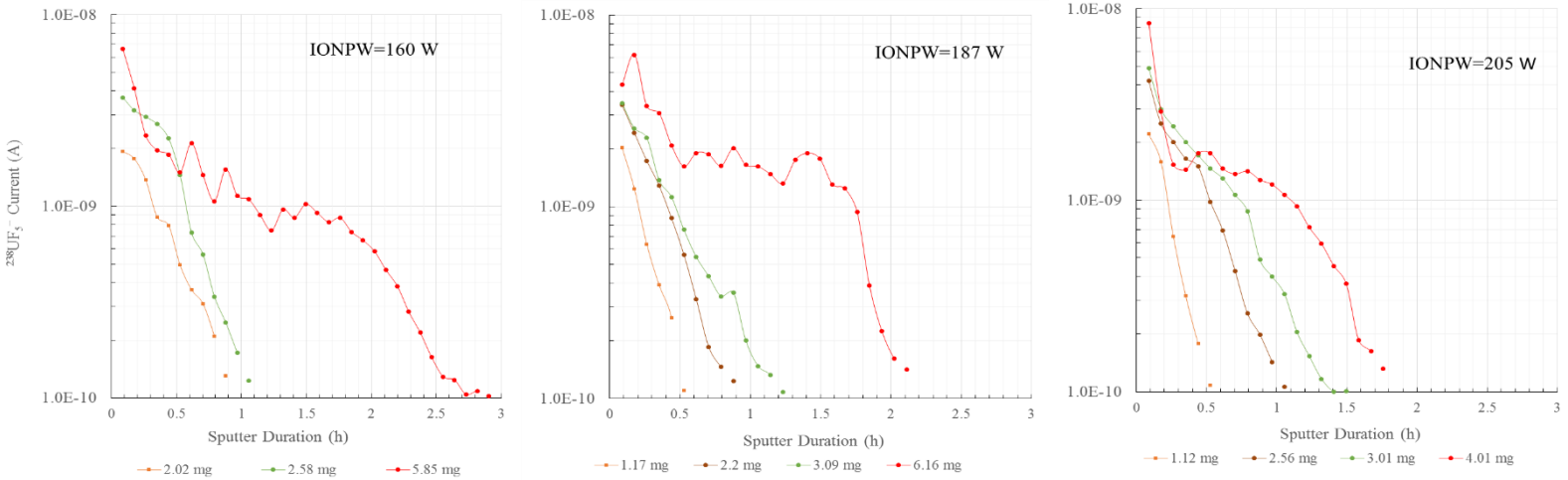

Figure 7.4.1 Temporal development of UF_5^- currents from UF_4 and PbF_2 mixtures (mass ration 1:8) with various ioniser power. An increase of the ioniser power did not seem to bring about an increase of the ion current intensity as such, but a shortening of targets' life time.

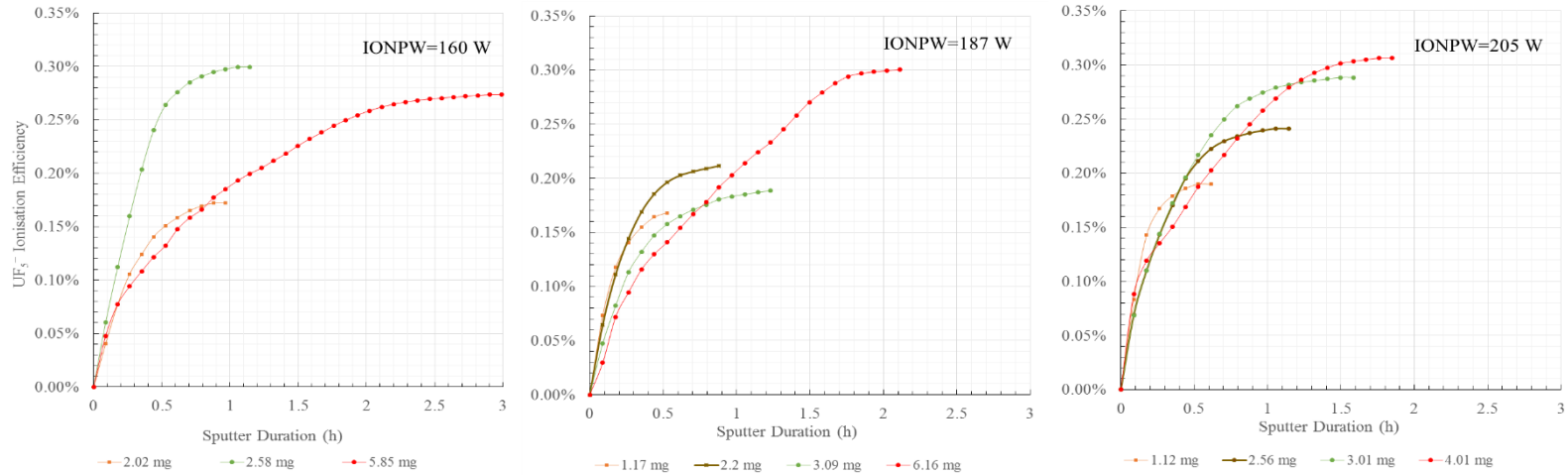

Figure 7.4.2 Temporal development of the integrated UF_5^- ionisation efficiencies of UF_4 and PbF_2 mixtures (mass ration 1:8) with various ioniser power. An increase of the ioniser power brought about a slight increase of the ionisation efficiency in most cases (around 3-10% with an increase from 187 to 2015 W).

7.5 EXPERIMENT 4

The fourth experiment, as was indicated in section 7.3.3, focussed on:

I. the investigation of the fluorides' potential reaction with the target holder material. Cathode inserts made from the noble metal gold were used.
II. examining the influence of iron proportion on the UO^- ionisation efficiency (mass ration of KkU D30 and iron: 1:1 and 1:2).
III. an examination of uranium carbides' applicability as secondary ions (see section 7.1).

7.5.1 Method

7.5.1.1 Sample Preparation

a. Preparation of Cathodes without Inserts

Targets consisting KkU D30 and iron were prepared with the procedures detailed in section 5.2.1.1. Sample specifications are shown in table 7.5.1 in section 7.5.2.1 c.

For uranium carbide extraction, KkU D30 and graphite were mixed to mass ratios of 1:1 and 1:2 respectively. However, since it offered no valid data for evaluation (see section 7.5.2.1), the specifications were left out in table 7.5.1.

b. Preparation of Cathodes with Inserts

The UF_4 material chosen to be tested with inserts was V4TA and PbF_2 mixture from Experiment 2, since it produced a UF_5^- current of around 0.2 nA after 8 hours of sputtering (see section 7.3.2.3) and seemed to be affected the most by the presumed reaction between the sample material and the target holder.

As a noble metal that is resistant to most chemical reactions, it was proposed that small gold target holders should be prepared for UF_4. Therefore, two cathode inserts were made from a gold wire[26].

Since the commercial 2.0 mm ø gold wire could not be encompassed in the cutting equipment, it was first made thinner (1.8 mm ø) with a sand paper and an electric drill which brought the wire into rotation. Afterwards, it was cut into 3 mm long sections and weighed. Two of these gold wire sections were used in this experiment.

Wells were created in the gold sections with a stamp (figure 7.5.1.a). The stamp pin used here was pointed (figure 7.5.1.b right). The wells were then filled with the residual V4TA and PbF_2 from experiment 2. The material was firmly pressed in the well with a

[26] Alfa Aesar 14729. Purity: 99.95%.

shorter and blunter stamp pin (figure 7.5.1.b, left). A filled gold insert is shown in figure 7.5.1 c.

In this way, targets held by inserts were double-pitted: not only was the sputter surface pre-pitted, but also the target holder.

The gold inserts were then weighed and brought into normal aluminium target holders. To make sure that the inserts do not fall out of normal target holders, they were pressed again with the blunter pin (figure 7.5.1.b, left). Figure 7.5.1.d shows a cathode with a gold insert prepared in this manner.

Copper inserts were made as practice before using the gold wire. One of the practice inserts was filled and used in the experiment as reference.

Also used as reference was a target with similar mass in a normal aluminium target holder.

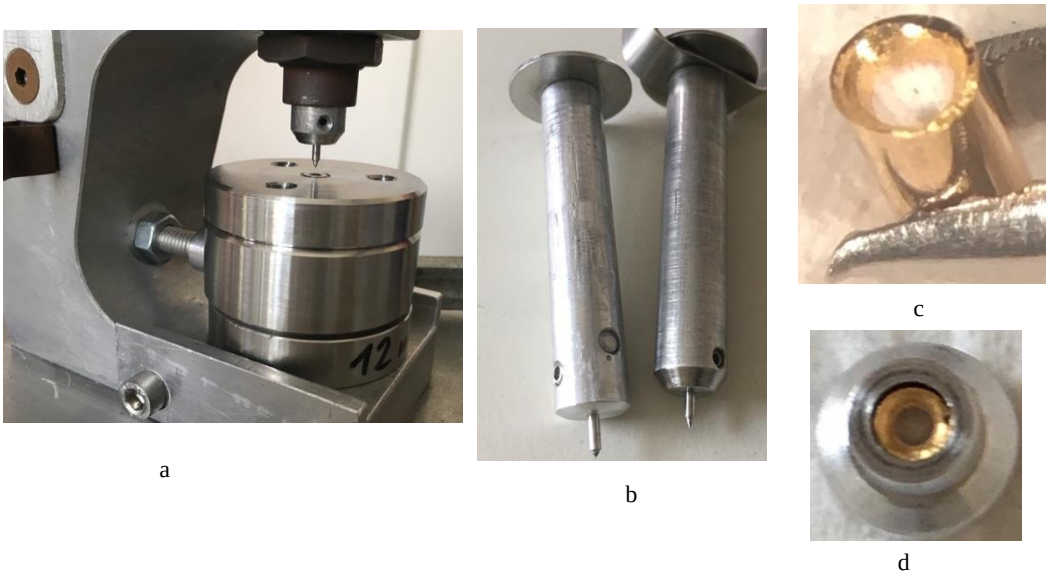

a b c d

Figure 7.5.1 a. aperture for pressing wells in gold wire as well as for pressing material into gold inserts. b. stamp pins used for creating wells in gold wire (right), pressing materials into the inserts (left) and pressing gold inserts into normal aluminium target holders (right) c. a gold insert filled with sample material d. a prepared cathode with a gold insert

7.5.1.2 Measurement Principle

To avoid potential negative influence of the presence of fluorides in the source on the extraction of other secondary ions than UF_5^-, uranium carbide as well as uranium oxide anions were measured before the measurement of uranium fluoride anions.

For the measurement of carbide anions, a mass range from 236 amu to 278 amu was scanned.

A target containing KkU D30 and niobium mixture, which was prepared for the first experiment and was not included, was measured along with targets containing KkU D30 and iron as reference.

7.5.2 Results

7.5.2.1 Applicability of Uranium Carbide Anions

a. Mass Scans

Figure 7.5.2 shows the third mass scans (sputter duration: 15 min) of six targets consisting KkU D30 and graphite with rough mass ratios of 1:1 and 1:2. Since the scanned mass range from 236 amu to 245 amu did not show any peaks at all, it was left out.

Three equidistant peaks at 253 amu, 265 amu and 276 amu could be recognised. In the cases of 253 amu and 276 amu, there was a positive correlation between the proportion of graphite in the material and the height of the peaks. Therefore, these peaks were identified as caesium carbide anions.

Uranium-containing ions collected were UO^- (around 2 nA) and UC_2^- (less than 0.2 nA). KkU D30 and graphite with rough mass ratios of 1:2 did not produce any carbide ion in this scan. This observation contributed to a premature termination of the measurement.

The measurement was terminated when a KkU D30 and graphite target with a mass ratio of 1:2, in the ninth scan (45 min), still provided no uranium carbide anions. It was only noticed after the measurement stop that there were targets (especially those with mass ratios of 1:1) which did provide UC_2^- currents that grew over time. In the 12^{th} scan (sputter duration: 1 hour), the value reached 0.7-0.8 nA. This is shown in figure 7.5.3.

Thus, it took around an hour for the UC_2^- current to develop to an applicable intensity. A possible explanation is that the used graphite powder (Alfa Aesar 14735) is very fine - grained (-100 mesh) and its mixture with KkU D30 was not homogeneous. Hence, carbon atoms needed to be first sputtered away so that uranium is exposed to the primary ion. This argument could find support in the general increase of the UO^- current over time in figure 7.5.3.

The UC^- intensity was, in this case, smaller than that of UC_2^-. It took 45 min of sputtering before the intensity of UC^- was sufficienctly high to be detectable by the FC. This is in accord with what Middleton (1989) and Buompane et al (2015) reported (see section 7.1).

The measurement was stopped before any more insights could be gained. Nevertheless, it could be taken as a suggestion for a smaller carbon proportion for the extraction of uranium carbides.

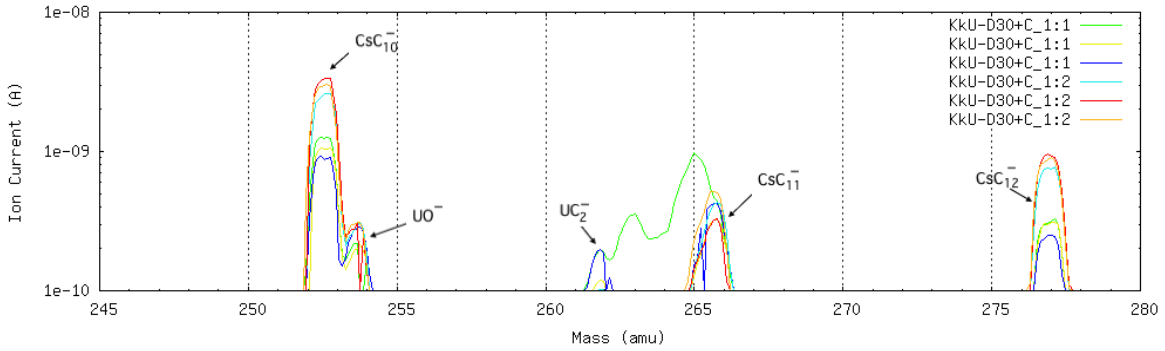

Figure 7.5.2 Mass scans (section 245-280 amu) of KkU D30 and graphite mixtures sputtered for 15 minutes. The highest peaks were identified as caesium carbide ions[27] because of the equal mass differences (12 amu) and the positive correlation between the height of the peak and the mass proportion of the graphite. Only a small amount of UO^- was produced and KkU D30 and graphite mixtures with a 1:1 mass ratio produced an amount of UC_2^- right above the resolution of the Faraday cup.

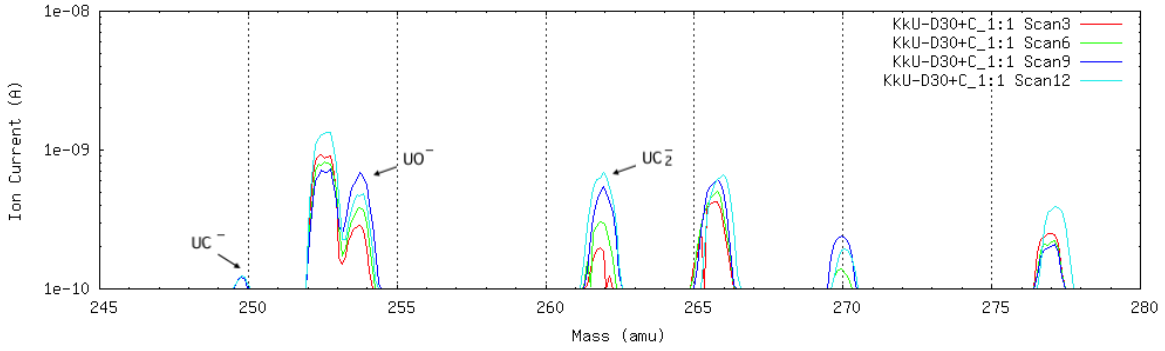

Figure 7.5.3 Mass scans of KkU D30 and graphite mixture sputtered for 15 (scan 3), 30 (scan 6), 45 (scan 9), and 60 (scan 12) minutes. The UC_x^- and generally the UO^- currents grew over time.

7.5.2.2 UO^- Ionisation Efficiency

a. Mass Scans

Figure 7.5.4 shows the third mass scan (sputter duration: 15 min) of targets intended for UO^- extraction. It can be read that niobium and KkU D30 mixture provided the highest UO^- beam intensity.

Further, KkU D30 and iron mixtures with a mass ratio of 1:2 outperformed those with mass ratio of 1:1 regarding all uranium oxide ions. Mass spectra of the two targets containing KkU D30 and iron with a mass ratio of 1:1 show differences which cannot be

[27] The peak at 265 amu UC_3^- appeared to have merged peaks at 265 (UC_3^-) and 266 (Cs_2^-).

explained by the different target sizes. Therefore, the reproducibility of this experiment could not be expected to be high.

Figure 7.5.5 shows the mass scans 1, 3, 5, 7 of KkU D30 and Fe with a mass ratio of 1:2, corresponding to 5 min, 15 min, 25 min and 35 min of sputter duration. Intensities of UO^- and UO_2^- increased, whereas UO_3^- and UO_4^- experienced intensity reduction during this time. This observation is in contrast with that in the first and the second experiment (see section 7.2.2.2.a and 7.3.2.1.a).

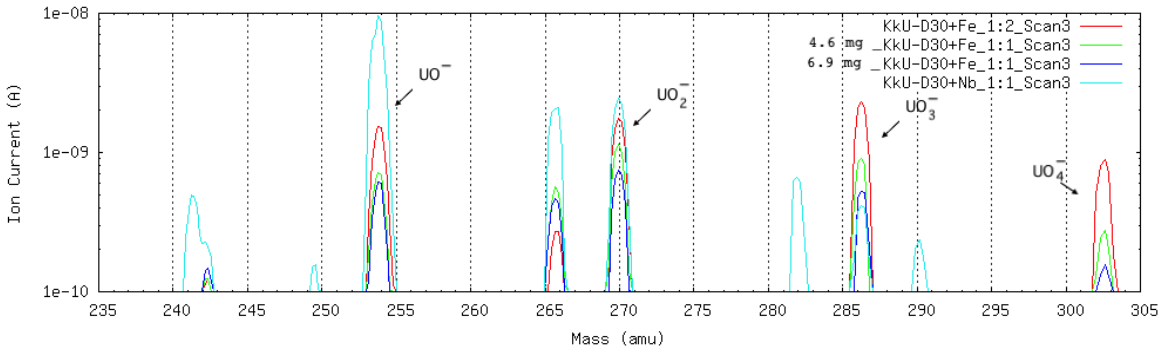

Figure 7.5.4 Third mass scans of targets for UO^- extraction. KkU D30 in a niobium matrix outperformed all other materials regarding UO^- beam intensity. KkU D30 and iron mixed with a mass ration of 1:2 produced UO_x^- of higher intensities than KkU D30 and iron with a mass ration of 1:2.

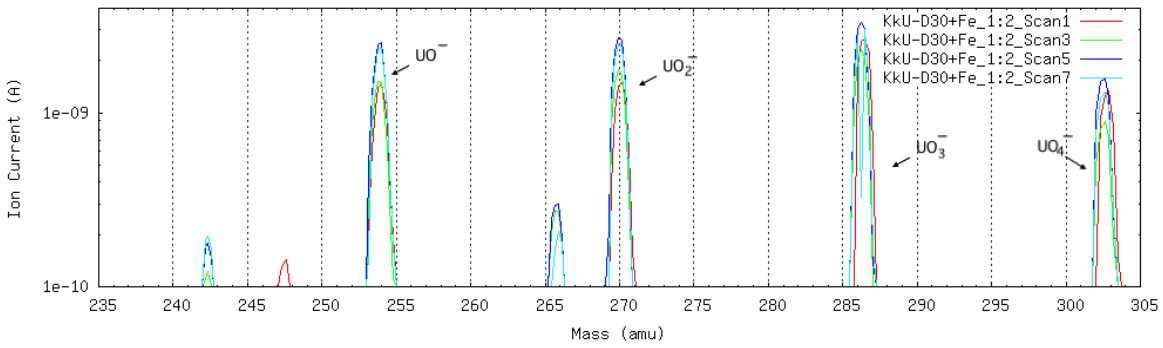

Figure 7.5.5 Mass scans 1, 3, 5, 7 of KkU D30 and Fe with a mass ratio of 1:2. In this time span, intensities of UO^- and UO_2^- increased, and those of UO_3^- and UO_4^- decreased.

b. Current Development

Figure 7.5.6 shows the temporal development of the UO^- currents. The KkU D30 and niobium mixture provided a UO^- beam with the highest intensity (around 10 nA) the whole time. The KkU D30 and iron mixture with a mass ratio of 1:2 produced a current five to six times larger than that with a mass ratio of 1:1 most of the time, while the sample masses were comparable.

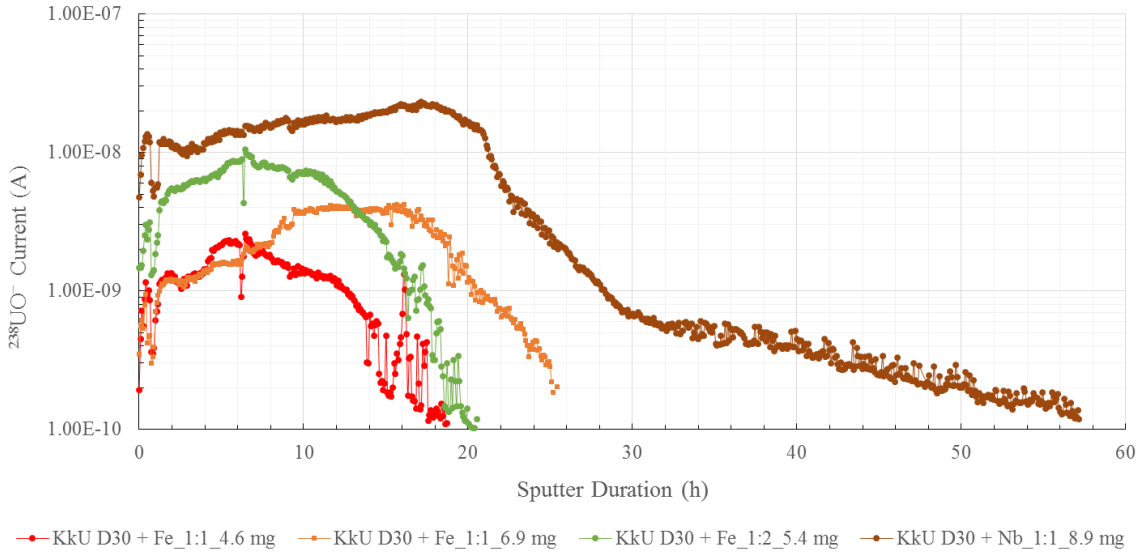

Figure 7.5.6 Temporal development of $^{238}UO^-$ currents. KkU D30 and niobium mixture provided UO^- with the highest intensity. An increase of the iron proportion in the KkU D30 and iron mixture had a positive influence on the UO^- intensity.

c. Ionisation Efficiency

Figure 7.5.7 shows the temporal development of the UO^- ionisation efficiencies. The results are also shown in table 7.5.1. The KkU and niobium mixture, though provided a higher ionisation efficiency in the long run, its sputter rate in the first 13 hours, however, is lower than that of the KkU and iron mixture with a mass ratio of 1:2.

Further, mixing KkU and iron to a mass ratio of 1:2 instead of 1:1 was not only beneficial for the UO^- ion beam intensity, but also for the overall ionisation efficiency. Under the condition of similar samples sizes, the KkU and iron mixture with a mass ratio of 1:2 had an ionisation efficiency almost 3.5 times higher than that of KkU and iron mixture with a mass ratio of 1:1.

A comparison of table 7.5.1 and table 7.3.2 shows that targets of the same composition (KkU D30 + Fe; mass ratio around 1:2) with similar mass (~ 5 mg) yielded a UO^- ionisation efficiency of 2.89% in this experiment, which is around 2.6 times of the value achieved in the second experiment (1.11%).

Further, UO^- ionisation efficiency of KkU D30 + Fe targets with a mass ratio of roughly 1:1 and a mass of 4.6 mg was 0.47% in this experiment; similar target (roughly the same composition, 5.88 mg) provided a UO^- ionisation efficiency of only 0.24% in the first experiment[28].

Like in the first experiment, KkU D30 embedded in a Nb matrix had a life time of around 60 hours (see figure 7.5.6), although the target size in this experiment (8.89 mg) is smaller

[28] The influence of the UO^- formation disorder described in section 7.2.2.1 should be considered.

than that in the first experiment (11.48 mg). The UO^- ionisation efficiency of this material in this experiment is around 3 times of that in the first experiment[27] (see also table 7.2.3).

These comparisons mark high UO^- ionisation efficiencies overall in this experiment and points, thus, to a low reproducibility of these ionisation efficiency measurements.

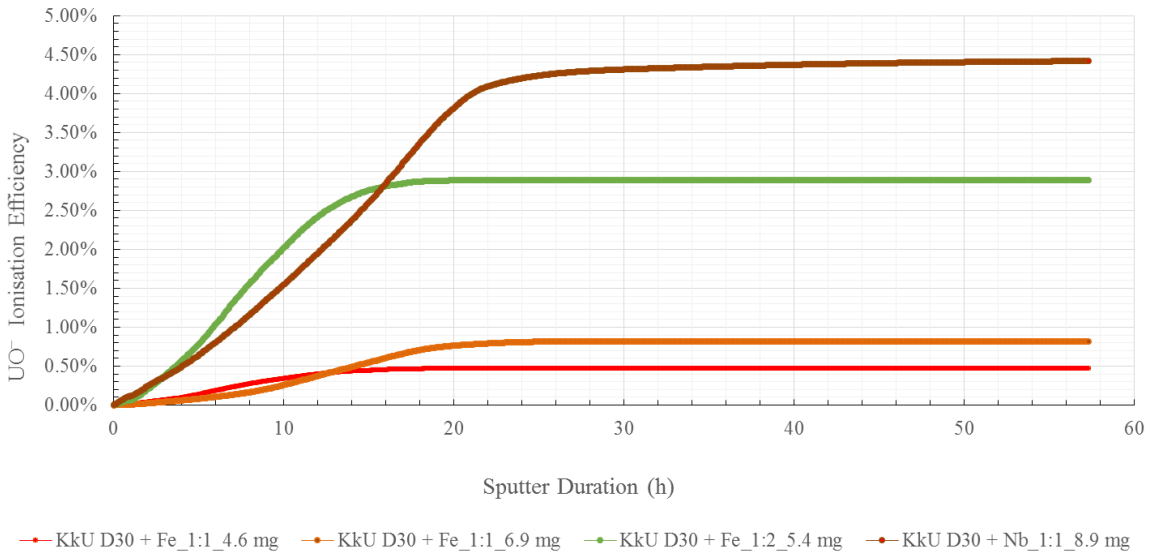

Figure 7.5.7 Temporal development of the integrated UO^- ionisation efficiencies

Material	Mass Ratio	Target Mass (mg)	UO^- Ionisation Efficiency (%)
KkUD30+Fe	1.00 : 0.93	4.60	0.47
KkUD30+Fe	1.00 : 0.93	6.86	0.82
KkUD30+Fe	1.00 : 2.12	5.35	2.89
KkUD30+Nb	1.00 : 0.98	8.89	4.42

Table 7.5.1 Targets specifications, UO^- ionisation efficiencies. Compared with what was achieved in the first and the second experiments, the UO^- ionisation efficiencies in this experiment of similar targets were much higher, which marks a low reproducibility of the ionisation efficiency measurements.

7.5.2.3 UF_5^- Extraction with Cathode Inserts

a. Mass Scans

Figure 7.5.8 shows the third mass scans (sputter duration: 15 min) of targets containing V4TA and PbF_2. In comparison to target contained in normal Al cathodes, targets in gold and copper inserts produced UF_5^- with a much higher intensity, although the mass of the targets are comparable (see table 7.5.2). Further, only the target in normal Al cathode provided a UO^- peak.

Further, no other UF_x^- peaks except for UF_5^- was measured within the sensitivity of the Faraday cup.

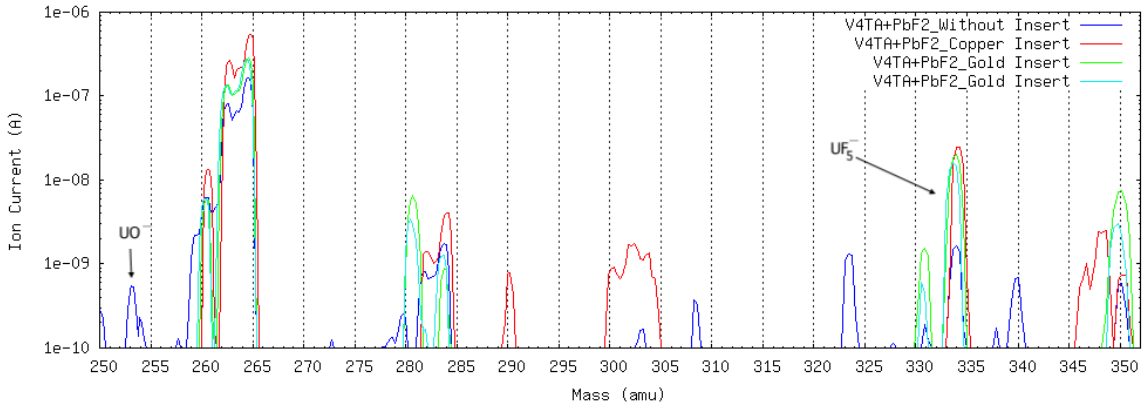

Figure 7.5.8 Third mass scans of V4TA and PbF_2 targets. Gold and copper inserts had a positive influence on the UF_5^- and negative influence on the UO^- intensity.

b. Current Development & Ionisation Efficiency

Figure 7.5.9 shows the temporal development of the UF_5^- current (up) and the integrated UF_5^- ionisation efficiency (down). Targets specifications as well as the results of the ionisation efficiency measurements are listed in table 7.5.2.

Using gold and copper inserts improved the UF_5^- current by a factor of 10 and the UF_5^- ionisation efficiency by a factor of around 30. The target in copper insert produced a UF_5^- current around 10 nA for 2.5 hours. Targets in gold inserts produced UF_5^- currents around 20 nA for roughly 1.5 hours. The ionisation efficiency of the target in copper insert is 20% higher than that of targets in gold inserts.

Strangely, the target in normal Al cathode had only a life time of 1 hour, which was in contrast with the life time of 12 hours of observed in experiment 2 (see section 7.3.2.3), even when considering that the mixing ratio was 1:9 (mass) and the sample mass was 5 mg in experiment 2.

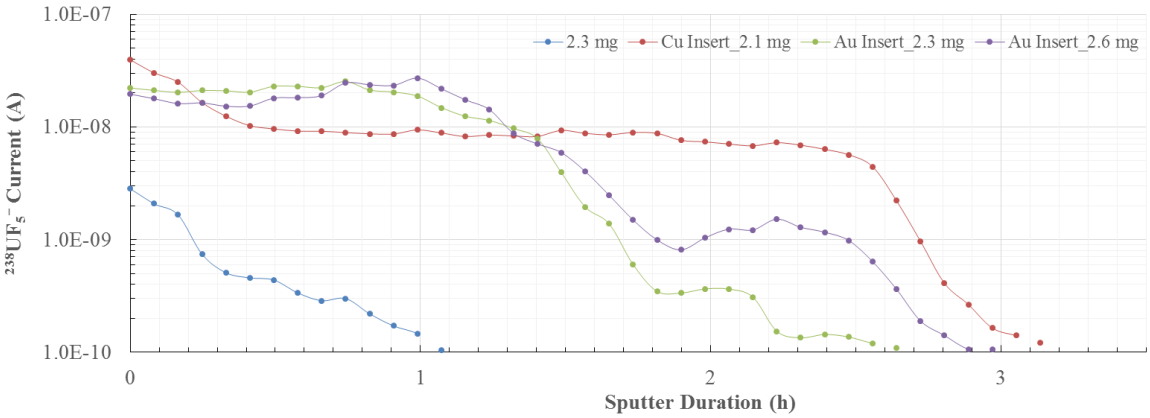

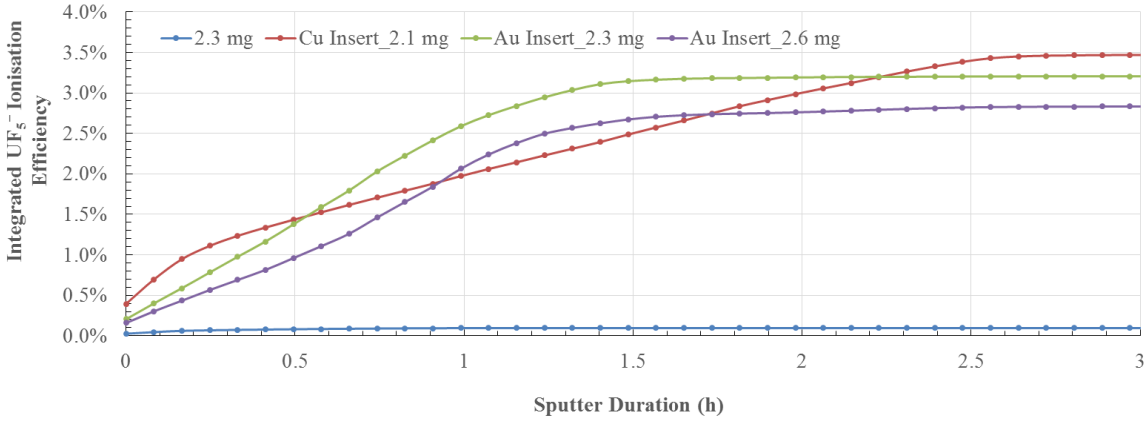

Figure 7.5.9 Temporal development of the $^{238}UF_5^-$ current (up) and the integrated UF_5^- ionisation efficiency (down) (legend denotes if inserts were used and target masses). Using inserts improved the UF_5^- ion beam intensity as well as the ionisation efficiency immensely.

Sample Material		**Target Mass (mg)**	**UF_5^- ionisation efficiency**
V4TA+PbF_2 Mass Ratio 1:8	No insert	2.25	0.10%
	Cu insert	2.11	3.47%
	Au insert	2.28	3.20%
	Au insert	2.60	2.83%

Table 7.5.2 Targets specifications, UF_5^- ionisation efficiencies

7.6 Outlook for Future Uranium Experiments

These four experiments showed that both the UF_5^- and UO^- ionisation efficiencies could be increased to around 3% (see also section 7.1: UO^- ionisation efficiency measured by Fifield et al (1996): 0.3%) with the appropriate target holder, sample material composition as well as ion source parameters. Since experiment 4 saw copper target holders as more advantageous than aluminium target holders for UF_4 samples, further experiments need to be carried out for the following aims:

- to see if this applies to all UF_4 materials prepared in FNSPE CTU Prague
- to see if the results in the experiment with different inserts (experiment 4) are reproducible, since this experiment included only one cathode with copper insert
- to see what difference does double-pitting make (a pitted sample well & target surface)

8. CONCLUSIONS AND OUTLOOK

The aim of the thesis was to examine and improve ionisation efficiency as well as the beam intensity of hafnium, caesium as well as uranium fluoride anions in a Middleton type Sputter Ion Source.

Experiments on HfF_5^- ion formation in relation to target composition as well as manner of sputtering showed that sample materials consisting of HfF_4, PbF_2 and Ag, especially in the case of high PbF_2 proportion, are superior than sample materials containing HfF_4 and Ag alone, with regard to HfF_5^- beam intensity as well as ionisation efficiency. The highest HfF_5^- ionisation efficiency was 5.9%, achieved by continuous sputtering of a HfF_4, PbF_2 and Ag mixture with a mass ratio of 1:3:1. This is almost a factor of 6 improvement compared to previous work (Vockenhuber 2004).

The experiment on CsF_2^- formation showed that PbF_2 is more effective than LaF_3 for the generation of CsF_2^-. Using PbF_2 as fluorine donor with a Cs:F atom ratio of 1:3 yielded a typical current of 40 - 100 nA, which is comparable with what was achieved at VERA previously (Kasberger 2015; Lachner et al 2015). The maximum CsF_2^- ionisation efficiency was around 0.08%.

Experiments on UO^- formation demonstrated that adding Fe to a mixture of U_3O_8 and Fe_2O_3 improves the UO^- beam intensity as well as ionisation efficiency. A 1:2 mass ratio of the U_3O_8 + Fe_2O_3 mixture to the added Fe proved to be more effective for the formation of UO^- than a 1:1 mass ratio. The maximum ionisation efficiency of around 2.9% was achieved by sputtering a U_3O_8 and Fe_2O_3 mixture added with Fe to a mass ratio of 1:2. Compared with what Fifield et al (1996) measured using a mixture of UO_3, FeO and Ag powder with a uranium and iron atom ratio of 1:1, this is nearly a factor of 10 improvement.

Experiments on UF_5^- ion formation showed that aluminium target holder are not suitable for UF_5^- measurement. The maximum ionisation efficiency of 3.9% was gained by using gold and copper inserts in normal aluminium cathodes for UF_4 and PbF_2 mixtures with a mass ratio of 1:8.

Since factors affecting ionisation efficiency are numerous and only a small fraction could be encompassed in this thesis, further studies would be required. Factors to be considered are, for example, ion source parameters in connection with the primary ion beam, cathode well geometry and sputter crater.

APPENDIX A CHECKLIST FOR IONISATION YIELD MEASUREMENTS WITH S2

1. Position 0 & 1 in target wheel: OldC. Also needed: a target for parametric optimisation/ peaks identification, which ideally has a similar mass number as the measured ion (For U: KkU-D30 + PbF2).
2. Create measurement using the following command: create_measurement dataaxel datavera2 heavy <folder name>
3. Fill out wheel.log & control.log: SOURCE_SELECT = 2
4. Mount the target wheel
5. i_script: source-S2 on -c -w 2e-6 0
6. Optional: use the command "/usr/vera/scripts/subscripts/i_info &" to indicate the present measurement in this vnc window
7. Load a recent setup for the corresponding ion, wait until the source is warm (OVN: around 145 degree) and a reasonable current (a few µA) can be collected in FC S2-1.
8. Check if slits S2-1 (x +/-10mm; y +/- 10 mm) are open (right-clicks show the actual position). The same applies to all slits that can be only adjusted manually. Also, check pg 202 if the ion beam attenuator is in the beamline.
9. chcat -S2 to a fresher OldC to centre the wheel: maximising the current in FC S2-1(which is inserted by default) by rotating the two upper knobs in the opposite direction (this adjusts the Left & Right position of the wheel)) and then the lower knob (this adjusts Up & Down).
10. Parameter optimisation with OldC: open FC S2-1, BLV S2-1 and insert FC I1-1.
    1. Under the following setting, the maximum of $^{12}C^-$ is at a setting of BM I1-1 of around 35 A. Scan the magnet and set the optimum.

CAT S2-1	-5.01 KV	-0.12 mA
EXT S2-1	15 KV	
HVS S2-1	-10.45 KV	

    2. Find out the bias current drawn by the shunt resistor of HVS S2-1: insert FC S2-1, set CAT S2-1 voltage to 0 kV, note down the HVS S2-1 current value I1, which denotes the current that flows through the resistors connected parallel to the power supply (1.5 GΩ); set CAT S2-1 voltage back to -5 KV and note down the HVS S2-1 CR current value I2. The difference (I2-I1) times a factor of **2.5** is the actual HVS S2-1 current (the meter reads wrong by a factor of 2.5). Compare it with the current in FC S2-1, there should not be much discrepancy (around 25% is fine). In the process, the HVS voltage value should be kept constant.
    3. Calculate and set a reasonable value for HVS S2-1CC current: if uranium is measured -> judging from experience, carbon targets produce a current of around 70 µA in the first FC. Uranium targets (extracted: UO^-) produce around 2/3 of the C^- current, which means that -0.020 mA is a reasonable HVS current value for UO^-. Since the initial UF_5^- current tends to be higher than the peak value of UO^- current, the range from -0.040 to -0.030 mA should be suitable.
    4. Set the source regulation REG S2-1 as HVS_CR, which will coordinate LNH and ION so that HVS S2-1 CR will reach the set value of HVS S2-1 CC. Set the CAT S2-1 CC value to -1.8 mA to allow for a regulation at a greater range (if HVS_CR is used as regulation target, EXT S2- 1 CR is only used as a maximum limit).
    5. Go to /usr/vera/exos_scripts/parfiles/regulate_hvscr.par and change the setting of Source_S2 to Cwarmup, if a process speed-up is needed, lnhfastC.

11. chcat to a cathode for parametric optimisation; open FC S2-1 and insert FC I1-1. Manually insert the 1 mm slit in front of FC I1-1 (take out the FC I1-1 to make sure that the slit does

not come together with the FC). Set a desired value for HVS VC (so that there is a defined peak position in HVS scans), scan BM I1-1 to find out a desired maximum and set the optimal value. Vienna KkU- D30 in PbF_2 matrix has PbF_3^- as its major peak, which has its maximum with the following setting.

CAT S2-1	-5.01 KV
EXT S2-1	15 KV
HVS S2-1	-10.45 KV
BM I1-1	Around 162A

12. Start script automax to maximise the current in FC I1-1 (excluding the parameter HVS VC). After the optimisation, change the 1mm slit to the 2mm one for measurement.
13. Scan HVS voltage, identify the peaks/one peak to for mass calibration.
14. Go to /usr/vera/exos_scripts/parfiles/regulate_hvscr.par and change the setting of Source_S2 (e.g. slow).
15. Check Page 202: the status of FC I1-1 CumulByp should be active, so that the measurement would stop automatically when no current is collected by the cup (status: bad).
16. Create a file "batch" by copying it from a similar previous measurement, and modify it to suit your needs.
17. Start the measurement by going to the right directory and enter **batch**. Should the permission be denied, then use either the command /**batch** or **chmod 775 batch**. chmod 775 (followed by a file name or directory name) changes the permissions mode of this file/directory so that the owner and group has full access.
18. Keep track of the source regulation at /dataaxel/tech/source/source_regulation_b_S2.plotdef: a fluctuation of the curve **catcr bias** possibly means too much caesium in the source; **capdr** denotes the LNH current, which should correspond with the set value (except when a fast source regulation, e.g. lnhfastC, applies); **catcr** denotes the cathode current, which, if it exceeds the limit of -2mA (<-10µA*200), indicates much caesium in the source and the insulator in the source may become conductive and thus disable the source until a cleaning is performed.
19. Should problems exist with the measurement: i_script diagnosis – x
20. Should the batch file be changed during the measurement, the measurement needs to be stopped and restarted. Start the Turn variable with a number that does not overlap with existing scans.
21. Should the scan range be changed during the measurement, change the value in "fsetpar "HVS S2-1|VC" -value" instead of the "-I" value in the batch file, since the scan duration will be changed otherwise.
22. Evaluation:
    1. create a file "extract_peak_mass<number>" by copying it from a similar previous measurement (modification might be needed).
    2. Note: changing the scanning range will lead to a change of "HVS patterns" that should be taken for evaluation.

APPENDIX B BATCH PROGRAM FOR MASS SCANS

by Ass.-Prof. Mag. Dr. Peter Steier

```
#!/bin/bash

. $SCRIPTDIR/scriptheader

CATHODES="2 3 4 5 6 7 8 9 10 11 12 13 14 15 16 17 18 19 20 21 22 23 24"

TURN=1
while true ; do
    for CAT in $CATHODES ; do
        SCANS=$(getinf "control.log:TARGETS :$CAT,SCANS")
        if test $SCANS == 0 ; then
            continue ;
          fi ;
        script chcat -S2 $CAT
        SCAN=0
        while test $SCAN -lt $SCANS ; do
            fsetpar "HVS S2-1|VC" -8.3
            script -i scan -Q -p 400 -I 5 -r 200 -i -s 0.1 -S 0.1  hvss2
fci1 MassScan_turn${TURN}_cat${CAT}_scan${SCAN}.plotdef
            SCAN=$(($SCAN+1))
          done
      done
    TURN=$(( $TURN + 1 ))
  done
```

APPENDIX C BATCH PROGRAM FOR DATA EVALUATION

by Ass.-Prof. Mag. Dr. Peter Steier

```
#!/bin/bash

MASS=254


HVS_PATTERN="^-11.1446\|^-11.1195\|^-11.0945\|^-11.0694\|^-11.0444\|^-
11.0193\|^-10.9942\|^-10.9692"

CATS="3 4 5 6 7 8 9 10 11 12 13 14"

SCANS="0 1 2"
TURNS="1 2 3 4 5 6 7 8 9 10 11 12 13 14 15 16 17 18 19 20 21 22 23 24 25
26 27 28 29 30 31 32 33 34 35 36 37 38 39 40 41 42 43 44 45 46 47 48 49
50 51 52 53 54 55 56 57 58 59 60 61 62 63 64 65 66 67 68 69 70 71 72 73
74 75 76 77 78 79 80"

for CAT in $CATS ; do
    {
    echo >&2 "cathode $CAT..."
    echo $CAT
    for TURN in $TURNS ; do
        for SCAN in $SCANS ; do
            grep "$HVS_PATTERN"
MassScan_turn${TURN}_cat${CAT}_scan${SCAN}.plotdef \
               | cut -d" " -f 2 \
               | awk 'BEGIN{a=0}{if (-$1>0+a) a=-$1} END{print a}'
          done ;
      done ; } > cat${CAT}_mass${MASS}_cur_vs_time.txt
  done

paste  $( for CAT in $CATS ; do echo
cat${CAT}_mass${MASS}_cur_vs_time.txt ; done ) >
mass${MASS}_cur_vs_time.txt
```

BIBILIOGRAPHY

Andersen, T., Haugen, H.K. and Hotop, H., 1999. Binding energies in atomic negative ions: III. *Journal of Physical and Chemical Reference Data*, *28*(6), pp.1511-1533.

Buompane, R., De Cesare, M., De Cesare, N., Di Leva, A., D'Onofrio, A., Fifield, L.K., Fröhlich, M., Gialanella, L., Marzaioli, F., Sabbarese, C. and Terrasi, F., 2015. Background reduction in 236U/238U measurements. *Nuclear Instruments and Methods in Physics Research Section B: Beam Interactions with Materials and Atoms*, *361*, pp.454-457.

Casacuberta, N., Christl, M., Lachner, J., van der Loeff, M.R., Masque, P. and Synal, H.A., 2014. A first transect of 236U in the North Atlantic Ocean. *Geochimica et Cosmochimica Acta*, *133*, pp.34-46.

Child, D.P., Hotchkis, M.A.C., Whittle, K. and Zorko, B., 2010. Ionisation efficiency improvements for AMS measurement of actinides. *Nuclear Instruments and Methods in Physics Research Section B: Beam Interactions with Materials and Atoms*, *268*(7-8), pp.820-823.

Eigl, R., Steier, P., Winkler, S.R., Sakata, K. and Sakaguchi, A., 2016. First study on 236U in the Northeast Pacific Ocean using a new target preparation procedure for AMS measurements. *Journal of environmental radioactivity*, *162*, pp.244-250.

Eliades, J., Zhao, X.L., Litherland, A.E. and Kieser, W.E., 2013. On-line ion chemistry for the AMS analysis of 90Sr and 135,137 Cs. *Nuclear Instruments and Methods in Physics Research Section B: Beam Interactions with Materials and Atoms*, *294*, pp.361-363.

Farwell, G.W., Roberts, J.E. and Wahl, A.C., 1954. Half-Lives of Pu 240 and Pu 239. *Physical Review*, *94*(2), p.363.

Fifield, L.K., Cresswell, R.G., Di Tada, M.L., Ophel, T.R., Day, J.P., Clacher, A.P., King, S.J. and Priest, N.D., 1996. Accelerator mass spectrometry of plutonium isotopes. *Nuclear Instruments and Methods in Physics Research Section B: Beam Interactions with Materials and Atoms*, *117*(3), pp.295-303.

Forstner, O., Gnaser, H., Golser, R., Hanstorp, D., Martschini, M., Priller, A., Rohlén, J., Steier, P., Vockenhuber, C. and Wallner, A., 2011. Reassessment of 182Hf AMS measurements at VERA. *Nuclear Instruments and Methods in Physics Research Section B: Beam Interactions with Materials and Atoms*, *269*(24), pp.3180-3182.

Hirose, K., Kikawada, Y., Igarashi, Y., Fujiwara, H., Jugder, D., Matsumoto, Y., Oi, T. and Nomura, M., 2017. Plutonium, 137Cs and uranium isotopes in Mongolian surface soils. *Journal of environmental radioactivity*, *166*, pp.97-103.

Hlavenka, J.D., Abrams, H., Roberts, M.L. and Longworth, B.E., 2017. Increased AMS Ion Source Efficiency and Ion Currents by Modifying SNICS Cathode Material and Geometry. *Physics Procedia*, *90*, pp.17-21.

Hotop, H. and Lineberger, W.C., 1975. Binding energies in atomic negative ions. *Journal of Physical and Chemical Reference Data*, *4*(3), pp.539-576.

IAEA. "Fission Product Yields". https://www-nds.iaea.org/wimsd/fpyield.htm#T3.

James, A.M. and Lord, M.P., 1992. *Macmillan's chemical and physical data*. Macmillan.

Lachner, J., Kasberger, M., Martschini, M., Priller, A., Steier, P. and Golser, R., 2015. Developments towards detection of 135Cs at VERA. *Nuclear Instruments and Methods in Physics Research Section B: Beam Interactions with Materials and Atoms*, *361*, pp.440-444.

Lee, T., Teh-Lung, K., Hsiao-Ling, L. and Ju-Chin, C., 1993. First detection of fallout Cs-135 and potential applications of 137Cs135Cs ratios. *Geochimica et cosmochimica acta*, *57*(14), pp.3493-3497.

MacDonald, C.M., Cornett, R.J., Charles, C.R.J., Zhao, X.L. and Kieser, W.E., 2016. Measurement of the Cs 135 half-life with accelerator mass spectrometry and inductively coupled plasma mass spectrometry. *Physical Review C*, *93*(1), p.014310.

Maden, C., 2003. *The potential of accelerator secondary ion mass spectrometry in environmental sciences* (Doctoral dissertation, ETH Zurich).

Maji, S., Lahiri, S., Wierczinski, B. and Korschinek, G., 2006. Separation of trace level hafnium from tungsten: A step toward solving an astronomical puzzle. *Analytical chemistry*, *78*(7), pp.2302-2305.

Martschini, M., Pitters, J., Moreau, T., Andersson, P., Forstner, O., Hanstorp, D., Lachner, J., Liu, Y., Priller, A., Steier, P. and Golser, R., 2017. Selective laser photodetachment of intense atomic and molecular negative ion beams with the ILIAS RFQ ion beam cooler. *International Journal of Mass Spectrometry*, *415*, pp.9-17.

Middleton, R., 1983. A versatile high intensity negative ion source. *Nuclear Instruments and Methods in Physics Research*, *214*(2-3), pp.139-150.

Middleton, R., 1989. A negative ion cookbook. *University of Pennsylvania*.

Pan, L. and Beck, D.R., 2009. Calculations of Hf^- electron affinity and photodetachment partial cross sections. *Journal of Physics B: Atomic, Molecular and Optical Physics*, *43*(2), p.025002.

Quinto, F., Steier, P., Wallner, G., Wallner, A., Srncik, M., Bichler, M., Kutschera, W., Terrasi, F., Petraglia, A. and Sabbarese, C., 2009. The first use of 236U in the general environment and near a shutdown nuclear power plant. *Applied Radiation and Isotopes*, *67*(10), pp.1775-1780.

Quinto, F., Lagos, M., Plaschke, M., Schaefer, T., Geckeis, H., Steier, P. and Golser, R., 2016. Multi-actinide analysis with AMS for ultra-trace determination and small sample sizes: advantages and drawbacks. *Verhandlungen der Deutschen Physikalischen Gesellschaft*.

Middleton, R. and Klein, J., 1999. Production of metastable negative ions in a cesium sputter source: Verification of the existence of $N2^-$ and CO^-. *Physical Review A*, *60*(5), p.3786.

NEC. 2001. Charging System. https://web.archive.org/web/20111108000948/http://www.pelletron.com/charging.htm.

Nomura, T., Sakaguchi, A., Steier, P., Eigl, R., Yamakawa, A., Watanabe, T., Sasaki, K., Watanabe, T., Golser, R., Takahashi, Y. and Yamano, H., 2017. Reconstruction of the temporal distribution of 236U/238U in the Northwest Pacific Ocean using a coral core sample from the Kuroshio Current area. *Marine Chemistry*, *190*, pp.28-34.

Shanks, R.P. and Freeman, S.P., 2015. Sputter-pits casting to measure AMS sample consumption. *Nuclear Instruments and Methods in Physics Research Section B: Beam Interactions with Materials and Atoms*, *361*, pp.168-172.

Steier, P., 2000. *Exploring the limits of VERA: A universal facility for accelerator mass spectrometry*. (Doctoral dissertation, University of Vienna).

Steier, P., Golser, R., Kutschera, W., Priller, A., Vockenhuber, C. and Winkler, S., 2004. VERA, an AMS facility for "all" isotopes. *Nuclear Instruments and Methods in Physics Research Section B: Beam Interactions with Materials and Atoms*, *223*, pp.67-71.

Steier, P., Bichler, M., Fifield, L.K., Golser, R., Kutschera, W., Priller, A., Quinto, F., Richter, S., Srncik, M., Terrasi, P. and Wacker, L., 2008. Natural and anthropogenic 236U in environmental samples. *Nuclear Instruments and Methods in Physics Research Section B: Beam Interactions with Materials and Atoms*, *266*(10), pp.2246-2250.

Steier, P., Dellinger, F., Forstner, O., Golser, R., Knie, K., Kutschera, W., Priller, A., Quinto, F., Srncik, M., Terrasi, F. and Vockenhuber, C., 2010. Analysis and application of heavy isotopes in the environment. *Nuclear Instruments and Methods in Physics Research Section B: Beam Interactions with Materials and Atoms*, *268*(7-8), pp.1045-1049.

Taylor, V.F., Evans, R.D. and Cornett, R.J., 2008. Preliminary evaluation of 135Cs/137Cs as a forensic tool for identifying source of radioactive contamination. *Journal of environmental radioactivity*, *99*(1), pp.109-118.

Vockenhuber, C., 2004. The upgrade of VERA for heavy ion AMS and the long-lived radionuclide 182 Hf (Doctoral dissertation, University of Vienna).

Vockenhuber, C., Bichler, M., Golser, R., Kutschera, W., Priller, A., Steier, P. and Winkler, S., 2004. 182Hf, a new isotope for AMS. *Nuclear Instruments and Methods in Physics Research Section B: Beam Interactions with Materials and Atoms*, *223*, pp.823-828.

Vockenhuber, C., Oberli, F., Bichler, M., Ahmad, I., Quitté, G., Meier, M., Halliday, A.N., Lee, D.C., Kutschera, W., Steier, P. and Gehrke, R.J., 2004. New Half-Life Measurement of Hf 182: Improved Chronometer for the Early Solar System. *Physical review letters*, *93*(17), p.172501.

Vogel, J.S., 2015. Anion formation by neutral resonant ionization. *Nuclear Instruments and Methods in Physics Research Section B: Beam Interactions with Materials and Atoms*, *361*, pp.156-162.

Vogel, J.S. and Giacomo, J.A., 2017. Increased 14 C AMS efficiency from reduced competitive ionization. *Radiocarbon*, *59*(3), pp.957-965.

Wang, Y.X., Pan, Z.Y., Ho, Y.K., Xu, Y. and Du, A.J., 2001. The structural and dynamical properties of Al clusters adsorbed on Ni surface. *Nuclear Instruments and Methods in Physics Research Section B: Beam Interactions with Materials and Atoms*, *180*(1-4), pp.251-256.

Wessells, C. 2012. "Cesium-137: a Deadly Hazard". http://large.stanford.edu/courses/2012/ph241/wessells1/.

Wilcken, K.M., Barrows, T.T., Fifield, L.K., Tims, S.G. and Steier, P., 2007. AMS of natural 236U and 239Pu produced in uranium ores. *Nuclear Instruments and Methods in Physics Research Section B: Beam Interactions with Materials and Atoms*, *259*(1), pp.727-732.

Winkler, S.R., Steier, P. and Carilli, J., 2012. Bomb fall-out 236U as a global oceanic tracer using an annually resolved coral core. *Earth and planetary science letters*, *359*, pp.124-130.

Winkler, S.R., Steier, P., Buchriegler, J., Lachner, J., Pitters, J., Priller, A. and Golser, R., 2015. He stripping for AMS of 236U and other actinides using a 3 MV tandem accelerator. *Nuclear Instruments and Methods in Physics Research Section B: Beam Interactions with Materials and Atoms*, *361*, pp.458-464.

Yang, G., Tazoe, H. and Yamada, M., 2016. 135 Cs activity and 135 Cs/137 Cs atom ratio in environmental samples before and after the Fukushima Daiichi Nuclear Power Plant accident. *Scientific reports*, *6*, p.24119.

Yin, X., He, M., Dong, K., Dou, L., Lan, X., Pang, F., Wu, S. and Jiang, S., 2015. Preliminary measurements of 135 Cs with AMS. *Nuclear Instruments and Methods in Physics Research Section B: Beam Interactions with Materials and Atoms*, *361*, pp.488-490.

Zhao, X.L., Kilius, L.R., Litherland, A.E. and Beasley, T., 1997. AMS measurement of environmental U-236 Preliminary results and perspectives. *Nuclear Instruments and Methods in Physics Research Section B: Beam Interactions with Materials and Atoms*, *126*(1-4), pp.297-300.

Zhao, X.L., Litherland, A.E., Eliades, J., Kieser, W.E. and Liu, Q., 2010. Studies of anions from sputtering I: Survey of MFn. *Nuclear Instruments and Methods in Physics Research Section B: Beam Interactions with Materials and Atoms*, *268*(7-8), pp.807-811.

Zhao, X.L., Charles, C.R.J., Cornett, R.J., Kieser, W.E., MacDonald, C., Kazi, Z. and St-Jean, N., 2016. An exploratory study of recycled sputtering and CsF_2^- current enhancement for AMS. *Nuclear Instruments and Methods in Physics Research Section B: Beam Interactions with Materials and Atoms*, *366*, pp.96-103.

Zheng, J., Tagami, K., Bu, W., Uchida, S., Watanabe, Y., Kubota, Y., Fuma, S. and Ihara, S., 2014. 135Cs/137Cs isotopic ratio as a new tracer of radiocesium released from the Fukushima nuclear accident. *Environmental science & technology*, *48*(10), pp.5433-5438.